

# 1            **Kinetic and structural characterization of the self-labeling** 2            **protein tags HaloTag7, SNAP-tag and CLIP-tag**

3  
4 Jonas Wilhelm<sup>1,9</sup>, Stefanie Kühn<sup>1,9</sup>, Mirosław Tarnawski<sup>2</sup>, Guillaume Gotthard<sup>3,7</sup>, Jana Tünner-  
5 mann<sup>1</sup>, Timo Tänzler<sup>4</sup>, Julie Karpenko<sup>4,8</sup>, Nicole Mertes<sup>1</sup>, Lin Xue<sup>1</sup>, Ulrike Uhrig<sup>5</sup>, Jochen Rein-  
6 stein<sup>6</sup>, Julien Hiblot<sup>1,4,10\*</sup> and Kai Johnsson<sup>1,4,10\*</sup>.

7  
8 <sup>1</sup>Department of Chemical Biology, Max Planck Institute for Medical Research, Heidelberg, Germany.  
9 <sup>2</sup>Protein Expression and Characterization Facility, Max Planck Institute for Medical Research, Heidelberg, Germany.  
10 <sup>3</sup>Structural Biology Group, European Synchrotron Radiation Facility (ESRF), Grenoble, France.  
11 <sup>4</sup>Institute of Chemical Sciences and Engineering, École Polytechnique Fédérale de Lausanne (EPFL), Lausanne, Swit-  
12 zerland.  
13 <sup>5</sup>Chemical Biology Core Facility, European Molecular Biology Laboratory, Heidelberg, Germany.  
14 <sup>6</sup>Department of Biomolecular Mechanisms, Max Planck Institute for Medical Research, Heidelberg, Germany.  
15 <sup>7</sup>Present addresses: Division of Biology and Chemistry–Laboratory for Biomolecular Research, Paul Scherrer Institute,  
16 Villigen, Switzerland. Department of Biology, Institute of Molecular Biology and Biophysics, ETH Zürich, Zürich, Swit-  
17 zerland.  
18 <sup>8</sup>Present address: Laboratoire d’Innovation Thérapeutique, UMR7200 CNRS/Université de Strasbourg, Strasbourg  
19 Drug Discovery and Development Institute (IMS), Illkirch-Graffenstaden, France.  
20 <sup>9</sup>These authors contributed equally: Jonas Wilhelm, Stefanie Kühn.  
21 <sup>10</sup>These authors contributed equally: Julien Hiblot, Kai Johnsson.  
22 \* e-mail: [julien.hiblot@mr.mpg.de](mailto:julien.hiblot@mr.mpg.de); [johnsson@mr.mpg.de](mailto:johnsson@mr.mpg.de).

1 **Abstract**

2 The self-labeling protein tags (SLPs) HaloTag7, SNAP-tag and CLIP-tag allow the covalent label-  
3 ing of fusion proteins with synthetic molecules for applications in bioimaging and biotechnology.  
4 To guide the selection of an SLP-substrate pair and provide guidelines for the design of substrates,  
5 we report a systematic and comparative study on the labeling kinetics and substrate specificities  
6 of HaloTag7, SNAP-tag and CLIP-tag. HaloTag7 reaches almost diffusion-limited labeling rates  
7 with certain rhodamine substrates, which are more than two orders of magnitude higher than those  
8 of SNAP-tag for the corresponding substrates. SNAP-tag labeling rates however are less affected  
9 by the structure of the label than those of HaloTag7, which vary over six orders of magnitude for  
10 commonly employed substrates. Solving the crystal structures of HaloTag7 and SNAP-tag labeled  
11 with fluorescent substrates allowed us to rationalize their substrate preferences. We also demon-  
12 strate how these insights can be exploited to design substrates with improved labeling kinetics.

## 1 **Introduction**

2 Modern high-resolution fluorescence imaging techniques require the specific labeling of proteins  
3 with appropriate fluorescent probes. Self-labeling protein tags (SLPs) have been shown to offer a  
4 straightforward way to achieve this goal as they undergo a specific and irreversible reaction with  
5 synthetic substrates such as fluorophores (1). SLPs are furthermore employed in various other  
6 applications such as *in vitro* biophysical studies (2, 3), the generation of semisynthetic biosensors  
7 (4-7) and yeast three-hybrid screenings (8). The three most popular SLPs are HaloTag7 (HT7)  
8 (9), SNAP-tag (SNAP) (10) and CLIP-tag (CLIP) (11) (**Fig. 1**).

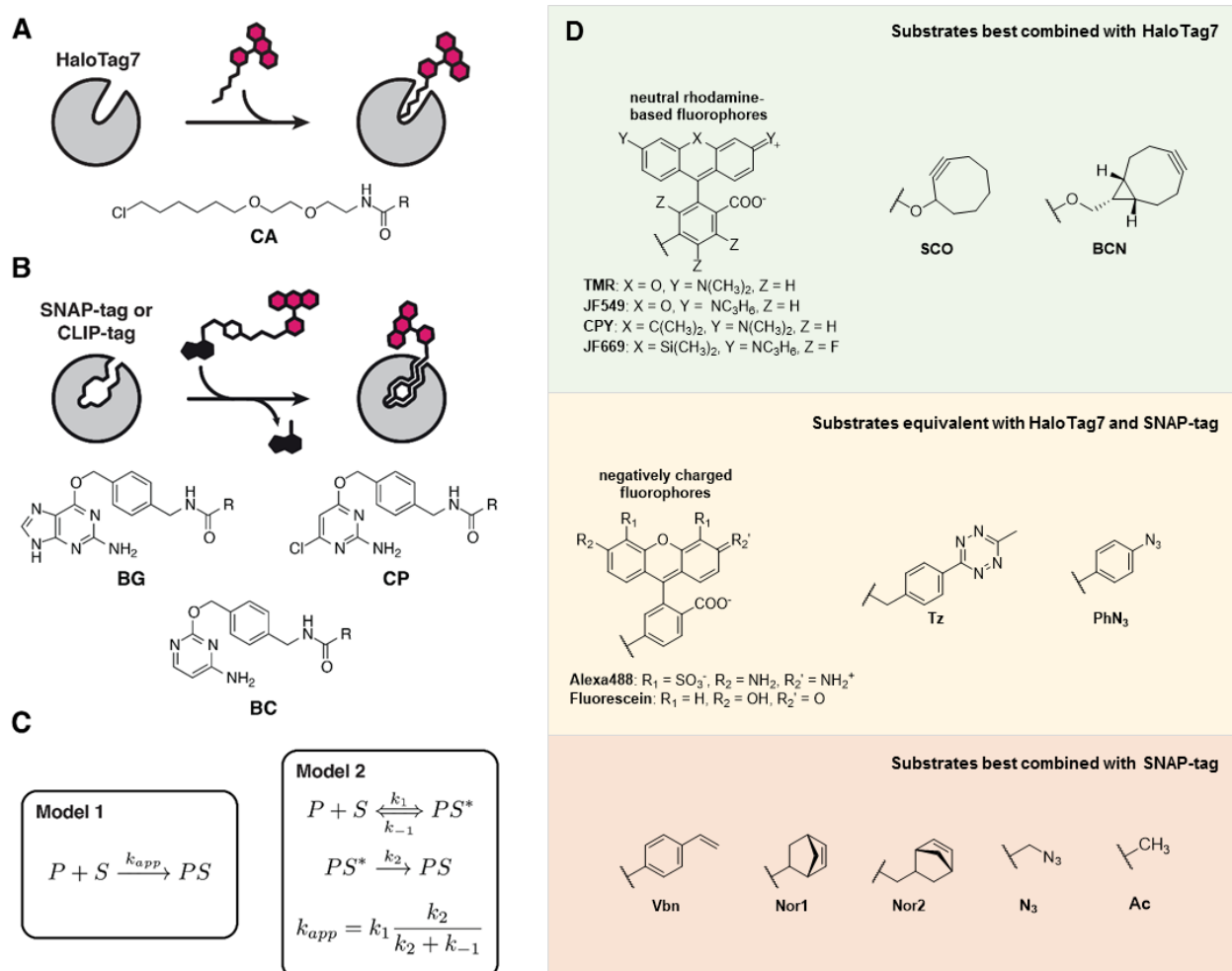
9 HT7 was engineered from a bacterial dehalogenase (DhaA from *Rhodococcus sp.*), an enzyme  
10 able to hydrolyze halogenated alkanes (12). Inactivating the second catalytic step of its enzymatic  
11 reaction (mutation H272N in HT7) abolished the hydrolysis of the ester formed with an active site  
12 aspartate residue and created an SLP. HT7 reacts specifically with chloroalkane-PEG (CA) mol-  
13 ecules resulting in covalent bonding of the alkane chain to the catalytic aspartate and release of  
14 a chloride ion (**Fig. 1A**). HT7 was further engineered for increased stability and efficient labeling  
15 kinetics toward CA-fluorophore substrates (13).

16 SNAP was engineered from the human *O*<sup>6</sup>-alkylguanine-DNA alkyltransferase (hAGT), a protein  
17 involved in the repair of alkylated DNA by transferring alkyl moieties to its reactive cysteine (14).  
18 SNAP was engineered to efficiently react with benzylguanine (BG) derivatives as substrates (**Fig.**  
19 **1B**) and to reduce its DNA binding properties (10). SNAP irreversibly transfers the benzyl moiety  
20 of the substrate to its reactive cysteine, leading to the release of guanine. SNAP also accepts  
21 substrates in which the guanine is replaced by a chloropyrimidine (CP) (**Fig. 1B**), reported to pos-  
22 sess higher cell permeability (15). Later, CLIP was engineered from SNAP as an orthogonal SLP  
23 system, accepting benzylcytosine (BC) derivatives as substrates (11) (**Fig. 1B**).

24 Even though it has become clear over the last years that the nature of the transferred label can  
25 have a significant impact on the reaction kinetics (9, 16, 17), no systematic study has been re-  
26 ported so far that addresses the influence of the transferred label on the SLP labeling kinetics.  
27 The structural reasons for the differences in labeling rates are poorly understood. Furthermore,  
28 the reaction kinetics of SLPs are usually characterized as a single step-reaction under pseudo-  
29 first order reaction conditions, *i.e.* in large excess of one of the reactants (Model 1, **Fig. 1C**). How-  
30 ever, the reaction mechanism of SLPs is more complex and should be characterized by a multi-  
31 step kinetic model comprising reversible substrate binding ( $k_1$ ), unbinding ( $k_{-1}$ ) and irreversible  
32 covalent reaction ( $k_2$ ) (Model 2, **Fig. 1C**). Here, we report an in-depth characterization of the re-  
33 action kinetics of HT7, SNAP and CLIP with different substrates, identifying those structural fea-

1 tures of labels that control labeling rates for the different tags. We complement these kinetic stud-  
 2 ies by reporting crystal structures of HT7 and SNAP covalently labeled with rhodamine-based  
 3 fluorophores, providing a detailed understanding of their substrate preferences. Our results will (i)  
 4 facilitate the use of SLPs in various applications, (ii) aid in the SLP engineering and (iii) help in the  
 5 design of improved labeling substrates.

6



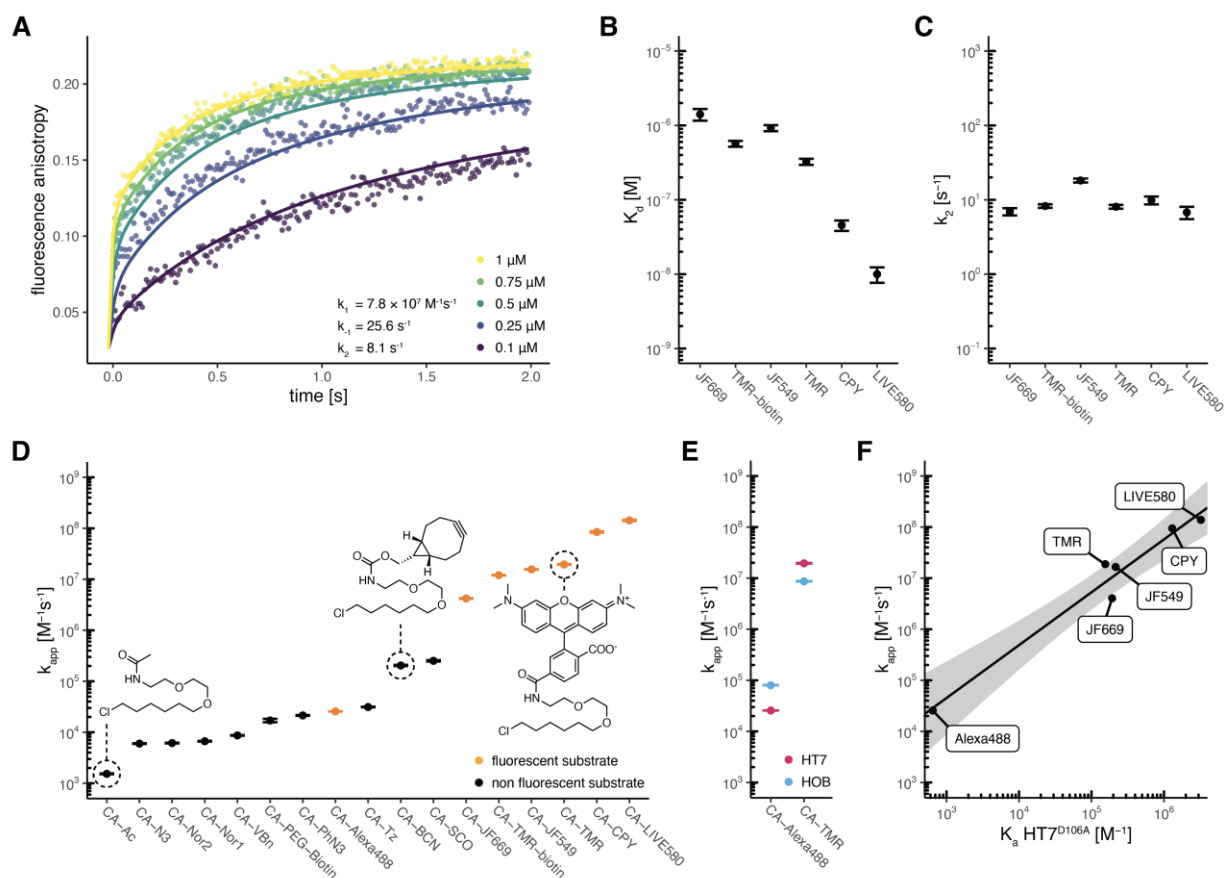
7

8 **Figure 1: Self-labeling reaction, substrates and kinetic models.**

9 **A.** Scheme of HT7 labeling reaction with fluorophore substrates. The chemical structure of HT7 substrates (CA) is  
 10 depicted below. R represents the functional moiety to be linked to HT7. **B.** Scheme of SNAP(f) / CLIP(f) labeling reaction  
 11 with fluorophore substrates. The chemical structures of SNAP/CLIP substrates (BG/CP/BC) are depicted below. R  
 12 represents the functional moiety to be linked to the SLP. **C.** Models employed to describe the SLP kinetics in this study.  
 13 **D.** Chemical structure of different SLP substrate substituents. Substrates are organized by their preferential use with  
 14 HT7 or SNAP.

## 1 **Results**

2 **HaloTag7 kinetic characterization.** Fluorophores represent the most popular class of labels em-  
3 ployed with SLPs. We characterized HT7 labeling kinetics with different CA-fluorophore sub-  
4 strates, namely CA-TMR, CA-JF549, CA-LIVE580, CA-CPY, CA-JF669 and CA-Alexa488 (**Fig.**  
5 **1D & S1**) by tracking fluorescence anisotropy change over time at different reactant concentra-  
6 tions. The very high labeling speed of HT7 towards most rhodamine-based CA substrates required  
7 a stopped-flow setup to precisely measure the labeling kinetics. Data were fitted to the kinetic  
8 model 2 (**Fig. 1C**), which described the reaction kinetics of most rhodamine-based HT7 substrates  
9 and allowed to determine the three kinetic parameters ( $k_1$ ,  $k_{-1}$  &  $k_2$ ) independently (**Fig. 2A-C, S2**  
10 **& Table S1**). Data fitted to the simplified model 1 resulted in a poorer fit, since curves show a clear  
11 biphasic character, indicating that model 2 should be preferred to describe these fast labeling  
12 kinetics (**Fig. S3**). It should be noted that fitting the data for the faster reacting substrates to model  
13 1 would lead to a significant overestimation of the labeling speed (**Fig. S4 & Table S2**). The slower  
14 labeling reaction with CA-Alexa488 allowed to perform measurements in a microplate reader.  
15 However, fitting model 2 to this data does not allow to determine the kinetic parameters ( $k_1$ ,  $k_{-1}$  &  
16  $k_2$ ) independently. Hence the data was fitted using the kinetic model 1 (**Fig. S5**). The kinetic model  
17 1 yields the apparent second-order rate constant  $k_{app}$  which describes the labeling reaction at  
18 reactant concentrations far below the  $K_d$  at which the substrate binding site is not saturated and  
19 the labeling rate depends linearly on the reactant concentrations. To compare the labeling rate  
20 constants of substrates analyzed through different kinetic models (**Fig. 2D & Table 1**),  $k_{app}$  can  
21 also be calculated from the individual rate constants obtained with kinetic model 2 (**Fig. 1C**).



1

2 **Figure 2: Characterization of HaloTag7 labeling kinetics.**

3 **A.** Fluorescence anisotropy traces (points) and fitted curves of HT7 labeling with CA-TMR in 1:1 stoichiometry at the  
 4 indicated concentrations. Kinetics were recorded by following fluorescence anisotropy over time using a stopped flow  
 5 device. Reactions were started by mixing equal volumes of HT7 and CA-TMR. Data were fitted to the kinetic model 2  
 6 (lines). **B.** HT7 affinities ( $K_d$ ) for different fluorophore substrates calculated from the kinetic parameters ( $k_{-1}/k_1$ ). **C.** HT7  
 7 reactivity ( $k_2$ ) for different fluorophore substrates obtained from fluorescence anisotropy kinetics. The minimal differ-  
 8 ences in  $k_2$  illustrate that labeling kinetics are mostly influenced by differences in  $K_d$ . **D.** Apparent second order labeling  
 9 rate constants ( $k_{app}$ ) of HT7 with different substrates. Rate constants span over six order of magnitude. Non-negatively  
 10 charged fluorophore substrates reach the fastest labeling kinetics. **E.** Comparison of  $k_{app}$  between HT7 and HOB for  
 11 CA-TMR and CA-Alexa488 labeling highlighting the preference of HOB for the negatively charged substrate CA-  
 12 Alexa488. **F.** Correlation between HT7 apparent second order rate constant ( $k_{app}$ ) and affinity ( $K_a = 1/K_d$ ) for different  
 13 fluorophore substrates. Affinities were obtained with the catalytically inactive variant HT7<sup>D106A</sup>. Log transformed values  
 14 were fitted to a linear model (black line,  $\log(k_{app}) = \log(K_a) \times 1.042 + 1.544$ ). The grey area represents the 95% confi-  
 15 dence bands (the area in which the true regression line lies with 95% confidence).

16

17 **HaloTag7 reaches fast kinetics with fluorophore substrates.** Among the tested fluorophore  
 18 substrates, CA-LIVE580 turned out to be the fastest substrate for HT7 with a  $k_{app}$  of  $1.39 \pm 0.03$   
 19  $\times 10^8 \text{ M}^{-1}\text{s}^{-1}$ , reaching an almost diffusion-limited labeling rate, and a calculated  $K_d$  ( $= k_{-1}/k_1$ ) of 9.99  
 20 nM (7.64 to 12.35 nM 95% CI). All other rhodamine-based substrates showed efficient labeling  
 21 kinetics as well ( $10^6 < k_{app} < 10^9 \text{ M}^{-1}\text{s}^{-1}$ ) with the exception of the negatively charged CA-Alexa488  
 22 ( $k_{app} = 2.57 \pm 0.01 \times 10^4 \text{ M}^{-1}\text{s}^{-1}$ ) (Table 1 & Fig. 2D). The HT7 variant HOB (halo-based oligonu-  
 23 cleotide binder) (18) features several positively charged surface mutations close to the substrate

1 binding site, which were introduced to increase the labeling rates with chloroalkanes attached to  
 2 oligonucleotides. We hypothesized that HOB may have increased labeling kinetics with the nega-  
 3 tively charged CA-Alexa488. Indeed, HOB shows a  $3.13 \pm 0.01$  fold increase in  $k_{app}$  compared to  
 4 HT7 with CA-Alexa488, while a decrease in  $k_{app}$  was observed with CA-TMR ( $2.09 \pm 0.01$  fold)  
 5 (**Fig. 1E, S5 & Table S3**). This suggests that kinetics of negatively charged substrates might suffer  
 6 from charge repulsions at the HT7 surface.

7

8 **Table 1:** Apparent labeling rate constants ( $k_{app}$ ) for different HT7, SNAP and CLIP substrates.

$k_{app}$  [ $M^{-1}s^{-1}$ ] (value | s.d.)

		Halo		SNAP		CLIP	
		CA		BG		CP	
		CA		BG		BC	
Fluorescent	Alexa488	$2.57 (\pm 0.01) \times 10^4$	$1.22 (\pm 0.01) \times 10^4$	$3.12 (\pm 0.01) \times 10^3$	$1.26 (\pm 0.01) \times 10^3$		
	Fluorescein	-	$1.17 (\pm 0.01) \times 10^5$	$*1.42 (\pm 0.01) \times 10^4$	$4.36 (\pm 0.01) \times 10^3$		
	JF669	$*4.03 (\pm 0.02) \times 10^6$	-	-	-		
	TMR-biotin	$*1.04 (\pm 0.01) \times 10^7$	-	-	-		
	JF549	$*1.66 (\pm 0.01) \times 10^7$	-	-	-		
	TMR	$*1.88 (\pm 0.01) \times 10^7$	$4.29 (\pm 0.01) \times 10^5$	$7.69 (\pm 0.01) \times 10^4$	$1.85 (\pm 0.01) \times 10^4$		
	CPY	$*9.44 (\pm 0.18) \times 10^7$	$2.17 (\pm 0.01) \times 10^5$	$*1.59 (\pm 0.01) \times 10^4$	$*2.65 (\pm 0.01) \times 10^4$		
	Live580	$*1.39 (\pm 0.03) \times 10^8$	-	-	-		
Non-fluorescent	Ac	$1.53 (\pm 0.02) \times 10^3$	$1.48 (\pm 0.05) \times 10^4$	$3.45 (\pm 0.38) \times 10^3$			
	-	-	$1.87 (\pm 0.05) \times 10^4$	$4.15 (\pm 0.62) \times 10^3$			
	N <sub>3</sub>	$6.00 (\pm 0.06) \times 10^3$	$3.70 (\pm 0.09) \times 10^4$	$6.36 (\pm 0.41) \times 10^3$			
	Nor2	$6.15 (\pm 0.07) \times 10^3$	-	-			
	Nor1	$6.68 (\pm 0.06) \times 10^3$	$7.34 (\pm 0.01) \times 10^4$	$1.77 (\pm 0.04) \times 10^4$			
	Vbn	$8.68 (\pm 0.07) \times 10^3$	$3.84 (\pm 0.07) \times 10^4$	$5.50 (\pm 0.45) \times 10^3$			
	PEG-biotin	$1.70 (\pm 0.08) \times 10^4$	-	-			
	PhN <sub>3</sub>	$2.14 (\pm 0.02) \times 10^4$	$4.78 (\pm 0.09) \times 10^4$	$2.91 (\pm 0.40) \times 10^3$			
	Tz	$3.13 (\pm 0.03) \times 10^4$	$3.94 (\pm 0.08) \times 10^4$	-			
	BCN	$2.04 (\pm 0.03) \times 10^5$	$3.88 (\pm 0.07) \times 10^4$	$3.34 (\pm 0.31) \times 10^3$			
	SCO	$2.52 (\pm 0.05) \times 10^5$	$3.75 (\pm 0.06) \times 10^4$	$4.22 (\pm 0.61) \times 10^3$			

9 Rate constants were obtained by fitting the data to kinetic model 1 or 2 (#). For some SNAP/CLIP substrates, a third  
 10 kinetic model was used which included a slow aging event of the labeled species (\*), see Table S5.

11  
 12 **HaloTag7 labeling kinetics correlate with substrate affinity.** For the substrates whose labeling  
 13 kinetics followed model 2, we observed that  $k_1$  and  $k_2$  values were rather constant among the  
 14 different HT7 fluorophore substrates, while larger differences were observed for the dissociation

1 rate constant  $k_{-1}$  (**Fig. S6 & Table S1**). The substrate preference of HT7 seems therefore mainly  
2 driven by the substrate affinity ( $K_d^{\text{kinetic}} = k_{-1}/k_1$ ) (**Fig. 2B**). After binding, the deeply buried CA moi-  
3 ety might adapt a similar conformation for all substrates, potentially explaining the minor effects of  
4 the substituent on the catalytic step ( $k_2$ ) (**Fig. 2C**). The trend observed for the  $K_d$  values calculated  
5 from the kinetic parameters was confirmed by measuring the affinity of the catalytically dead var-  
6 iant HT7<sup>D106A</sup> for the same CA-fluorophore substrates using fluorescence polarization (**Fig. S6F &**  
7 **S7**). The  $K_d^{\text{kinetic}}$  correlates with  $K_d^{\text{D106A}}$  (**Fig. S6E**) and as a consequence the association constant  
8  $K_a^{\text{D106A}}$  ( $= 1/K_d$ ) correlates with  $k_{\text{app}}$  (**Fig. 2F**). Hence, the  $K_a^{\text{D106A}}$  can be used to estimate the  $k_{\text{app}}$   
9 for fluorescent HT7 substrates.

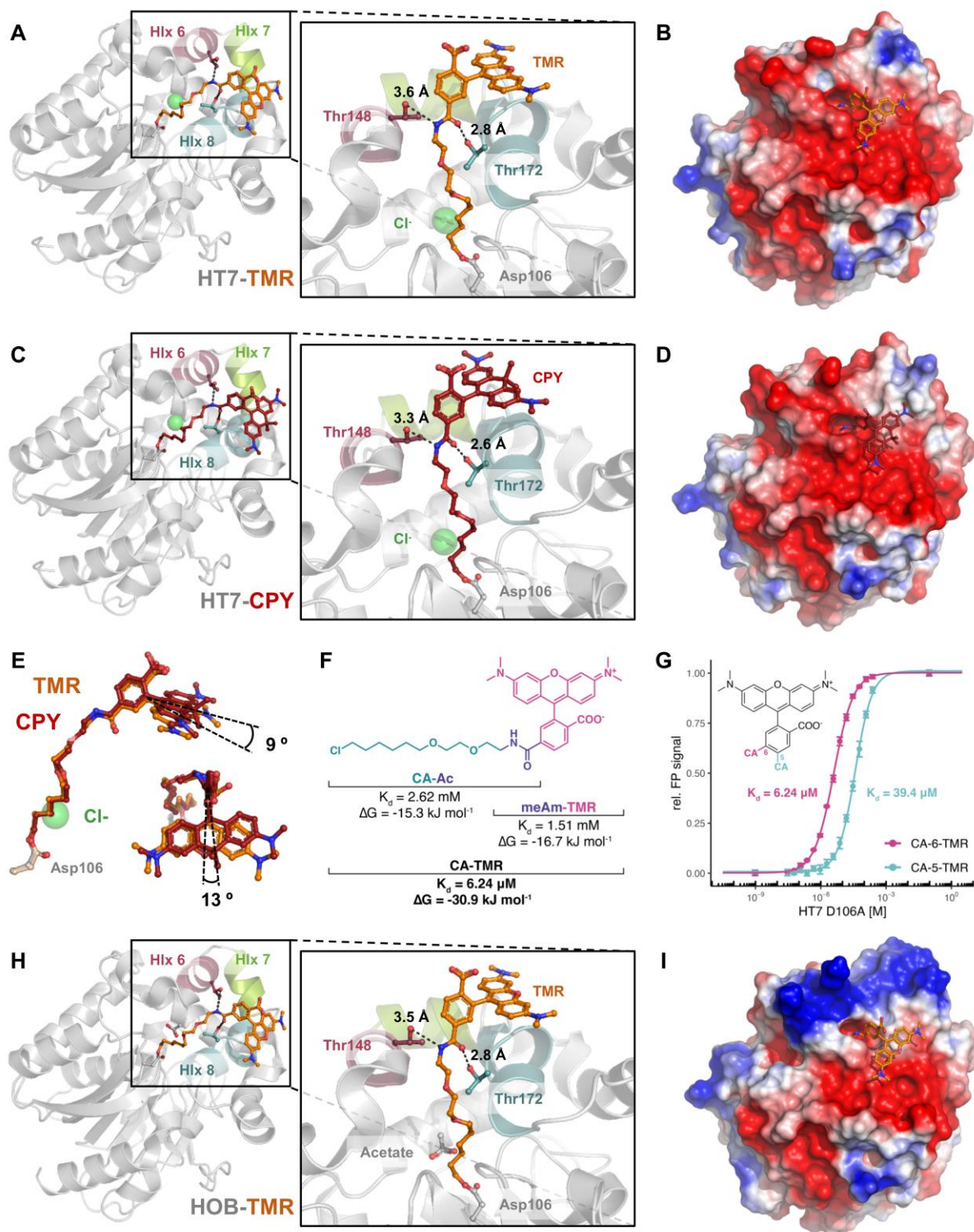
10  
11 ***HaloTag7 reacts slower with non-fluorophore substrates.*** In order to determine  $k_{\text{app}}$  for non-  
12 fluorescent CA substrates, we developed a competitive kinetic assay in which the non-fluorescent  
13 CA substrates compete with CA-Alexa488 for protein labeling. Non-fluorescent substrates were  
14 significantly slower than zwitterionic rhodamine substrates ( $10^3 < k_{\text{app}} < 10^6 \text{ M}^{-1}\text{s}^{-1}$ ), highlighting  
15 the strong preference of HT7 for the rhodamine core structure. Larger alkynes (e.g. SCO, BCN)  
16 and aromatic structures (e.g. Tz, PhN<sub>3</sub>, VBn) were preferred over alkenes (Nor) and small moieties  
17 (Ac, N<sub>3</sub>) (**Fig. 2D, S8 & Table 1**).

18  
19 ***HaloTag7 substrate design.*** Overall, HT7 can reach labeling kinetics near the diffusion limit but  
20 its apparent rate constants span over six orders of magnitude, depending on the nature of the  
21 label (**Fig. 2D**). HT7 exhibits a strong preference for rhodamine derivatives, with the exception of  
22 negatively charged rhodamines. It is noteworthy that the substrate with the slowest labeling rate  
23 carries the smallest label, i.e. an acetate group (CA-Ac). The preference for rhodamines can be  
24 exploited to increase labeling rates of poor substrates. As an example, the commercially available  
25 CA-PEG-biotin substrate presents slow reaction kinetics ( $k_{\text{app}} = 1.70 \pm 0.08 \times 10^4 \text{ M}^{-1}\text{s}^{-1}$ , **Table 1**  
26 **& Fig. S8**), but synthesizing a CA-TMR-biotin ligand led to an over 500 fold increase in labeling  
27 kinetics ( $k_{\text{app}} = 1.04 \pm 0.01 \times 10^7 \text{ M}^{-1}\text{s}^{-1}$ , **Table 1, S1 & Fig. S2**), greatly facilitating biotinylation of  
28 HT7 fusion proteins. This strategy to improve labeling rates of HT7 ligands should be applicable  
29 to various other labels.

30  
31 ***Structural analysis of rhodamine-bound HaloTag.*** In order to better understand the substrate  
32 preference of HT7 for rhodamine-based CA substrates, we solved the X-ray structure of TMR-  
33 (PDB ID 6Y7A) and CPY-bound HT7 (PDB ID 6Y7B) at 1.4 Å and 3.1 Å resolution, respectively  
34 (**Fig. 3A, 3C, S9 & Table S4**). Additionally, the TMR-bound structure of HOB was obtained at 1.5



1 Å resolution (PDB ID 6ZCC) (**Fig. 3H, S9 & Table S4**). These structures present the same  $\alpha/\beta$   
2 hydrolase fold of the superfamily with minimal deviation from already available HT7 X-ray struc-  
3 tures (19-22) (**Fig. S9C**). In addition to the conventional  $\alpha/\beta$  hydrolase topology, HT7 features an  
4 extra capping domain made of six  $\alpha$ -helices (Hlx4 to 9) which partially cover the catalytic site and  
5 form an entry channel for the CA substrate. After reaction, the PEG-alkane ligand is buried in the  
6 protein, while the xanthene moiety of the dye lays on the distorted  $\alpha$ -helix 8 (Hlx8) in a confor-  
7 mation partially constrained by the crystal packing (**Fig. 3A, 3C & S9D**). A recently published HT7-  
8 TMR X-ray structure (PDB ID 6U32) shows the fluorophore bound in two alternative conformations  
9 (23). In one conformation, the fluorophore lays on Hlx8 similar to what we report here and in the  
10 other, it lays on the Hlx7-turn-Hlx8 motif (**Fig. S10**). This second conformation is incompatible with  
11 our HT7-TMR structure due to steric clashes caused by the crystal packing. The alkane-fluoro-  
12 phore is positioned by the Hlx6-turn-Hlx7-turn-Hlx8 motif of the HT7 capping domain from which  
13 T172<sup>Hlx8</sup> and, to a lesser extent, T148<sup>Hlx6</sup> form hydrogen bonds with the oxygen and the nitrogen  
14 of the amide bond linking PEG-alkane and fluorophore (**Fig. 3A & 3C**). CA-TMR and CA-CPY  
15 have similar conformations in both structures (**Fig. S11A**) with only minor differences in their tor-  
16 sion angles (**Fig. 3E**). In comparison to TMR, one of the additional methyl groups of CPY is forming  
17 van-der-Waals interactions at the protein surface, potentially explaining the increased affinity of  
18 CA-CPY relative to CA-TMR.



1  
2 **Figure 3: Structure-function analysis of HaloTag7 substrate interactions.**

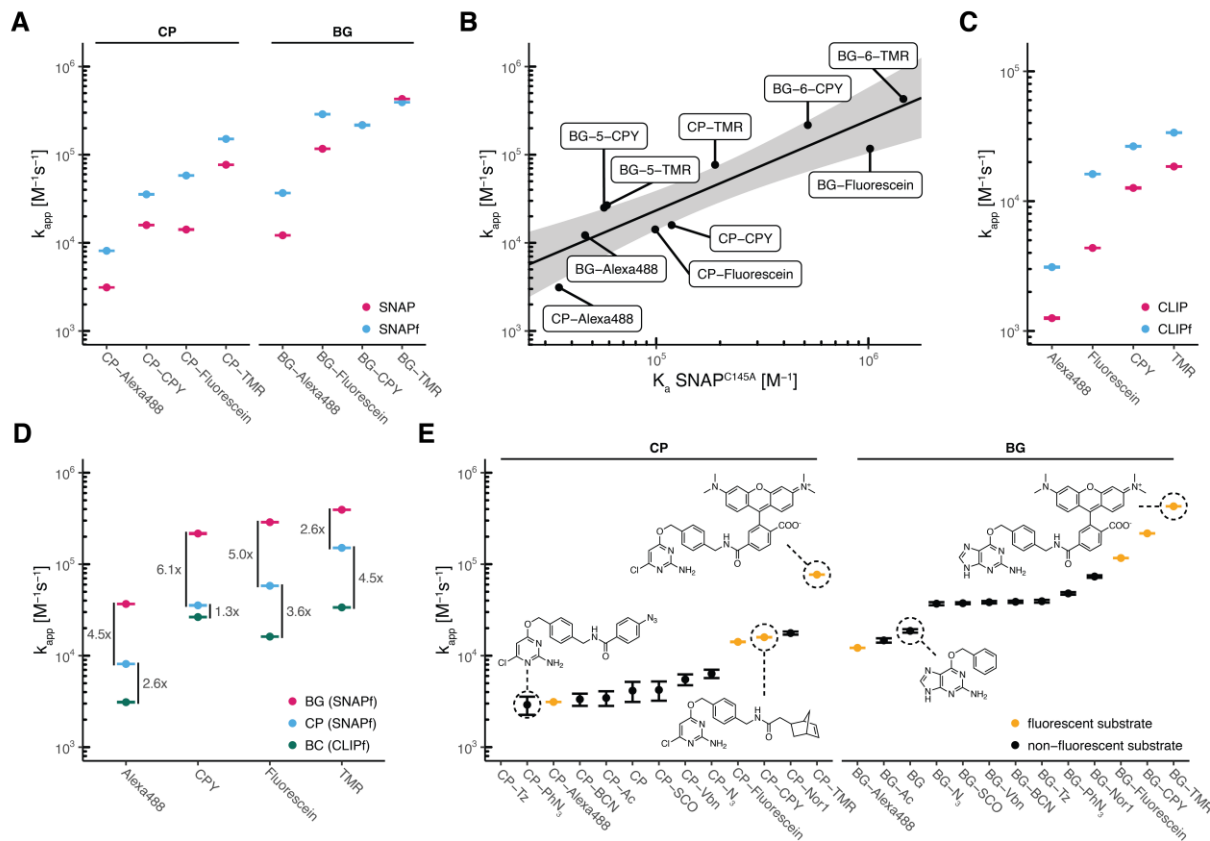
3 Crystal structures of HT7-TMR (PDB ID 6Y7A, **A**), HT7-CPY (PDB ID 6Y7B, chain A, **C**) and HOB-TMR (PDB ID 6ZCC,  
4 **H**). Proteins are represented as grey cartoons, the fluorophore substrates and residues as sticks. Putative hydrogen  
5 bonds are represented as black dashed lines with annotated distances. Electrostatic potentials at protein surfaces (**B**,  
6 **D** & **I**, respectively) are drawn at -2.0 (red) to 2.0 (blue) kJ/mol/e and were obtained using the APBS software with  
7 standard parameters. **E**. Comparison of the TMR and CPY conformation on HT7. **F**. HT7 affinities ( $K_d$ ) and free binding  
8 energies ( $\Delta G$ ) for different TMR substrate substructures. **G**. Comparison of HT7 affinity for CA-6-TMR and CA-5-TMR.

1 **Fluorophore and CA core contribute both to HaloTag7 substrate affinity.** To characterize the  
2 contributions of rhodamine structures and the CA core to the overall affinity of HT7 substrates, we  
3 measured affinities of the catalytically dead variant HT7<sup>D106A</sup> for the acetylated chloroalkane (CA-  
4 Ac) and *N*-methylamide-fluorophores (meAm-TMR/CPY). Although the acetylated chloroalkane  
5 should form hydrogen bonds to the protein (via T148/T172) and is well buried in the cavity, we  
6 observed a rather low affinity ( $K_d$ ) of 2.62 mM (2.44 to 2.72 mM CI 95%, **Fig. 3F & S12**), which is  
7 consistent with the low apparent labeling rate constant of CA-Ac (**Fig. 2D**). The protein binds the  
8 meAm-TMR fluorophore with a slightly higher affinity ( $K_d = 1.51$  mM, 1.40 to 1.64 mM CI 95%)  
9 (**Fig. 3F & S12**). The free binding energies for both fragments calculated from the  $K_d$  values (CA-  
10 Ac:  $-15.3$  kJ.mol<sup>-1</sup> and meAm-TMR:  $-16.7$  kJ.mol<sup>-1</sup>) are thus comparable and almost sum up to the  
11 calculated free binding energy of the full CA-TMR substrate ( $30.9$  kJ mol<sup>-1</sup>,  $K_d = 6.24$   $\mu$ M), *i.e.* no  
12 synergistic effect in binding is observed (24). Similar results were obtained for meAm-CPY (**Fig.**  
13 **S12**). The CA-fluorophore binding is thus driven by interactions with both the CA core and the  
14 fluorophore, explaining the high impact of fluorophore structure changes on the overall labeling  
15 kinetics.

16 The importance of substrate geometry was interrogated by synthesizing CA-fluorophore sub-  
17 strates linked via the 5 position of the rhodamine benzyl ring instead of the usual 6 position (**Fig.**  
18 **3G**). According to the observed conformations in the presented crystal structures, these 5-sub-  
19 strates should not be able to interact with Hlx8 after HT7 binding since the xanthene would be  
20 turned 60° away from the protein surface. HT7<sup>D106A</sup> showed reduced affinities towards these sub-  
21 strates compared to the 6-substituted rhodamine substrates (6.31 fold and 22.7 fold decrease for  
22 CA-TMR and CA-CPY, respectively) (**Fig. 3G**). This result emphasizes the importance of the in-  
23 teraction between the xanthene ring and the Hlx8.

24  
25 **HaloTag7 surface charge impacts substrate recognition.** HOB comprises four surface muta-  
26 tions compared to HT7 close to the substrate entry channel but opposite to the TMR binding site  
27 (**Fig. S11B**). These mutations lead to faster labeling rates with negatively charged CA substrates  
28 relative to HT7. Only minor differences can be observed between the crystal structures of HOB  
29 and HT7 labeled with CA-TMR (**Fig. 3H & S11B**). Since the HOB mutations replace mostly neg-  
30 ative by positively charged residues, we analyzed the electrostatic potential of both proteins. While  
31 HT7 features an overall negatively charged surface around the substrate entry channel (**Fig. 3B**  
32 **& 3D**), HOB shows a positively charged patch opposite to the fluorophore binding site (**Fig. 3I**).  
33 Hence, a putative electrostatic steering effect (25) could explain the altered substrate preference  
34 of HOB despite that its positive charges are on the opposite side of the fluorophore binding site.

1 **Kinetic characterization of SNAP-tag.** SNAP labeling kinetics were characterized for both BG-  
2 and CP-fluorophore substrates (*i.e.* TMR, CPY, Alexa488 and Fluorescein) (**Fig. 1D & S1**), by  
3 following fluorescence polarization changes during the labeling reaction at different protein con-  
4 centrations in a plate reader assay. The kinetic model 2 did not allow to determine the kinetic  
5 parameters ( $k_1$ ,  $k_{-1}$  &  $k_2$ ) independently. Hence, data were fitted to model 1 in order to obtain  
6 apparent second order rate constants ( $k_{app}$ ) of the labeling reactions (**Table 1 & Fig. S13**). SNAP's  
7 apparent labeling rate constants are ranging between  $10^4$  and  $10^6$   $M^{-1}s^{-1}$  for BG-fluorophore sub-  
8 strates (**Fig. 4A**), among which BG-TMR presents the fastest labeling rate ( $k_{app} = 4.29 \pm 0.01 \times$   
9  $10^5$   $M^{-1}s^{-1}$ ) (**Table 1**). CP substrates show 4 – 14 times slower reaction kinetics than the corre-  
10 sponding BG substrates ( $10^3 < k_{app} < 10^5$   $M^{-1}s^{-1}$ ) (**Fig. 4A**). Some CP substrates (CPY and Fluor-  
11 escein) exhibit a slow additional phase of fluorescence polarization increase or decrease after  
12 labeling that might be due to a slow conformational change of the labeled protein. In order to fit  
13 these traces, the kinetic model 1 was extended by adding a step that occurs after labeling. The  
14 rate constants of this additional process ( $k_3$ ) ranged between  $10^{-2}$  and  $10^{-3}$   $s^{-1}$  (**Fig. S13 & Table**  
15 **S5**). SNAP labeling with BG-TMR and CP-TMR was further investigated by measuring stopped  
16 flow fluorescence anisotropy kinetics at higher protein concentrations (**Fig. S14 & Table S6**). Fit-  
17 ting the data to the kinetic model 2 allowed to estimate the kinetic parameters  $k_1$ ,  $k_{-1}$  and  $k_2$  inde-  
18 pendently and to calculate  $K_d$  values (**Fig. S14C**). The calculated  $k_{app}$  for both substrates were  
19 similar to the  $k_{app}$  determined via the plate reader assay using model 1 (**Fig. S14C**). CP-TMR  
20 presents similar  $k_1$  and  $k_2$  as BG-TMR, while  $k_{-1}$  is significantly higher for CP-TMR (8.8 fold), indi-  
21 cating that both substrates feature the same chemical reactivity but differ in their affinity towards  
22 SNAP.



1  
2 **Figure 4: Characterization of SNAP- and CLIP-tag labeling kinetics.**  
3 **A.** Comparison of labeling kinetics ( $k_{app}$ ) between SNAP and SNAPf. **B.** Correlation between SNAP apparent second  
4 order rate constant ( $k_{app}$ ) and affinity ( $K_a = 1/K_d$ ) for different fluorophore substrates. Affinities were obtained for the  
5 catalytically inactive variant  $SNAP^{C145A}$ . Log transformed values were fitted to a linear model (black line,  $\log(k_{app}) =$   
6  $\log(K_a) * 1.0217 - 0.7407$ ). The grey area represents the 95% confidence bands (the area in which the true regression  
7 line lies with 95% confidence). **C.** Comparison of labeling kinetics ( $k_{app}$ ) between CLIP and CLIPf. **D.** Comparison of  
8 labeling kinetics ( $k_{app}$ ) between SNAPf and CLIPf. **E.** Apparent second order labeling rate constants ( $k_{app}$ ) of SNAP with  
9 different substrates. Kinetics span over three orders of magnitude (two orders of magnitude within each substrate class  
10 BG/CP). BG-based, non-negatively charged fluorophore substrates reach the fastest labeling kinetics.

11  
12 **SNAP-tag labeling kinetics correlate with substrate affinity.** To confirm the previous finding,  
13 affinities for different fluorescent substrates were measured using the catalytically inactive mutant  
14  $SNAP^{C145A}$  (**Fig. S15**). A strong preference for BG-TMR over CP-TMR was observed with almost  
15 one order of magnitude difference in  $K_d^{C145A}$ .  $SNAP^{C145A}$  presents a 3 fold lower  $K_d^{C145A}$  for BG-  
16 TMR (0.68  $\mu$ M; 0.63 to 0.75  $\mu$ M CI 95%) than calculated from stopped-flow experiments using  
17 active SNAP.  $SNAP^{C145A}$  showed similar affinities as for BG-TMR towards various xanthene-based  
18 fluorophores such as BG-MaP555, BG-JF549 and BG-fluorescein (**Fig. S15**), indicating that mod-  
19 ifications of the rhodamine structure seem not to affect the affinity of the protein as much as ob-  
20 served for HT7 substrates. However,  $SNAP^{C145A}$  has very low affinity for sulfonated fluorophore  
21 substrates such as BG-Alexa488 (21.6  $\mu$ M; 20.5 to 22.9  $\mu$ M CI 95%) or BG-sulfo-Cy3/5 (Cy3, 68.1

1  $\mu\text{M}$ ; 63.8 to 72.7  $\mu\text{M}$  CI 95%) (**Fig. S15**). A good correlation between  $K_d^{C145A}$  and  $k_{\text{app}}$  was observed  
2 for the tested fluorophore substrates (**Fig. 4B**), highlighting again the importance of high affinity  
3 for a quick labeling reaction. As for HT7, we attempt to decipher SNAP substrate recognition by  
4 measuring its affinity towards BG-Ac and meAm-TMR. While no affinity could be measured for  
5 meAm-TMR, SNAP<sup>C145A</sup> presented a relatively high affinity for BG-Ac (88.0  $\mu\text{M}$ ; 88.6 to 91.5  $\mu\text{M}$   
6 CI 95%) and CP-Ac (201  $\mu\text{M}$ ; 192 to 212  $\mu\text{M}$  CI 95%) compared to HT7 affinity for CA-Ac (**Fig.**  
7 **S16**), which could explain the promiscuity of SNAP.

8  
9 **Kinetic characterization of CLIP-tag and SNAP-tag variants.** The mutant SNAPf (SNAP<sup>E30R</sup>) is  
10 a SNAP variant with faster labeling rates for BG-Alexa488, BG-TMR, BG-Atto549 and BG-  
11 AlexaFluor647 (26) (**Fig. 4A, Fig. S17**). Fluorescence polarization kinetics of SNAPf revealed a 2  
12 to 4 fold  $k_{\text{app}}$  increase compared to SNAP for most BG- and CP-fluorophore substrates (**Fig. 4A,**  
13 **S7, S18 & Table S7**). Nevertheless, no increase in labeling kinetics was observed for the best  
14 SNAP substrates BG-TMR and BG-CPY (**Fig. 4A**). CLIP (11) and CLIPf (CLIP<sup>E30R</sup>) (26) are or-  
15 thogonal variants of SNAP accepting BC instead of BG substrates (**Fig. S17**). Labeling kinetics of  
16 CLIP and CLIPf (**Table S7 & Fig. S19**) yielded apparent second order rate constants ( $k_{\text{app}}$ ) ranging  
17 from  $10^3$  to  $10^5 \text{ M}^{-1}\text{s}^{-1}$  with a 2 to 4 fold increase for CLIPf compared to CLIP (**Fig. 4C**). The fastest  
18 labeling kinetics were achieved with CLIPf and BC-TMR showing a  $k_{\text{app}}$  of  $3.37 \pm 0.01 \times 10^4 \text{ M}^{-1}\text{s}^{-1}$   
19 <sup>1</sup>. However, CLIPf is significantly slower than SNAPf (**Fig. 4D**).

20  
21 **Cross-reactivity of SNAP- and CLIP-tag substrates.** SNAP and CLIP originate from hAGT (10,  
22 11) (**Fig. S17**), which can potentially react with SNAP and CLIP substrates. We therefore meas-  
23 ured the labeling activity of hAGT for the corresponding TMR-based substrates (**Fig. S20**). BG/CP-  
24 TMR labeling of hAGT is 130 / 20 times slower than the labeling of SNAP ( $k_{\text{app}}^{\text{BG-TMR}} = 3.38 \pm 0.01$   
25  $\times 10^3 \text{ M}^{-1}\text{s}^{-1}$ ;  $k_{\text{app}}^{\text{CP-TMR}} = 3.13 \pm 0.01 \times 10^3 \text{ M}^{-1}\text{s}^{-1}$ ) (**Table 2**). Interestingly, hAGT shows no preference  
26 for BG over CP substrates. BC-TMR reaction with hAGT is 25'000 times slower than with CLIP  
27 ( $k_{\text{app}} = 0.70 \pm 0.01 \text{ M}^{-1}\text{s}^{-1}$ ) (**Table 2**). Our results suggest that CLIP should be preferred over SNAP  
28 in cases where cross-reactivity of substrates with endogenous hAGT is a concern.

29 CLIP development was motivated by the perspective to use both SLPs together for multicolor  
30 labeling. However, the cross-reactivities of the fastest reacting SNAP and CLIP rhodamine sub-  
31 strates have not yet been determined. Hence, we measured cross-reactivity of BG/CP-TMR with  
32 CLIP and BC-TMR with SNAP (**Table 2**). SNAP reacts more than 1000 times slower with BC-TMR  
33 (SNAP  $k_{\text{app}}^{\text{BC-TMR}} = 3.20 \pm 0.02 \times 10^2 \text{ M}^{-1}\text{s}^{-1}$ ) than with BG-TMR despite the noticeable affinity of

1 SNAP<sup>C145A</sup> for BC-Ac (416  $\mu\text{M}$ , 408 to 421  $\mu\text{M}$  CI 95%) which is only 5 times lower than for BG-Ac  
2 (**Fig. S16**). On the other hand, CLIP reacts 100 times slower with BG-TMR (CLIP  $k_{\text{app}}^{\text{BG-TMR}} = 8.26$   
3  $\pm 0.05 \times 10^1 \text{ M}^{-1}\text{s}^{-1}$ ) than with BC-TMR. These data are in agreement with values previously re-  
4 ported for fluorescein substrates (11). Since both proteins show residual reactivity towards their  
5 non-respective substrates, simultaneous co-labeling of both proteins or prior SNAP labeling is  
6 advisable to minimize cross-reactions.

7

8 **Table 2:** Labeling kinetics ( $k_{\text{app}}$ ) of hAGT, SNAP and CLIP with TMR substrates.

		$k_{\text{app}} [\text{M}^{-1}\text{s}^{-1}]$ (value   s.d.)		
		hAGT	SNAP	CLIP
BG-TMR		$3.38 (\pm 0.01) \times 10^3$	$4.29 (\pm 0.01) \times 10^5$	$8.26 (\pm 0.05) \times 10^1$
CP-TMR		$3.13 (\pm 0.01) \times 10^3$	$7.69 (\pm 0.01) \times 10^4$	$7.22 (\pm 0.04) \times 10^0$
BC-TMR		$6.25 (\pm 0.01) \times 10^{-1}$	$3.20 (\pm 0.02) \times 10^2$	$1.85 (\pm 0.01) \times 10^4$

9

10 **SNAP-tag is a promiscuous SLP.** Labeling kinetics of non-fluorescent SNAP substrates were  
11 characterized by competition kinetics against BG-Alexa488 (**Fig. S21**). Non-fluorescent BG sub-  
12 strates ( $10^4 < k_{\text{app}} < 10^5 \text{ M}^{-1}\text{s}^{-1}$ ) were preferred over CP substrates ( $10^3 < k_{\text{app}} < 10^4 \text{ M}^{-1}\text{s}^{-1}$ ) (**Fig. 4E**  
13 **& Table 1**). In general, SNAP kinetics with non-fluorescent substrates were slower than with fluo-  
14 rescent substrates with the exception of the negatively charged Alexa488. However, in compari-  
15 son to HT7, the labeling rates of SNAP show much less dependence on the nature of the label  
16 (**Fig. 4E & Table 1**).

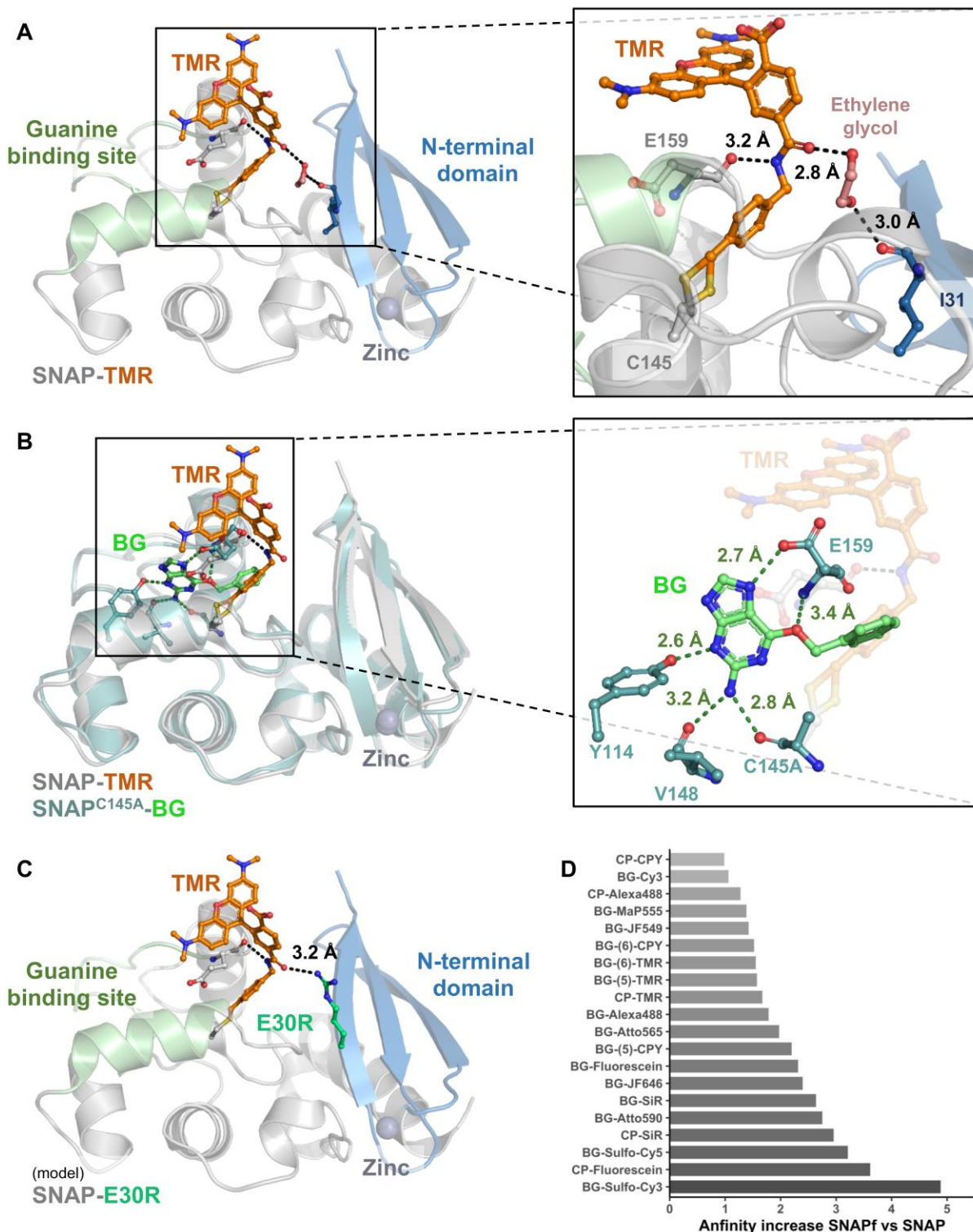
17

18 **Structural analysis of TMR-bound SNAP-tag.** To better understand the preference of SNAP for  
19 TMR substrates, the X-ray structure of SNAP labeled with TMR was solved at 2.3 Å resolution  
20 (PDB ID 6Y8P) (**Fig. 5A, S22 & Table S4**). The structure shows the same  $\alpha/\beta$  topology with two  
21 domains as observed for hAGT and other SNAP structures (27, 28). The active site is very similar  
22 to the benzylated SNAP structure (PDB ID 3L00) (28), despite the presence of an alternative cys-  
23 teine conformation (**Fig. S22C**). The TMR moiety strongly participates in the crystal packing, en-  
24 gaging in interactions with the neighboring xanthene ring and protein in a sandwich-like topology  
25 (**Fig. S22D**). As a consequence, and in contrast to HT7-TMR, SNAP does not interact with the  
26 bound fluorophore in the present X-ray structure.

27 We next evaluated the relative preference for 6- versus 5-carboxy isomers of TMR and CPY sub-  
28 strates by studying their labeling rates (**Fig. S23 & Table S8**) and affinities (**Fig. S15**) for SNAP,  
29 SNAPf and their dead variants. SNAP and SNAPf showed 10 times slower reaction rates with 5-

1 fluorophores ( $k_{app} \approx 10^4 - 10^5 \text{ M}^{-1}\text{s}^{-1}$ ) compared to the corresponding 6-fluorophores ( $k_{app} \geq 10^5 \text{ M}^{-1}\text{s}^{-1}$ ). These differences were even more pronounced for the affinities, which were up to 25 fold  
2  
3 higher for the 6-carboxy isomers.  
4 In the crystal structure of TMR-labeled SNAP, a structural ethylene glycol forms hydrogen bonds  
5 with both the backbone carbonyl oxygen of I31 and the carbonyl oxygen of the amide linking the  
6 benzyl to the fluorophore (**Fig. 5A**). This benzyl-fluorophore amide is also forming a hydrogen  
7 bond to the backbone carbonyl oxygen of the catalytically important E159 residue via its  $N\alpha$  atom.  
8 Comparison with the BG-bound SNAP<sup>C145A</sup> structure (PDB ID 3KZZ, **Fig. 5B**) suggests that, after  
9 catalytic reaction, the E159 side chain flips inside the BG binding cavity, resulting in a reorientation  
10 of its backbone carbonyl oxygen that can then interact with the amide of the substrate (**Fig. 5B**).





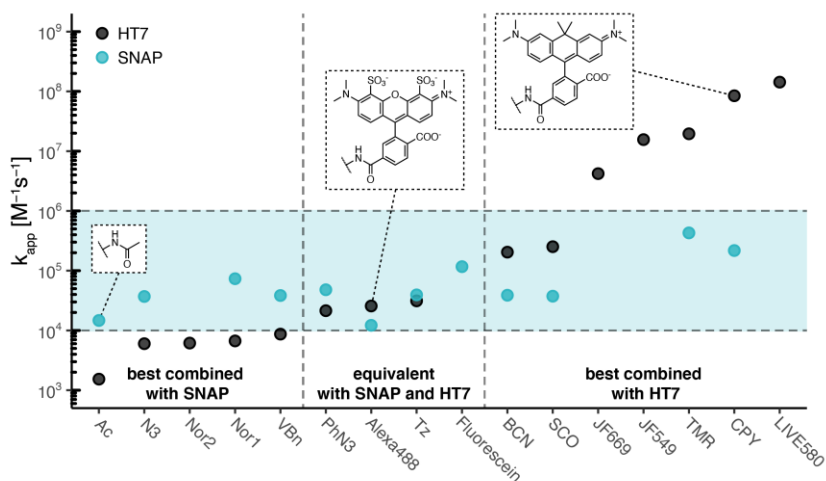
1  
2 **Figure 5:** Structure-function analysis of SNAP-tag fluorophore substrate interactions.  
3 **A.** Crystal structure of SNAP labeled with a TMR substrate. **B.** Structural comparison between SNAP-TMR and the BG  
4 bound variant of SNAP<sup>C145A</sup>. **C.** Modeling of the E30R mutation in the SNAP-TMR crystal structure. SNAP is represented  
5 as cartoon, the fluorophore substrate and residues as sticks. Putative hydrogen bonds and corresponding distances  
6 are indicated by black dashes. **D.** Affinity increase between SNAP<sup>C145A</sup> and SNAP<sup>fC145A</sup> for different fluorophore sub-  
7 strates. Number in brackets indicate different linkage of the fluorophore benzyl group to BG.

1 **SNAPf has a higher affinity for its substrates.** We modeled the SNAPf mutation E30R in the  
2 structure of TMR-labeled SNAP to gain a better understanding of how it affects the labeling kinet-  
3 ics (**Fig. 5C**). Results suggest that an arginine in position 30 could interact with the carbonyl oxy-  
4 gen of the amide group in the label via a moderate hydrogen bond (3.2 Å), replacing the hydrogen  
5 bond observed with the ethylene glycol in the crystal structure. This could lead to an increased  
6 affinity for the substrate or a better substrate positioning resulting in a quicker labeling. To probe  
7 this hypothesis, the affinities of SNAP<sup>C145A</sup> and SNAPf<sup>C145A</sup> were compared side by side for various  
8 fluorophore substrates (**Fig S16**). Among the 21 fluorophore substrates tested, only five did not  
9 show a significant increase in affinity (*i.e.* above 50%) and nine showed more than a 2 fold affinity  
10 increase (**Fig. 5D**). As observed for SNAP, SNAPf<sup>C145A</sup> substrate affinities correlate well with the  
11 corresponding  $k_{app}$  values for SNAPf (**Fig. S24**). It is noteworthy to mention that negatively charged  
12 substrates such as BG-sulfo-Cy3 show the strongest increase in the protein affinities and labeling  
13 rates when comparing SNAP to SNAPf. This could be due to the exchange of the negatively  
14 charged glutamic acid by a positively charged arginine resulting in a potential electrostatic steering  
15 effect as mentioned for HT7 (25).

16  
17 **Comparison between SNAP-tag and SsOGT-H<sup>5</sup>.** Recently, an homologue of hAGT from an ex-  
18 tremophile archaea was converted to an SLP (SsOGT-H<sup>5</sup>) by introducing mutations that have  
19 been shown to increase the reactivity of SNAP (29). Its crystal structure labeled with SNAP-Vista  
20 Green<sup>®</sup> (SVG, *i.e.* BG-5-fluorescein) (30) shows a different fluorophore conformation, constrained  
21 by the crystal packing (**Fig. S25**). Interestingly, the SsOGT-H<sup>5</sup>-SVG structure was obtained with a  
22 fluorophore connected via the 5-carboxy isomer of the fluorophore and presents a substrate con-  
23 formation that could not exist in the SNAP structure due to steric clashes (**Fig. S25A**). We com-  
24 pared the kinetics of SNAP and SsOGT-H<sup>5</sup> (**Fig. S26 & Table S9**) toward the substrates BG-TMR  
25 (5- and 6-substituted) and BG-6-Alexa488 at 37°C. In contrast to SNAP, SsOGT-H<sup>5</sup> showed a  
26 preference for BG-5-TMR ( $k_{app} = 1.45 \pm 0.92 \times 10^2 \text{ M}^{-1}\text{s}^{-1}$ ) over BG-6-TMR ( $k_{app} = 6.78 \pm 0.67 \times$   
27  $10^1 \text{ M}^{-1}\text{s}^{-1}$ ). Furthermore, the negatively charged BG-6-Alexa488 ( $k_{app} = 1.24 \pm 0.01 \times 10^2 \text{ M}^{-1}\text{s}^{-1}$ )  
28 presents kinetics in the same range as BG-5-TMR, highlighting a different substrate preference  
29 between SNAP and SsOGT-H<sup>5</sup>. For all substrates, SsOGT-H<sup>5</sup> presents kinetics 100 times slower  
30 than SNAP or CLIP, making it less suitable for labeling applications at physiological temperatures.

## 1 **Discussion**

2 We provide here a systematic comparison of the labeling kinetics of HT7, SNAP and CLIP towards  
3 a large panel of substrates. A structure-function relationship analysis complements this compari-  
4 son, thereby yielding insights into the origins of the different substrate specificities of HT7 and  
5 SNAP. The data should assist scientists in choosing SLP-substrate pairs for specific purposes.



6  
7 **Figure 6:** Labeling kinetics comparison between SNAP-tag and HaloTag7.  
8 Apparent labeling rate constants ( $k_{app}$ ) of HT7 span over six orders of magnitude while rate constants of SNAP span  
9 only over two orders of magnitude (BG-substrates). The blue area highlights the span of SNAP apparent labeling rate  
10 constants. Depending on the application, some substrates should preferentially be employed with HT7 or SNAP to  
11 ensure quick labeling.

12 The direct comparison of SNAP and HT7 reveals that HT7 features significantly higher labeling  
13 rates with various fluorescent rhodamine derivatives (**Fig 6 & Table 1**). These differences in re-  
14 activity can be explained by specific interactions of the rhodamine's xantheno ring with selected  
15 surface residues of HT7. The high reactivity of HT7 towards rhodamines is important as rhoda-  
16 mines up to now represent the most relevant class of cell-permeable fluorophores for live-cell  
17 imaging. The interactions between rhodamines and HT7 also help to explain why some rhoda-  
18 mine-based HT7 substrates tend to have improved spectroscopic properties and are more fluoro-  
19 genic than the corresponding SNAP or CLIP substrates (16). Most rhodamine-based fluorophores  
20 exist in an equilibrium between spirocyclic non-fluorescent and zwitterionic fluorescent forms.  
21 While in solution the spirocyclic form might be favored, labeling reaction with an SLP switches this  
22 equilibrium toward the zwitterionic form, leading to a fluorescence intensity increase (31). This  
23 property is of particular interest in wash-free live-cell fluorescence microscopy since it leads to  
24 higher signal over background (26, 32-35) and can also be exploited for sensor design (23, 36).  
25 Furthermore, the dynamic equilibrium between the spirocyclic non-fluorescent and zwitterionic  
26 fluorescent form is crucial for cell permeability (33). The mechanism underlying the equilibrium

1 shift from the spirocyclic non-fluorescent to the zwitterionic fluorescent form is not fully understood  
2 yet but our results indicate that the planar, zwitterionic form of rhodamines (e.g. TMR and CPY)  
3 features energetically favorable interactions with HT7 surface, thus potentially favoring this state  
4 of the fluorophore when labeled to the protein.

5 While HT7 reacts quicker with most rhodamine-based fluorophore substrates than SNAP, the dif-  
6 ferences become much less pronounced or reversed for negatively charged substrates. For ex-  
7 ample, SNAP reacts faster with Alexa488 than HT7 and the reactivity for most other non-fluores-  
8 cent substrates tends to be higher for SNAP as well (**Fig 6 & Table 1**). It is interesting to hypoth-  
9 esize about the origin of the substrate specificity differences between SNAP and HT7. Most likely,  
10 these differences are, at a least partially, a consequence of the substrates used in the engineering  
11 of the tags. For HT7, TMR was used in most screening assays (9, 13) and, as a result, HT7 shows  
12 a specificity for zwitterionic rhodamines. In contrast, different substrates such as BG-fluorescein  
13 (37), BG-Cy3 (38) as well as affinity reagents such as BG-biotin (37) were used in SNAP screening  
14 and selection assays. As a consequence, SNAP is more promiscuous than HT7. Differences in  
15 labeling speed of both SLPs are mostly driven by differences in substrate affinity: an overall cor-  
16 relation between affinity and rate constants was observed for both proteins that was more pro-  
17 nounced for HT7. Indeed, HT7 presents a very low affinity toward the e.g. unsubstituted CA-Ac  
18 substrate highlighting that HT7 affinity toward substrates is highly driven by the substituent and so  
19 are the kinetics. We show here how the low reactivity of HT7, for example towards CA-PEG-biotin,  
20 can be overcome by designing substrates in which the label of interest is attached to a CA-TMR  
21 core and anticipate that such strategy could be expanded to other substituents.

22 A key property of SLP substrates for live-cell applications that we have not addressed in this study  
23 is their cell permeability. Generally speaking, the CA core is less polar than BG, CP and BC. The  
24 permeability of HT7 substrates therefore can be expected to be higher than the corresponding  
25 SNAP-tag substrates. However, this question will have to be more systematically addressed in  
26 future studies.

27 For future engineering of SLPs, it would be particularly interesting to increase the affinity of SNAP  
28 and CLIP towards rhodamine-based substrates. Given the importance of these fluorophores for  
29 live-cell fluorescence (super-resolution) microscopy (1), additional tags that display labeling kinet-  
30 ics towards rhodamines similar to those of HT7 would be highly welcomed. Our results suggest  
31 that increasing the reactivity towards these dyes might come with the risk of reducing the activity

- 1 towards other substrates, thereby limiting the flexibility of such tags. However, given the im-
- 2 portance of SLPs and rhodamine-based probes for live-cell imaging, the generation of such spe-
- 3 cialized tags is warranted.

## 1 **Materials and Methods**

2 **Labeling substrates and chemical synthesis.** Labeling substrates for HaloTag, SNAP-tag and  
3 CLIP-tag were synthesized according to literature procedures (10, 11, 15, 32-34, 39-45); pur-  
4 chased from Promega Corp. (Madison, WI, USA), Abberior GmbH (Göttingen, Germany), Santa  
5 Cruz Biotechnology Inc. (Dallas, TX, USA) and NEB Inc. (Ipswich, MA, USA); were kind gifts from  
6 Dr. L. Lavis (Janelia research campus, USA) and Dr. A.D.N. Butkevich (MPI for Medical Research,  
7 Germany) or were synthesized according to the procedure available in the supplementary infor-  
8 mation.

9 **Cloning, protein expression and purification.** SNAP, SNAPf, SNAP<sup>ox</sup>, CLIP, CLIPf, HT7 and  
10 HOB were cloned in a pET51b(+) vector (Novagen) for production in *Escherichia coli*, featuring an  
11 N-terminal His<sub>10</sub> tag and a Tobacco Etch Virus (TEV) cleavage site. SsOGT-H<sup>5</sup> and hAGT were  
12 cloned in the same plasmid featuring an N-terminal StrepTag-II and an enterokinase cleavage site  
13 together with a C-terminal His<sub>10</sub> tag. Cloning was performed by Gibson assembly (46) using E.cloni  
14 10G cells (Lucigen) and point mutations were performed using the Q5 site-directed mutagenesis  
15 kit (NEB). Proteins were expressed in *E. coli* strain BL21(DE3)-pLysS (Novagen). Lysogeny broth  
16 (LB) (47) cultures were grown at 37°C to optical density at 600 nm (OD<sub>600nm</sub>) of 0.8. Transgene  
17 expression was induced by the addition of 0.5 mM isopropyl-β-D-thiogalactopyranoside (IPTG)  
18 and cells were grown at 17°C overnight in the presence of 1 mM MgCl<sub>2</sub>. Cells were harvested by  
19 centrifugation and lysed by sonication.

20 For N-terminally His-tagged proteins, the cell lysate was cleared by centrifugation (75 000g, 4° C,  
21 10 min) before affinity-tag purification using a HisTrap FF crude column (Cytiva, Marlborough, MA,  
22 USA) and an ÄktaPure FPLC (Cytiva). Buffer was exchanged using a HiPrep 26/10 Desalting  
23 column (Cytiva) to HEPES 50 mM, NaCl 50 mM pH 7.3 (*i.e.* activity buffer). Proteins were con-  
24 centrated using Ultra-15 mL centrifugal filter devices (Amicon, Merck KGaA, Darmstadt, Germany)  
25 with a molecular weight cut-off (MWCO) smaller than the protein size to a final concentration of  
26 500 μM. Proteins were aliquoted and stored at -80°C after flash freezing in liquid nitrogen. Double-  
27 tagged proteins, after similar cell lysis and clearing, were purified using HisPur Ni-NTA Superflow  
28 Agarose (Thermo Fisher Scientific, Waltham, MA, USA) by batch incubation followed by washing  
29 and elution steps on a polypropylene column (Qiagen). Proteins were subsequently purified using  
30 a StrepTrap HP column (Cytiva) on an ÄktaPure FPLC. Proteins were then concentrated using  
31 Ultra-5 mL centrifugal filter devices with a MWCO smaller than the protein size and conserved in  
32 glycerol 45 % (w/v) at -20°C.

1 Correct size and purity of proteins were assessed by SDS-PAGE and liquid chromatography-mass  
2 spectrometry (LC-MS) analysis.

3 **Affinity of HT7 and HOB towards CA substrates.** Binding affinities of HT7<sup>D106A</sup> or HOB<sup>D106A</sup> to  
4 chloroalkane (CA) substrates were determined by fluorescence polarization (FP, equation 1)  
5 measurements using a microplate reader (Spark20M®, Tecan Group AG, Männedorf, Switzer-  
6 land). The fluorescent substrates (10 nM) were titrated against different protein concentrations  
7 (0 – 250 μM) in activity buffer supplemented with 0.5 g/L BSA. Assays were performed in black  
8 low-volume non-binding 384-well plates (Corning Inc., Corning, NY, USA) with a final volume of  
9 20 μL. All measurements were performed in triplicates at 37°C, filter settings are listed in **Table 3**.  
10 Obtained FP values were averaged and fitted to a single site binding model (equation 2) to esti-  
11 mate  $K_d$  values for each fluorescent substrate. The FP value of each dye fully reacted with the  
12 native HT7 was used to improve fitting of the curves upper plateau by adding an extra data point  
13 at protein concentration of 0.1 M.

14 
$$FP = \frac{I_{\parallel} - I_{\perp} * G}{I_{\parallel} + I_{\perp} * G} \quad (1)$$

15 with FP: fluorescence polarization,  $I_{\parallel}$ : fluorescence intensity parallel to the excitation light polari-  
16 zation,  $I_{\perp}$ : fluorescence intensity perpendicular to the excitation light polarization and G: grating  
17 factor ( $G = I_{\parallel}/I_{\perp}$ ).

18 
$$FP = FP_{min} + \frac{FP_{max} - FP_{min}}{1 + \frac{K_d}{[prot]}} \quad (2)$$

19 with  $FP_{min}$ : fluorescence polarization of the free fluorophore (lower plateau),  $FP_{max}$ : maximal fluo-  
20 rescence polarization of fully bound fluorophore (upper plateau),  $K_d$ : dissociation constant and  
21  $[prot]$  = protein concentration.

22 **Affinity of SNAP and SNAPf towards BG and CP substrates.** Binding affinities of SNAP<sup>C145A</sup>  
23 and SNAP<sup>fC145A</sup> toward BG-Alexa488, CP-Alexa488, BG-Fluorescein, CP-Fluorescein, BG-  
24 MAP555, BG-JF549, BG-TMR(6), BG-TMR(5), CP-TMR, BG-CPY(6), BG-CPY(5), CP-CPY, BG-  
25 SiR, CP-SiR, BG-JF646, BG-Atto565, BG-Atto590, BG-sulfo-Cy3, BG-Cy3, BG-sulfo-Cy5, BG-  
26 Cy5 were determined by fluorescence polarization analogous to HT7 affinities towards CA sub-  
27 strates described above with the following changes: fluorescent substrates were titrated at a final  
28 concentration of 50 nM against protein concentrations ranging from (0 – 250 μM) at room temper-  
29 ature using 0.1 g/L BSA and 1 mM DTT (SNAP-FP buffer). The FP value of each dye fully reacted  
30 with the native SNAP/SNAPf was used to improve fitting of the upper plateau of the curves by  
31 adding an extra data point at protein concentration of 0.005 M.

1 **Table 3:** Filter settings used in FP measurements.

Fluorophore	Excitation filter (BW)	Emission filter (BW)
Alexa488, Fluorescein, Oregon green, JF503, 500R	485 (20) nm	535 (25) nm
TMR, JF549, JF525, TMR-az-F2, TMR-CN, TMR-SCH3, TMR-SNH2, MaP555, 510R, 515R, 580CP, Atto565, Atto590, (sulfo-)Cy3	535 (25) nm	595 (35) nm
CPY, SiR, LIVE580, JF608, JF646, JF669, (sulfo-)Cy5	620 (20) nm	680 (30) nm

2 **Affinity of HT7 towards methyl-amide fluorophores.** Binding affinities of HT7 towards methyl-  
3 amide fluorophores were determined by fluorescence polarization analogous to CA substrates  
4 described above with following changes: fluorescent substrates were used at a final concentration  
5 of 50 nM and measurements were performed at room temperature.

6 **Affinity of HT7<sup>D106A</sup> towards CA-Ac via FP competition assay.** Binding affinity of HT7<sup>D106A</sup> to-  
7 wards CA-Ac was determined by a fluorescence polarization competition assay against CA-TMR.  
8 5 μM protein and 50 nM CA-TMR were titrated against CA-Ac concentrations ranging from 80 μM  
9 to 10 mM in activity buffer supplemented with 0.5 g/L BSA. Assays were performed in low-volume  
10 non-binding black 384-well plates (Corning Inc.) with a final volume of 20 μL using a microplate  
11 reader (Spark20M®, Tecan). All measurements were performed in triplicates at 37°C, filter set-  
12 tings are listed in **Table 3**. Obtained FP values were averaged and fitted to a 4 parameter logistic  
13 curve (equation **3**) to estimate the I<sub>50</sub> value. The lower plateau was fixed to the measured FP value  
14 of the free dye to improve the fit. The dissociation constant of CA-Ac was calculated as described  
15 by Rossi and Taylor (2011) (48).

$$FP = FP_{max} + \frac{FP_{min} - FP_{max}}{1 + \left(\frac{I_{50}}{[ligand]}\right)^{HillSlope}} \quad (3)$$

16  
17 with FP<sub>min</sub>: fluorescence polarization of the free fluorophore (lower plateau), FP<sub>max</sub>: maximal fluo-  
18 rescence polarization of fully bound fluorophore (upper plateau), I<sub>50</sub>: half maximal effective con-  
19 centration, HillSlope: hill slope and [ligand]: ligand concentration.

20 **Affinity of SNAP<sup>C145A</sup> towards non-fluorescent substrates via FP competition assay.** Binding  
21 affinities of SNAP<sup>C145A</sup> towards BG, CP, BG-Ac, CP-Ac and BC-Ac to were obtained as previously  
22 described for HT7 by titrating 5 μM protein and 50 nM CP-TMR against non-fluorescent substrate  
23 concentrations ranging from 150 nM to 1.5 mM. Experimental conditions and data analysis were



1 identical despite that 1 mM DTT was added to the buffer and the assay was performed at room  
2 temperature.

3 **Calculation of free binding energy from  $K_d$ .** Free binding energies were calculated from  $K_d$   
4 values according to equation 4:

$$\Delta G = -RT * \ln \left( \frac{1}{K_d} \right) \quad (4)$$

5  
6 with  $\Delta G$ : free binding energy, R: universal gas constant, T: temperature and  $K_d$ : dissociation con-  
7 stant.

8 **HT7 and HOB labeling kinetics via stopped-flow.** Labeling kinetics of HT7 with CA-TMR, CA-  
9 JF549, CA-CPY, CA-LIVE580 and CA-JF669 and labeling kinetics of HOB with CA-TMR were  
10 measured by recording fluorescence anisotropy changes over time using a BioLogic SFM-400  
11 stopped-flow instrument (BioLogic Science Instruments, Claix, France) in single mixing configura-  
12 tion at 37°C. Monochromator wavelengths for excitation and long pass filters used for detection  
13 are listed in **Table 4**. HT7 protein and substrates in activity buffer were mixed in a 1:1 stoichiometry  
14 in order to reach recordable speed of these fast reactions and increase information content of the  
15 traces. Concentrations were varied from 0.125  $\mu\text{M}$  to 1  $\mu\text{M}$ . The anisotropy of the free substrate  
16 was measured to obtain a baseline.

17 The dead time of the instrument was measured according to the manufacturer protocol (BioLogic  
18 Technical note #53) by recording the fluorescence decay during the pseudo-first order reaction of  
19 *N*-acetyl-L-tryptophanamide with a large excess of *N*-bromosuccinimide and fitting the data to the  
20 first order reaction rate law.

21 **Table 4:** Monochromator excitation wavelengths and filters used for stopped-flow measurements

Fluorophore	Excitation wavelength [nm]	Emission filter [nm]
TMR / JF549	555	570 Long Path
CPY	610	630 Long Path
LIVE580	603	630 Long Path
JF669	669	690 Long Path

22 **SNAP labeling kinetics via stopped-flow.** Labeling kinetics of SNAP with BG-TMR were meas-  
23 ured via stopped-flow analogous to HT7 kinetics described above but final substrate concentration  
24 was fixed at 2  $\mu\text{M}$  and the protein concentration was varied from 1.875  $\mu\text{M}$  to 50  $\mu\text{M}$ . The activity  
25 buffer was supplemented with 1 mM DTT.

26 **HT7 and HOB labeling kinetics via microplate reader.** Labeling kinetics of HT7 and HOB with  
27 CA-Alexa488 were measured by recording FP over time using a microplate reader (Spark20M®),

1 Tecan). The final concentration of fluorophore substrate remained constant (50 nM) with varying  
2 protein concentrations (200 nM – 256  $\mu$ M) in activity buffer supplemented with 0.5 g/L of BSA.  
3 Labeling reactions were started by adding the fluorophore substrate using either multichannel pi-  
4 pets or the injector module of the plate reader. Assays were performed in black non-binding flat  
5 bottom 96-well plates (Corning Inc.) with a final reaction volume of 200  $\mu$ L. All measurements were  
6 performed in triplicates at 37°C with filter settings listed in **Table 3**. The FP of the free substrate  
7 was measured to obtain a baseline.

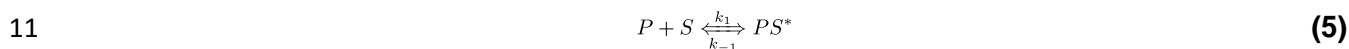
8 ***HT7-tag competitive labeling kinetics.*** Competitive kinetics were measured by recording FP  
9 over time using a microplate reader (Spark20M®, Tecan). The final concentration of CA-Alexa488  
10 (50 nM) and HT7 protein (200 nM) remained constant with varying concentrations of non-fluores-  
11 cent substrates (0 – 1  $\mu$ M) in activity buffer supplemented with 0.5 g/L of BSA. Assays were per-  
12 formed in black non-binding flat bottom 96-well plates with a final reaction volume of 200  $\mu$ L. La-  
13 beling reactions were started by adding the HT7 protein to wells containing CA-Alexa488 and non-  
14 fluorescent substrates using an electronic 96 channel pipettor (Integra Bioscience Corp., Hudson,  
15 NH, USA). All measurements were performed in triplicates at 37°C with filter settings listed in  
16 **Table 3**. The FP of free CA-Alexa488 was measured to obtain a baseline.

17 ***SNAP and CLIP labeling kinetics via microplate reader.*** Labeling kinetics of SNAP and CLIP  
18 substrates were measured by recording FP over time using a microplate reader analogously to  
19 HT7 labeling kinetics described above with the following changes: fluorescent substrate concen-  
20 tration was fixed to 20 nM and protein concentrations were varied from 15 nM to 900 nM. Meas-  
21 urements were performed in SNAP-FP buffer. Kinetics with substrates that showed adsorption to  
22 plastic were recorded in a black quartz 96-well plate (Hellma GmbH, Müllheim, Germany).

23 ***SNAP competitive labeling kinetics.*** Competitive kinetics were measured by recording FP over  
24 time using a microplate reader analogous to HT7 competition kinetics described above using  
25 100 nM of BG-Alexa488 as fluorescent substrate in SNAP-FP buffer.

26 ***Analysis of stopped-flow data.*** Kinetic stopped-flow data was pre-processed using a custom R  
27 script (49, 50). Recorded pre-trigger time points were removed and time points were adjusted to  
28 start at  $t = 0$ . Values from replicates were averaged. The anisotropy of the free dye was calculated  
29 by averaging anisotropy values of the baseline measurements. Pre-processed data was fit to a  
30 kinetic model (5, 6) described by the differential equations 7-10 using the DynaFit software (51).  
31 The anisotropy of the free dye and the mixing delay of the stopped-flow machine were set as fixed  
32 offset and delay parameters in DynaFit. It was assumed that the protein substrate complex and

1 the reacted product are contributing equally to the anisotropy signal. Hence, the response for both  
2 species was set equal in DynaFit and fitted together with the kinetic constants. Standard deviations  
3 (normal distribution verified) and confidence intervals of fitted parameters were estimated with the  
4 Monte Carlo method (52) with standard settings ( $N = 1000$ , 5% worst fits discarded). In case of  
5 SNAP kinetics with BG-TMR, the substrate concentration was fitted by DynaFit in order to rule out  
6 quantification errors of the BG quenched fluorophore. Accurate fitting of the concentration was  
7 ensured by including conditions in which protein is limiting and no maximum FP value was  
8 reached. Data points and predictions based on the fitted models were plotted using R. Fluores-  
9 cence intensity changes upon protein binding were verified to be minimal ( $< 12\%$ ) and hence not  
10 noticeably biasing the fluorescence anisotropy.



13 with P: SLP protein, S: SLP substrate,  $PS^*$ : protein substrate complex and PS: protein substrate  
14 conjugate.

$$15 \quad \frac{d[P]}{dt} = -k_1[P][S] + k_{-1}[PS^*] \quad (7)$$

$$16 \quad \frac{d[S]}{dt} = -k_1[P][S] + k_{-1}[PS^*] \quad (8)$$

$$17 \quad \frac{d[PS^*]}{dt} = +k_1[P] - k_{-1}[PS^*] - k_2[PS^*] \quad (9)$$

$$18 \quad \frac{d[PS]}{dt} = +k_2[PS^*] \quad (10)$$

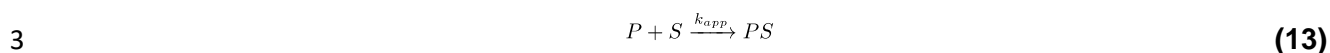
19  
20 The derived parameters  $K_d$  (dissociation constant) and  $k_{app}$  (apparent first order reaction rate) were  
21 calculated using the following equations:

$$22 \quad K_d = \frac{k_{-1}}{k_1} \quad (11)$$

$$23 \quad k_{app} = k_1 \frac{k_2}{k_2 + k_{-1}} \quad (12)$$

24  
25 **Analysis of kinetic microplate reader data.** Kinetic data from microplate reader assays was  
26 fitted to a simplified kinetic model (13) described by the differential equations 14-16 using DynaFit.  
27 Dead time of the measurements and baseline FP value were put in as fixed parameters. Standard  
28 deviations (normal distribution verified) and confidence intervals of fitted parameters were esti-  
29 mated with the Monte Carlo method with standard settings ( $N = 1000$ , 5% worst fits discarded).  
30 In case of BG, CP and BC kinetics, the substrate concentration was fitted by DynaFit in order to  
31 rule out quantification errors of the BG, CP or BC fluorophores. Accurate fitting of the concentration

1 was ensured by including conditions in which protein is limiting and no maximum FP value was  
2 reached. Data points and predictions based on the fitted models were plotted using R.



4 with P: SLP protein, S: SLP substrate and PS: protein substrate conjugate.

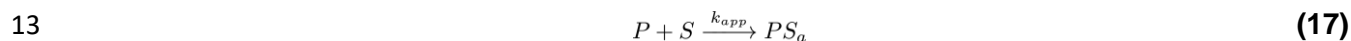
5  
6 
$$\frac{d[P]}{dt} = -k_{app}[P][S] \quad (14)$$

7 
$$\frac{d[S]}{dt} = -k_{app}[P][S] \quad (15)$$

8 
$$\frac{d[PS]}{dt} = +k_{app}[P][S] \quad (16)$$

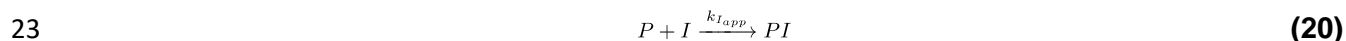
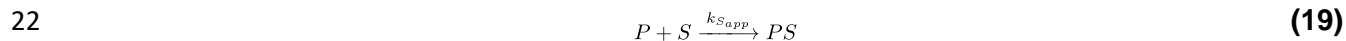
9

10 In some cases, a slow second phase ( $k_3$ ) was observed in the kinetic data that could not be de-  
11 scribed by the simplified model **13**. This data was fit to an expanded model that includes a potential  
12 conformational change in a second step (**17**, **18**).



15 with P: SLP protein, S: SLP substrate,  $PS_a$ : protein substrate conjugate state A and  $PS_b$ : protein  
16 substrate conjugate state B.

17 **Analysis of competition kinetics.** Data was fitted to a simplified kinetic competition model (**19**,  
18 **20**) described by the differential equations **21-25** using DynaFit. Dead time of the measurements  
19 and baseline FP value were put in as fixed parameters. Standard deviations (normal distribution  
20 verified) and confidence intervals of fitted parameters were estimated with the Monte Carlo method  
21 with standard settings ( $N = 1000$ , 5% worst fits discarded).



24 with P: SLP protein, S: fluorescent SLP substrate, I: non-fluorescent SLP substrate (inhibitor), PS:  
25 protein fluorescent substrate conjugate and PI: protein non-fluorescent substrate conjugate.

26

27

1 
$$\frac{d[P]}{dt} = -k_{S_{app}}[P][S] - k_{I_{app}}[P][I] \quad (21)$$

2 
$$\frac{d[S]}{dt} = -k_{S_{app}}[P][S] \quad (22)$$

3 
$$\frac{d[I]}{dt} = -k_{I_{app}}[P][I] \quad (23)$$

4 
$$\frac{d[PS]}{dt} = +k_{S_{app}}[P][S] \quad (24)$$

5 
$$\frac{d[PI]}{dt} = +k_{I_{app}}[P][I] \quad (25)$$

6

7 **Protein crystallization.** For crystallization trials, protein purification tags were removed by over-  
8 night cleavage with TEV protease at 30°C as previously described (53). Cleaved proteins were  
9 purified by affinity-tag purification using a HisTrap FF crude column (Cytiva) on an ÄktäPure FPLC,  
10 collecting the flow-through. Proteins were further separated by size exclusion chromatography  
11 (HiLoad 26/600 Superdex 75, Cytiva) and concentrated using Ultra-4 or 15 mL centrifugal filter  
12 devices (Amicon, Merck). Correct size and high purity were verified via SDS-PAGE and LC-MS  
13 analysis. Protein labeling was performed in activity buffer, overnight at RT using fluorophore sub-  
14 strates at 10 μM (CA-TMR/CA-CPY and BG-TMR for HT7/HOB and SNAP, respectively) in pres-  
15 ence of 5 μM (3 mg) of protein. After concentration to about 200 μL, excess of fluorophore sub-  
16 strate was removed by buffer exchange using Illustra microspin G-25 columns (Cytiva) according  
17 to the manufacturer instructions. Protein labeling was verified by SDS-PAGE fluorescence scan  
18 and LC-MS analysis. Protein concentrations were adjusted between 10 and 20 mg/mL and sub-  
19 mitted to crystallization trials using different commercial screens mixing in 200 nL final volume  
20 protein solution:crystallization solution (1:1) using a Mosquito robot (TTP Labtech).

21 **HT7 crystal structures.** Crystallization was performed at 20°C using the vapor-diffusion method.  
22 Crystals of HT7 labeled with a chloroalkane-PEG-tetramethylrhodamine (CA-TMR) fluorophore  
23 substrate were grown by mixing equal volumes of protein solution at 20 mg/ml in 50 mM HEPES  
24 pH 7.3, 50 mM sodium chloride and a reservoir solution containing 0.1 M MES pH 6.0, 1.0 M  
25 lithium chloride and 15% (m/v) PEG 6000. The crystals were briefly washed in cryoprotectant  
26 solution consisting of the reservoir solution with glycerol added to a final concentration of 20%  
27 (v/v), prior to flash-cooling in liquid nitrogen. Crystals of HT7 labeled with a chloroalkane-PEG-  
28 carbopyronine (CA-CPY) fluorophore substrate were obtained by mixing equal volumes of protein  
29 solution at 15 mg/ml in 50 mM HEPES pH 7.3, 50 mM sodium chloride and precipitant solution  
30 containing 0.1 M Bicine pH 9.0 and 1.7 M ammonium sulfate. The crystals were briefly washed in  
31 cryoprotectant solution consisting of the reservoir solution supplemented with 20% (v/v) ethylene  
32 glycol before flash-cooling in liquid nitrogen. Crystals of HT7-based Oligonucleotide Binder (HOB)  
33 labeled with a CA-TMR fluorophore substrate were grown by mixing equal volumes of protein

1 solution at 9.0 mg/ml in 50 mM HEPES pH 7.3, 50 mM sodium chloride and a reservoir solution  
2 composed of 0.2 M calcium acetate and 20% (m/v) PEG 3350. Prior to flash-cooling in liquid  
3 nitrogen, the crystals were stepwise transferred into a reservoir solution with PEG 3350 concen-  
4 tration increased to 30 and 40% (m/v).

5 Single crystal X-ray diffraction data was collected at 100 K on the X10SA beamline at the SLS  
6 (PSI, Villigen, Switzerland). All data were processed with XDS (54). The structures of HT7 labeled  
7 with TMR was determined by molecular replacement (MR) using Phaser (55) and PDB ID 5UY1  
8 coordinates as a search model. The structure of HT7 labeled with CPY and HOB labeled with  
9 TMR were subsequently determined by molecular replacement using HT7-TMR as a search  
10 model. Geometrical restraints for TMR and CPY were generated using Grade server (56). The  
11 final models were optimized in iterative cycles of manual rebuilding using Coot (57) and refinement  
12 using Refmac5 (58) and phenix.refine (59). Data collection and refinement statistics are summa-  
13 rized in **Table S4**, model quality was validated with MolProbity (60) as implemented in PHENIX.

14 **SNAP crystal structure.** SNAP-TMR crystals were obtained on the crystallography platform of  
15 EPFL using the SNAP<sup>ox</sup>-tag construct that features the sequence of SNAP identical to available  
16 SNAP crystal structures (PDB ID 3L00, 3KZZ and 3KZY). Previously crystallized SNAP features  
17 the mutation P179R involved in the crystal packing suggesting its important role for crystallization  
18 (28). Crystals were obtained in different conditions including in 100 mM Sodium HEPES pH 7.5,  
19 25% PEG 8000 from the PEG suite screen (Qiagen) after 48 hours at 18°C. Single crystals were  
20 fished and placed in a cryoprotectant solution (containing the crystallization solution supplemented  
21 with 20% (v/v) glycerol) before being flash frozen in liquid nitrogen. Single crystal X-ray diffraction  
22 data was collected on the ID29 beamline at the ESRF (Grenoble, France). Integration, scaling,  
23 molecular replacement (using PDB ID 3L00 as starting model) and refinement were performed as  
24 explained for HT7. Refinement statistics can be found in **Table S4**.

25 **SNAPf in silico modeling.** The glutamic acid in position 30 of the SNAP-TMR structure (PDB ID  
26 6Y8P) was modeled as an arginine using the mutate function using the software SYBYL-X1.3  
27 (Tripos Int., USA). A side-chain conformation for the arginine was selected from the rotamer  
28 source library of Lovell and minimized with few steps with no steric clashes and no direct contact  
29 with another positive charges as criteria.

30 **Data availability and analysis.** Atomic coordinates and structure factors were deposited in the  
31 Protein Data Bank (PDB) under accession codes 6Y7A (HT7-TMR), 6ZCC (HOB-TMR), 6Y7B  
32 (HT7-CPY) and 6Y8P (SNAP-TMR). Analysis was conducted on PyMOL (61). OMIT maps were

1 generated using Phenix (62). Root mean square deviations (RMSDs) were obtained using the  
2 cealign command from PyMOL. Electrostatic potentials were generated using the adaptive pois-  
3 son–boltzmann solver (APBS) (63) as PyMOL plugin including the PDB2PQR software (64). Plas-  
4 mids from this study are available at Addgene (167266-167275).

## 5 **Acknowledgements**

6 The authors thank Ilme Schlichting for X-ray data collection. HaloTag diffraction data were col-  
7 lected at the Swiss Light Source, beamline X10SA, of the Paul Scherrer Institute, Villigen, Swit-  
8 zerland. The authors thank Florence Pojer for supporting the SNAP-TMR crystallization on the  
9 EPFL platform. The ESRF is acknowledged for access to beamlines and facilities for molecular  
10 biology via its in-house research programme. The authors thank Andrea Bergner (MPIMF) and  
11 Bettina Mathes (MPIMF) for providing proteins and fluorophore substrates, respectively. The au-  
12 thors thank Dr. L. Lavis (HHMI, Ashburn, VA, USA) and Dr. A.D.N. Butkevich (MPI-MF, Heidel-  
13 berg, Germany) for providing HaloTag substrates. We thank all members of the Johnsson lab for  
14 critical discussions. This work was supported by the Ecole Polytechnique Federale de Lausanne  
15 (EPFL), the Max Planck Society and the Deutsche Forschungsgemeinschaft (DFG, German Re-  
16 search Foundation), SFB 1129.

17

## 18 **Author contributions**

19 J.W., S.K., J.R., J.H. and K.J. designed the experiments.

20 J.W., S.K., J.H. and J.T. performed the biochemistry experiments.

21 J.H., T.T., G.G. crystalized and solved the SNAP-TMR structure.

22 M.T. and J.H. crystalized and solved the HaloTag structures.

23 U.U. performed the structural modeling work.

24 S.K., J.W., J.K., N.M. and L.X. synthesized the compounds used in the study.

25 K.J., J.H., J.W. and S.K. wrote the manuscript with input from all authors.

26

## 27 **Competing financial information**

28 K.J. is inventor on patents filed by MPG and EPFL on fluorophores and labeling technologies.

29

## 30 **Additional information**

31 Further information and requests for resources and reagents should be directed to and will be  
32 fulfilled by Julien Hiblot ([julien.hiblot@mr.mpg.de](mailto:julien.hiblot@mr.mpg.de)) and Kai Johnsson ([johnsson@mr.mpg.de](mailto:johnsson@mr.mpg.de)).

33

## 1 References

- 2
- 3 1. Xue L, Karpenko IA, Hiblot J, Johnsson K. Imaging and manipulating proteins in live cells through
- 4 covalent labeling. *Nature chemical biology*. 2015;11(12):917-23.
- 5 2. England CG, Luo H, Cai W. HaloTag Technology: A Versatile Platform for Biomedical Applications.
- 6 *Bioconjugate Chemistry*. 2015;26(6):975-86.
- 7 3. Haruki H, Gonzalez MR, Johnsson K. Exploiting ligand-protein conjugates to monitor ligand-
- 8 receptor interactions. *PLoS One*. 2012;7(5):e37598.
- 9 4. Farrants H, Hiblot J, Griss R, Johnsson K. Rational Design and Applications of Semisynthetic
- 10 Modular Biosensors: SNIFITs and LUCIDs. *Methods Mol Biol*. 2017;1596:101-17.
- 11 5. Sallin O, Reymond L, Gondrand C, Raith F, Koch B, Johnsson K. Semisynthetic biosensors for
- 12 mapping cellular concentrations of nicotinamide adenine dinucleotides. *Elife*. 2018;7.
- 13 6. Yu Q, Xue L, Hiblot J, Griss R, Fabritz S, Roux C, et al. Semisynthetic sensor proteins enable
- 14 metabolic assays at the point of care. *Science*. 2018;361(6407):1122-6.
- 15 7. Abdelfattah AS, Kawashima T, Singh A, Novak O, Liu H, Shuai Y, et al. Bright and photostable
- 16 chemigenetic indicators for extended in vivo voltage imaging. *Science*. 2019.
- 17 8. Chidley C, Haruki H, Pedersen MG, Muller E, Johnsson K. A yeast-based screen reveals that
- 18 sulfasalazine inhibits tetrahydrobiopterin biosynthesis. *Nature chemical biology*. 2011;7(6):375-83.
- 19 9. Los GV, Encell LP, McDougall MG, Hartzell DD, Karassina N, Zimprich C, et al. HaloTag: a novel
- 20 protein labeling technology for cell imaging and protein analysis. *ACS chemical biology*. 2008;3(6):373-82.
- 21 10. Keppler A, Gendreizig S, Gronemeyer T, Pick H, Vogel H, Johnsson K. A general method for the
- 22 covalent labeling of fusion proteins with small molecules in vivo. *Nature biotechnology*. 2003;21(1):86-9.
- 23 11. Gautier A, Juillerat A, Heinis C, Correa IR, Jr., Kindermann M, Beaufils F, et al. An engineered
- 24 protein tag for multiprotein labeling in living cells. *Chem Biol*. 2008;15(2):128-36.
- 25 12. Damborský J, Koča J. Analysis of the reaction mechanism and substrate specificity of haloalkane
- 26 dehalogenases by sequential and structural comparisons. *Protein Engineering, Design and Selection*.
- 27 1999;12(11):989-98.
- 28 13. Encell LP, Friedman Ohana R, Zimmerman K, Otto P, Vidugiris G, Wood MG, et al. Development of
- 29 a dehalogenase-based protein fusion tag capable of rapid, selective and covalent attachment to
- 30 customizable ligands. *Curr Chem Genomics*. 2012;6:55-71.
- 31 14. Pegg AE, Dolan ME, Moschel RC. Structure, Function, and Inhibition of O6-Alkylguanine-DNA
- 32 Alkyltransferase. *Progress in Nucleic Acid Research and Molecular Biology*1995. p. 167-223.
- 33 15. Correa I, Baker B, Zhang A, Sun L, Provost C, Lukinavic.ius Gz, et al. Substrates for Improved Live-
- 34 Cell Fluorescence Labeling of SNAP-tag. *Current Pharmaceutical Design*. 2013;19(30):5414-20.
- 35 16. Erdmann RS, Baguley SW, Richens JH, Wissner RF, Xi Z, Allgeyer ES, et al. Labeling Strategies Matter
- 36 for Super-Resolution Microscopy: A Comparison between HaloTags and SNAP-tags. *Cell Chem Biol*.
- 37 2019;26(4):584-92 e6.
- 38 17. Jonker CTH, Deo C, Zager PJ, Tkachuk AN, Weinstein AM, Rodriguez-Boulan E, et al. Accurate
- 39 measurement of fast endocytic recycling kinetics in real time. *Journal of Cell Science*. 2020;133(2).
- 40 18. Kossmann KJ, Ziegler C, Angelin A, Meyer R, Skoupi M, Rabe KS, et al. A Rationally Designed
- 41 Connector for Assembly of Protein-Functionalized DNA Nanostructures. *Chembiochem*. 2016;17(12):1102-
- 42 6.
- 43 19. Liu Y, Fares M, Dunham NP, Gao Z, Miao K, Jiang X, et al. AgHalo: A Facile Fluorogenic Sensor to
- 44 Detect Drug-Induced Proteome Stress. *Angew Chem Int Ed Engl*. 2017;56(30):8672-6.
- 45 20. Liu Y, Miao K, Dunham NP, Liu H, Fares M, Boal AK, et al. The Cation- $\pi$  Interaction Enables a Halo-
- 46 Tag Fluorogenic Probe for Fast No-Wash Live Cell Imaging and Gel-Free Protein Quantification.
- 47 *Biochemistry*. 2017;56(11):1585-95.



- 1 21. Kang MG, Lee H, Kim BH, Dunbayev Y, Seo JK, Lee C, et al. Structure-guided synthesis of a protein-  
2 based fluorescent sensor for alkyl halides. *Chem Commun (Camb)*. 2017;53(66):9226-9.
- 3 22. Newman J, Peat TS, Richard R, Kan L, Swanson PE, Affholter JA, et al. Haloalkane dehalogenases:  
4 structure of a *Rhodococcus* enzyme. *Biochemistry*. 1999;38(49):16105-14.
- 5 23. Deo C, Abdelfattah AS, Bhargava HK, Berro AJ, Falco N, Farrants H, et al. The HaloTag as a general  
6 scaffold for far-red tunable chemigenetic indicators. *Nature chemical biology*. 2021.
- 7 24. Jencks WP. On the attribution and additivity of binding energies. *Proceedings of the National  
8 Academy of Sciences*. 1981;78(7):4046-50.
- 9 25. Wade RC, Gabdoulline RR, Ludemann SK, Lounnas V. Electrostatic steering and ionic tethering in  
10 enzyme-ligand binding: insights from simulations. *Proc Natl Acad Sci U S A*. 1998;95(11):5942-9.
- 11 26. Sun X, Zhang A, Baker B, Sun L, Howard A, Buswell J, et al. Development of SNAP-Tag Fluorogenic  
12 Probes for Wash-Free Fluorescence Imaging. *ChemBioChem*. 2011;12(14):2217-26.
- 13 27. Wibley JEA. Crystal structure of the human O6-alkylguanine-DNA alkyltransferase. *Nucleic Acids  
14 Research*. 2000;28(2):393-401.
- 15 28. Mollwitz B, Brunk E, Schmitt S, Pojer F, Bannwarth M, Schiltz M, et al. Directed evolution of the  
16 suicide protein O(6)-alkylguanine-DNA alkyltransferase for increased reactivity results in an alkylated  
17 protein with exceptional stability. *Biochemistry*. 2012;51(5):986-94.
- 18 29. Perugino G, Vettone A, Illiano G, Valenti A, Ferrara MC, Rossi M, et al. Activity and Regulation of  
19 Archaeal DNA Alkyltransferase. *Journal of Biological Chemistry*. 2012;287(6):4222-31.
- 20 30. Rossi F, Morrone C, Massarotti A, Ferraris DM, Valenti A, Perugino G, et al. Crystal structure of a  
21 thermophilic O6-alkylguanine-DNA alkyltransferase-derived self-labeling protein-tag in covalent complex  
22 with a fluorescent probe. *Biochemical and Biophysical Research Communications*. 2018;500(3):698-703.
- 23 31. Lavis LD. Teaching Old Dyes New Tricks: Biological Probes Built from Fluoresceins and Rhodamines.  
24 *Annual Review of Biochemistry*. 2017;86(1):825-43.
- 25 32. Lukinavicius G, Umezawa K, Olivier N, Honigmann A, Yang G, Plass T, et al. A near-infrared  
26 fluorophore for live-cell super-resolution microscopy of cellular proteins. *Nat Chem*. 2013;5(2):132-9.
- 27 33. Wang L, Tran M, D'Este E, Roberti J, Koch B, Xue L, et al. A general strategy to develop cell  
28 permeable and fluorogenic probes for multicolour nanoscopy. *Nat Chem*. 2020;12(2):165-72.
- 29 34. Grimm JB, English BP, Chen J, Slaughter JP, Zhang Z, Revyakin A, et al. A general method to improve  
30 fluorophores for live-cell and single-molecule microscopy. *Nat Methods*. 2015;12(3):244-50, 3 p following  
31 50.
- 32 35. Grimm JB, Muthusamy AK, Liang Y, Brown TA, Lemon WC, Patel R, et al. A general method to fine-  
33 tune fluorophores for live-cell and in vivo imaging. *Nat Methods*. 2017;14(10):987-94.
- 34 36. Wang L, Hiblot J, Popp C, Xue L, Johnsson K. Environmentally Sensitive Color-Shifting Fluorophores  
35 for Bioimaging. *Angewandte Chemie*. 2020;132(49):22064-8.
- 36 37. Juillerat A, Gronemeyer T, Keppler A, Gendreizig S, Pick H, Vogel H, et al. Directed Evolution of O6-  
37 Alkylguanine-DNA Alkyltransferase for Efficient Labeling of Fusion Proteins with Small Molecules In Vivo.  
38 *Chemistry & Biology*. 2003;10(4):313-7.
- 39 38. Gronemeyer T, Chidley C, Juillerat A, Heinis C, Johnsson K. Directed evolution of O6-alkylguanine-  
40 DNA alkyltransferase for applications in protein labeling. *Protein Eng Des Sel*. 2006;19(7):309-16.
- 41 39. Hiblot J, Yu Q, Sabbadini MDB, Reymond L, Xue L, Schena A, et al. Luciferases with Tunable  
42 Emission Wavelengths. *Angew Chem Int Ed Engl*. 2017;56(46):14556-60.
- 43 40. Zhang Y, So M-k, Loening AM, Yao H, Gambhir SS, Rao J. HaloTag Protein-Mediated Site-Specific  
44 Conjugation of Bioluminescent Proteins to Quantum Dots. *Angewandte Chemie International Edition*.  
45 2006;45(30):4936-40.
- 46 41. Masharina A, Reymond L, Maurel D, Umezawa K, Johnsson K. A fluorescent sensor for GABA and  
47 synthetic GABA(B) receptor ligands. *Journal of the American Chemical Society*. 2012;134(46):19026-34.

- 1 42. Ueno Y, Jose J, Loudet A, Pérez-Bolívar Cs, Anzenbacher P, Burgess K. Encapsulated Energy-  
2 Transfer Cassettes with Extremely Well Resolved Fluorescent Outputs. *Journal of the American Chemical*  
3 *Society*. 2011;133(1):51-5.
- 4 43. Mudd G, Pi IP, Fethers N, Dodd PG, Barbeau OR, Auer M. A general synthetic route to isomerically  
5 pure functionalized rhodamine dyes. *Methods and Applications in Fluorescence*. 2015;3(4).
- 6 44. Bottanelli F, Kromann EB, Allgeyer ES, Erdmann RS, Wood Baguley S, Sirinakis G, et al. Two-colour  
7 live-cell nanoscale imaging of intracellular targets. *Nature communications*. 2016;7(1).
- 8 45. Keppler A, Pick H, Arrivoli C, Vogel H, Johnsson K. Labeling of fusion proteins with synthetic  
9 fluorophores in live cells. *Proceedings of the National Academy of Sciences*. 2004;101(27):9955-9.
- 10 46. Gibson DG, Young L, Chuang RY, Venter JC, Hutchison CA, 3rd, Smith HO. Enzymatic assembly of  
11 DNA molecules up to several hundred kilobases. *Nat Methods*. 2009;6(5):343-5.
- 12 47. Bertani G. Lysogeny at mid-twentieth century: P1, P2, and other experimental systems. *J Bacteriol*.  
13 2004;186(3):595-600.
- 14 48. Rossi AM, Taylor CW. Analysis of protein-ligand interactions by fluorescence polarization. *Nature*  
15 *Protocols*. 2011;6(3):365-87.
- 16 49. Team RDC. R: A language and environment for statistical computing  
17 Vienna, Austria: R Foundation for Statistical Computing; 2010.
- 18 50. Wickham H, Averick M, Bryan J, Chang W, McGowan L, François R, et al. Welcome to the Tidyverse.  
19 *Journal of Open Source Software*. 2019;4(43).
- 20 51. Kuzmič P. Program DYNAFIT for the Analysis of Enzyme Kinetic Data: Application to HIV Proteinase.  
21 *Analytical Biochemistry*. 1996;237(2):260-73.
- 22 52. Straume M, Johnson ML. Monte Carlo method for determining complete confidence probability  
23 distributions of estimated model parameters. *Methods Enzymol*. 1992;210:117-29.
- 24 53. Cabrita LD, Gilis D, Robertson AL, Dehouck Y, Rooman M, Bottomley SP. Enhancing the stability  
25 and solubility of TEV protease using in silico design. *Protein Sci*. 2007;16(11):2360-7.
- 26 54. Kabsch W. Xds. *Acta Crystallogr D Biol Crystallogr*. 2010;66(Pt 2):125-32.
- 27 55. McCoy AJ, Grosse-Kunstleve RW, Adams PD, Winn MD, Storoni LC, Read RJ. Phaser crystallographic  
28 software. *Journal of applied crystallography*. 2007;40(Pt 4):658-74.
- 29 56. Smart OS, Womack TO, Sharff A, Flensburg C, Keller P, Paciorek W, et al. Grade Web Server. 2011.
- 30 57. Emsley P, Lohkamp B, Scott WG, Cowtan K. Features and development of Coot. *Acta*  
31 *crystallographica Section D, Biological crystallography*. 2010;66(Pt 4):486-501.
- 32 58. Murshudov GN, Skubak P, Lebedev AA, Pannu NS, Steiner RA, Nicholls RA, et al. REFMAC5 for the  
33 refinement of macromolecular crystal structures. *Acta crystallographica Section D, Biological*  
34 *crystallography*. 2011;67(Pt 4):355-67.
- 35 59. Adams PD, Afonine PV, Bunkoczi G, Chen VB, Davis IW, Echols N, et al. PHENIX: a comprehensive  
36 Python-based system for macromolecular structure solution. *Acta crystallographica Section D, Biological*  
37 *crystallography*. 2010;66(Pt 2):213-21.
- 38 60. Chen VB, Arendall WB, 3rd, Headd JJ, Keedy DA, Immormino RM, Kapral GJ, et al. MolProbity: all-  
39 atom structure validation for macromolecular crystallography. *Acta crystallographica Section D, Biological*  
40 *crystallography*. 2010;66(Pt 1):12-21.
- 41 61. DeLano WL. Pymol: An open-source molecular graphics tool. *CCP4 Newsletter On Protein*.  
42 *Crystallography*. 2002;40:82-92.
- 43 62. Adams PD, Afonine PV, Bunkóczi G, Chen VB, Davis IW, Echols N, et al. PHENIX: a comprehensive  
44 Python-based system for macromolecular structure solution. *Acta Crystallogr D Biol Crystallogr*.  
45 2010;66(Pt 2):213-21.
- 46 63. Jurrus E, Engel D, Star K, Monson K, Brandi J, Felberg LE, et al. Improvements to the APBS  
47 biomolecular solvation software suite. *Protein Sci*. 2018;27(1):112-28.

1 64. Dolinsky TJ, Czodrowski P, Li H, Nielsen JE, Jensen JH, Klebe G, et al. PDB2PQR: expanding and  
2 upgrading automated preparation of biomolecular structures for molecular simulations. *Nucleic Acids Res.*  
3 2007;35(Web Server issue):W522-5.

4



1	<b>Supplementary information table of content</b>	
2		
		Page
	<b>Chemistry</b>	4-27
	General information	4
	<b>Material Table:</b> Sources of substrates and chemicals used in this study	5-7
	Chemical Synthesis	8-27
	<b>Supplementary figures</b>	28-54
	<b>Figure S1:</b> Chemical structure of SLP substrates	28-29
	<b>Figure S2:</b> Labeling kinetics of HT7 with fluorescent CA substrates	30
	<b>Figure S3:</b> Comparison of model 1 and model 2 fitted to HT7 labeling kinetics	31
	<b>Figure S4:</b> Modeling of HT7 labeling kinetics using measured parameters to compare the kinetic models 1 and 2	32
	<b>Figure S5:</b> Labeling kinetics of HT7 and HOB with CA-TMR and CA-Alexa488	33
	<b>Figure S6:</b> Rate and equilibrium constants of HT7 labeling with various fluorescent CA substrates	34
	<b>Figure S7:</b> Affinity of the dead mutant HT7D106A to fluorescent CA substrates	35
	<b>Figure S8:</b> Labeling kinetics of HT7 with non-fluorescent CA substrates	36
	<b>Figure S9:</b> Validation of HT7-TMR and HT7-CPY X-ray structures	37-38
	<b>Figure S10:</b> Structural comparison between HT7-TMR structures 6U32 and 6Y7A	39-40
	<b>Figure S11:</b> Structural comparison between HT7-TMR, HT7-CPY and HOB-TMR	41
	<b>Figure S12:</b> Biochemical study of the interaction of HT7 with chloroalkane-fluorophores	42
	<b>Figure S13:</b> Labeling kinetics of SNAP with fluorescent BG and CP substrates	43
	<b>Figure S14:</b> Labeling kinetics of SNAP measured by stopped flow anisotropy	44
	<b>Figure S15:</b> Comparison of fluorophore substrate affinities between the dead mutants SNAP <sup>C145A</sup> and SNAPf <sup>C145A</sup>	45
	<b>Figure S16:</b> Comparison of non-derivatized core substrate affinities to the dead mutant SNAP <sup>C145</sup>	46
	<b>Figure S17:</b> Sequence alignment and structural comparison between SNAP and CLIP variants	47
	<b>Figure S18:</b> Labeling kinetics of SNAPf with fluorescent BG and CP substrates	48
	<b>Figure S19:</b> Labeling kinetics of CLIP and CLIPf with fluorescent BC	49
	<b>Figure S20:</b> Labeling kinetics of hAGT, SNAP and CLIP with the non-respective BG-, CP- and BC-TMR substrates	50
	<b>Figure S21:</b> Labeling kinetics of SNAP with non-fluorescent BG and CP substrates	51
	<b>Figure S22:</b> Validation and analysis of the SNAP-TMR X-ray structure	52
	<b>Figure S23:</b> Labeling kinetics of SNAP and SNAPf with BG-5-TMR and BG-5-CPY	53
	<b>Figure S24:</b> Correlation between SNAPf labeling kinetics and substrate affinity	53
	<b>Figure S25:</b> SsOGT-H5-VistaGreen alternative fluorophore conformation	54
	<b>Figure S26:</b> Labeling kinetics of SsOGT-H5 with BG-Alexa488 and BG-TMR	54
	<b>Supplementary tables</b>	55-57
	<b>Table S1:</b> Kinetic parameters of HT7 labeling with fluorescent CA substrates	55
	<b>Table S2:</b> Comparison $k_{app}$ of HT7 labeling kinetics analyzed using models 1 and 2	55
	<b>Table S3:</b> Comparison of HT7 and HOB labeling kinetics with fluorescent CA substrates	55
	<b>Table S4:</b> Data collection and refinement statistics the X-ray crystal structures	56
	<b>Table S5:</b> Kinetic parameters of SNAP and SNAPf labeling with fluorescent substrates analyzed using model 1.2	57
	<b>Table S6:</b> Kinetic parameters of SNAP labeling with BG-/CP-TMR measured via stopped flow	57
	<b>Table S7:</b> Comparison of SNAP/CLIP with SNAPf/CLIPf labeling kinetics with fluorescent substrates	57
	<b>Table S8:</b> Comparison of SNAP labeling with 5- and 6-fluorophores.	57

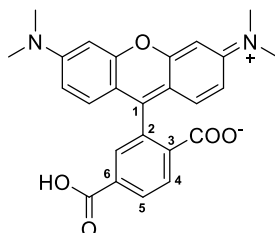
<b>Table S9:</b> Kinetic parameters of SsOGT-H <sup>5</sup> labeling	57
<b>Protein sequences</b>	58-59
<b>Examples DynaFit scripts</b>	60-64
<b>References</b>	65

1

## 1 Chemical Synthesis

### 2 General information

3 All chemical reagents and (anhydrous) solvents for synthesis were purchased from commercial suppliers (Merck KGaA, Darmstadt,  
4 Germany; Honeywell, Charlotte, NC, USA; TCI, Tokyo, Japan; Thermo Fisher Scientific, Waltham, MA, USA; SiChem, Bremen,  
5 Germany) and were used without further purification or distillation. Anhydrous solvents were handled under argon atmosphere. SLP  
6 substrates were purchased from commercial sources, synthesized according to published procedures or gifts from colleagues. Details  
7 are given in **Material Table**.



8  
9 <sup>1</sup>H- and <sup>13</sup>C-NMR spectra were recorded in deuterated solvents on a Bruker (Bruker Corp., Billerica, MA, USA) DPX400 (400 MHz for  
10 <sup>1</sup>H, 101 MHz for <sup>13</sup>C, respectively) or on a Bruker AVANCE III HD 400 (400 MHz for <sup>1</sup>H, 101 MHz for <sup>13</sup>C, respectively) equipped with  
11 a CryoProbe. Chemical shifts ( $\delta$ ) are reported in ppm referenced to the residual solvent peaks of DMSO-*d*<sub>6</sub> ( $\delta_{\text{H}} = 2.50$  ppm,  $\delta_{\text{C}} = 39.52$   
12 ppm), acetone-*d*<sub>6</sub> ( $\delta_{\text{H}} = 2.05$  ppm,  $\delta_{\text{C}}(\text{CH}_3) = 29.84$  ppm,  $\delta_{\text{C}}(\text{CO}) = 206.26$  ppm) or CDCl<sub>3</sub> ( $\delta_{\text{H}} = 7.26$  ppm,  $\delta_{\text{C}} = 77.16$  ppm). Coupling  
13 constants *J* are reported in Hz and corresponding multiplicities are abbreviates as follows: s = singlet, d = doublet, t = triplet,  
14 q = quartet, p = pentet, m = multiplet and br = broad.

15 Reaction progress was monitored by thin layer chromatography (TLC) (Silica gel 60G F<sub>254</sub> on TLC glass plates) in appropriate solvents.  
16 Reaction spots were visualized under UV lamp (254 nm or 366 nm) and/or by staining solutions. LC-MS was performed on a Shimadzu  
17 MS2020 (Shimadzu Corp., Kyoto, Japan) connected to a Nexera UHPLC system equipped with a Waters (Waters Corp., Milford, MA,  
18 USA) ACQUITY UPLC BEH C18 (1.7  $\mu\text{m}$ , 2.1x50 mm) column. Buffer A: 0.1% formic acid in H<sub>2</sub>O, Buffer B: acetonitrile. Measurements  
19 were done with an analytical gradient from 10% to 90% B over 6 min or from 1% to 90% B over 10 min.

20 Normal phase flash chromatography was performed on self-packed silica gel (60 M, 0.04 - 0.063 mm, Macherey-Nagel GmbH & Co.  
21 KG, Düren, Germany) columns or by using an Isolera One system (Biotage Sweden AB, Uppsala, Sweden) using pre-packed silica  
22 gel columns (ultra pure silica gel 12 g or 25 g). Solvent compositions are reported individually in parentheses.

23 Preparative reversed phase high-performance liquid chromatography (RP-HPLC) was conducted using a Waters SunFire™ Prep C18  
24 OBDM column (10 x 150 mm, 5  $\mu\text{m}$  pore size, 4 mL/min. flow rate) or an Ascentis (Merck KGaA, Darmstadt, Germany) C18 column  
25 (10 x 250 mm, 5  $\mu\text{m}$  pore size, 8 mL/min. flow rate) on either a Waters Alliance e2695 separation module connected to a 2998 PDA  
26 detector or a Dionex system equipped with an UVD (170 U, UV-Vis detector). Solvent A: 0.1%TFA in H<sub>2</sub>O, Solvent B: acetonitrile.

27 High resolution mass spectra (HRMS) were measured by the MS-service of the EPF Lausanne (SSMI) on a Waters Xevo® G2-S Q-  
28 ToF spectrometer (Waters, Milford, MA, USA) with electron spray ionization (ESI) or by the MS-facility of the Max Planck Institute for  
29 Medical Research on a Bruker maXis IITM ETD.

1 **Material Table:** Substrate and chemical source used in the study

	<b>Substrate</b>	<b>Source / reference</b>
<b>General</b>	CPY-6-COOH	Butkevich <i>et al.</i> , (2016) (1)
	CPY-5-COOH	Butkevich <i>et al.</i> , (2016) (1)
	TMR-5-COOH	Mudd <i>et al.</i> , (2015) (2)
	TMR-6-COOH	Mudd <i>et al.</i> , (2015) (2)
	Cy3-COOH	Ueno <i>et al.</i> , (2011) (3)
	Cy5-COOH	Ueno <i>et al.</i> , (2011) (3)
	SiR-COOH	Lukinavicius <i>et al.</i> , (2013) (4)
	meAm-6-TMR	this study
	meAm-5-TMR	this study
	meAm-6-CPY	this study
	meAm-5-CPY	this study
	<b>HaloTag substrates</b>	CA-TMR
CA-Alexa488		Purchased from Promega, Madison, WI, USA
CA-Fluorescein		Purchased from Promega, Madison, WI, USA
CA-Oregon green		Purchased from Promega, Madison, WI, USA
CA-JF549		Gift from Dr. Luke Lavis, HHMI, Ashburn, VA, USA
CA-JF503		Gift from Dr. Luke Lavis, HHMI, Ashburn, VA, USA
CA-JF525		Gift from Dr. Luke Lavis, HHMI, Ashburn, VA, USA
CA-JF608		Gift from Dr. Luke Lavis, HHMI, Ashburn, VA, USA
CA-JF669		Gift from Dr. Luke Lavis, HHMI, Ashburn, VA, USA
CA-TMR-az-F <sub>4</sub>		Gift from Dr. Luke Lavis, HHMI, Ashburn, VA, USA
CA-TMR-CN		Wang <i>et al.</i> , (2020) (5)
CA-TMR-SCH <sub>3</sub>		Wang <i>et al.</i> , (2020) (5)
CA-TMR-SNH <sub>2</sub>		Wang <i>et al.</i> , (2020) (5)
CA-MaP555		Wang <i>et al.</i> , (2020) (5)
CA-CPY		Butkevich <i>et al.</i> , (2016) (1)
CA-500R		Butkevich <i>et al.</i> , (2016) (1)
CA-510R		Purchased from Abberior GmbH, Göttingen, Germany
CA-515R		Purchased from Abberior GmbH, Göttingen, Germany
CA-580CP		Gift from Dr. Alexey N. Butkevich, MPI-MF, Heidelberg, Germany
CA-LIVE580		Purchased from Abberior GmbH, Göttingen, Germany
CA-Cy3		this study
CA-Cy5		this study
CA-TMR-biotin		this study
CA-PEG-biotin		Purchased from Promega, Madison, WI, USA
CA-Ac		this study
CA-N <sub>3</sub>		this study
CA-Nor1		this study
CA-Nor2		this study
CA-Tz		this study



	CA-PhN <sub>3</sub>	this study
	CA-Vbn	this study
	CA-BCN	this study
	CA-SCO	this study
SNAP substrates	BG	Purchased from Santa Cruz Biotechnology, Dallas, TX, USA
	CP	this study
	BG-NH <sub>2</sub>	Keppler <i>et al.</i> , (2003) (6)
	CP-NH <sub>2</sub>	Srikun <i>et al.</i> , (2010) (7)
	BG-TMR	Keppler <i>et al.</i> , (2004) (8)
	CP-TMR	Correa <i>et al.</i> , (2013) (9)
	BG-Alexa488	Purchased from NEB as SNAP-Surface® Alexa Fluor® 488, Ipswich, MA, USA
	CP-Alexa488	this study
	BG-Fluorescein	Keppler <i>et al.</i> , (2003) (6)
	CP-Fluorescein	this study
	BG-CPY	Hiblot <i>et al.</i> , (2017) (10)
	CP-CPY	this study
	BG-5-TMR	this study
	BG-5-CPY	this study
	BG-MaP555	Wang <i>et al.</i> , (2020) (5)
	BG-SiR	Lukinavicius <i>et al.</i> , (2013) (4)
	CP-SiR	this study
	BG-JF549	Grimm <i>et al.</i> , (2015) (11)
	BG-JF646	Grimm <i>et al.</i> , (2015) (11)
	BG-Cy3	this study
	BG-sulfo-Cy3	Gautier <i>et al.</i> , (2008) (12)
	BG-Cy5	this study
	BG-sulfo-Cy5	Gautier <i>et al.</i> , (2008) (12)
	BG-Atto565	Correa <i>et al.</i> , (2013) (9)
	BG-Atto590	Bottanelli <i>et al.</i> , (2016) (13)
	BG-N <sub>3</sub>	this study
	CP-N <sub>3</sub>	this study
	BG-Nor2	this study
	CP-Nor2	this study
	BG-Tz	this study
	CP-Tz	this study
	BG-PhN <sub>3</sub>	this study
	CP-PhN <sub>3</sub>	this study
	BG-Vbn	this study
	CP-Vbn	this study
	BG-BCN	this study
CP-BCN	this study	
BG-Ac	this study	
CP-Ac	this study	

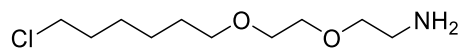
	BG-SCO	this study
	CP-SCO	this study
CLIP substrates	BC-NH <sub>2</sub>	Gautier <i>et al.</i> , (2008) (12)
	BC-TMR	Gautier <i>et al.</i> , (2008) (12)
	BC-Alexa488	Purchased from NEB as CLIP-Surface® Alexa Fluor® 488, Ipswich, MA, USA
	BC-Fluorescein	Gautier <i>et al.</i> , (2008) (12)
	BC-CPY	this study

1

## 1 Chemical Synthesis

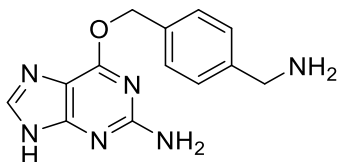
### 2 1.1 Synthesis of substrate amines

#### 3 1.1.1 2-(2-((6-chlorohexyl)oxy)ethoxy)ethan-1-amine (CA-NH<sub>2</sub>)



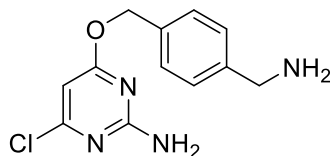
4 CA-NH<sub>2</sub> was synthesized according to the procedure from Zhang *et al.* 2006 (14).

#### 7 1.1.2 6-((4-(aminomethyl)benzyl)oxy)-9H-purin-2-amine (BG-NH<sub>2</sub>)



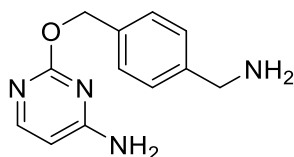
9 BG-NH<sub>2</sub> was synthesized according to the procedure from Keppler *et al.* 2003 (6).

#### 11 1.1.3 4-((4-(aminomethyl)benzyl)oxy)-6-chloropyrimidin-2-amine (CP-NH<sub>2</sub>)



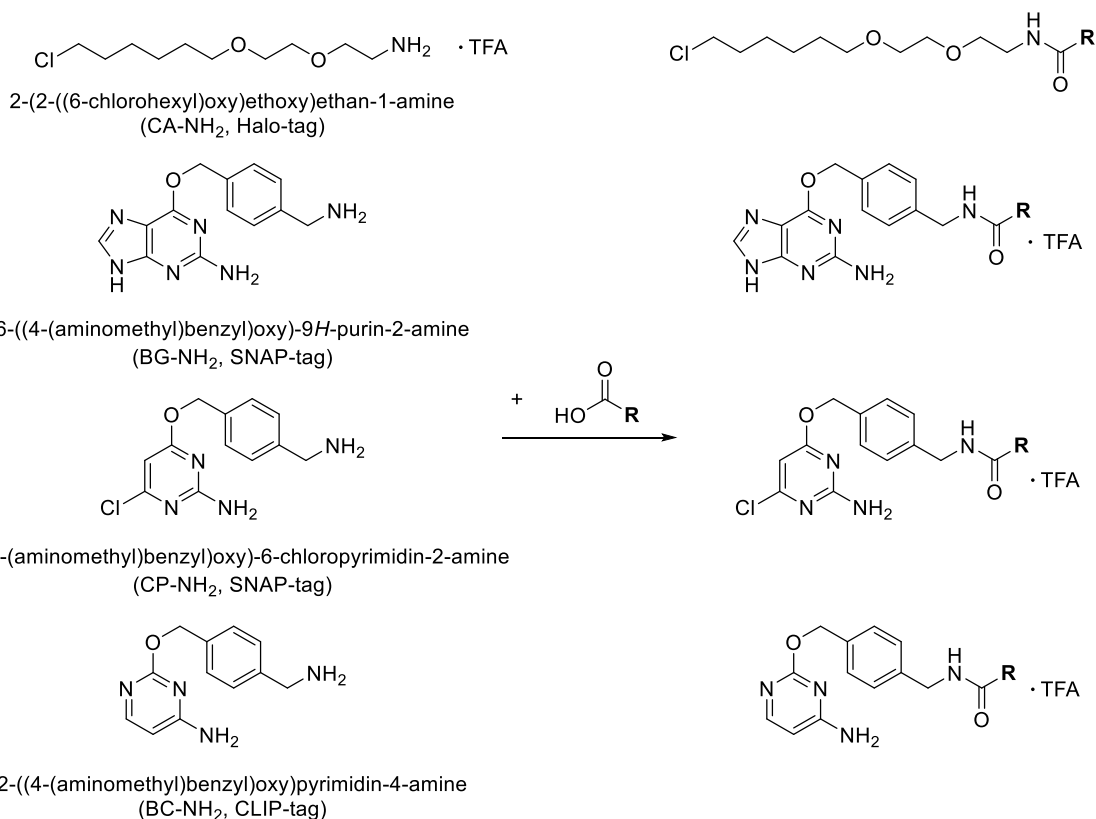
12 CP-NH<sub>2</sub> was synthesized according to the procedure from Srikun *et al.* 2010 (7).

#### 15 1.1.4 2-((4-(aminomethyl)benzyl)oxy)pyrimidin-4-amine (BC-NH<sub>2</sub>)



16 BC-NH<sub>2</sub> was synthesized according to the procedure from Gautier *et al.* 2008 (12).

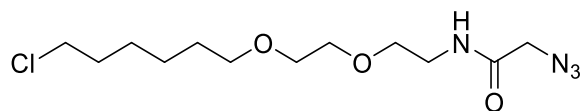
## 1 1.2 General procedure A for peptide coupling reactions



2  
3 To a solution of TSTU (1.2 equiv.) in dry DMSO (0.3 mL), DIPEA (10.2 equiv. for Halo-tag-, 5.0 equiv. for SNAP-substrates) and  
4 different carboxylic acids (1.1 equiv.) were added. After 5 min., a solution of 10 mg of corresponding amine (1.0 equiv.) in dry DMSO  
5 (0.1 mL) was added and the reaction mixture was stirred at r.t. for 2 hours. The reaction mixture was quenched by addition of water  
6 (100  $\mu$ L) and acidified with acetic acid (50  $\mu$ L), then purified by semi-preparative HPLC, eluted with a gradient of MeCN/H<sub>2</sub>O + 0.1%  
7 TFA (equilibration at 15% MeCN for 5 min, then gradient of 15 - 100% MeCN over 25 min, followed by 100% MeCN for 10 min.).  
8 Fractions containing the desired product were combined and lyophilized. Final compounds were stored as DMSO stocks for  
9 biochemical testing.

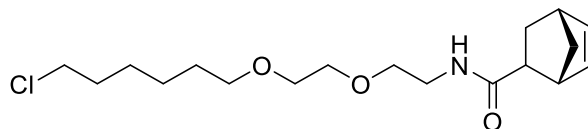
## 10 1.3 HT7 substrates

### 11 1.3.1 2-azido-N-(2-(2-((6-chlorohexyl)oxy)ethoxy)ethyl)acetamide (CA-N<sub>3</sub>)



12  
13 Reaction was conducted according to general procedure A using CA-NH<sub>2</sub> and 2-azidoacetic acid (4.6  $\mu$ L, 32.6  $\mu$ mol). The desired  
14 product (4.6 mg, 15.0  $\mu$ mol) was obtained as a yellowish oil in 51% yield.  
15 <sup>1</sup>H NMR (400 MHz, DMSO-*d*<sub>6</sub>)  $\delta$  [ppm] = 8.15 (t, *J* = 5.8 Hz, 1H), 3.81 (s, 2H), 3.62 (t, *J* = 6.6 Hz, 2H), 3.53 – 3.40 (m, 6H), 3.37 (t, *J*  
16 = 6.6 Hz, 2H), 3.24 (dd, *J* = 5.7 Hz, *J* = 5.8 Hz, 2H), 1.75 – 1.65 (m, 2H), 1.54 – 1.43 (m, 2H), 1.43 – 1.25 (m, 4H).  
17 <sup>13</sup>C NMR (101 MHz, DMSO-*d*<sub>6</sub>)  $\delta$  [ppm] = 167.31, 70.17, 69.56, 69.40, 68.83, 50.69, 45.36, 38.67, 32.00, 29.04, 26.10, 24.91.  
18 HRMS (ESI): calc. for C<sub>12</sub>H<sub>23</sub>ClN<sub>4</sub>NaO<sub>3</sub><sup>+</sup> [M+Na]<sup>+</sup>: 329.1351; found 329.1354.  
19

1 **1.3.2 (1R,4R)-N-(2-(2-((6-chlorohexyl)oxy)ethoxy)ethyl)bicyclo[2.2.1]hept-5-ene-2-carboxamide (CA-Nor1)**



2  
3 Reaction was conducted according to general procedure A using CA-NH<sub>2</sub> and (1R,4R)-bicyclo[2.2.1]hept-5-ene-2-carboxylic acid  
4 (6.2 μL, 32.6 μmol). The desired endo-isomer (5.6 mg, 16.3 μmol) of was obtained in 55% yield.

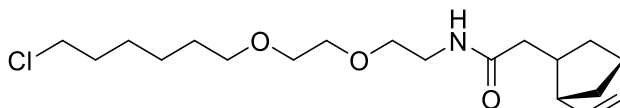
5 **<sup>1</sup>H NMR** (400 MHz, DMSO-*d*<sub>6</sub>) δ [ppm] = 7.59 (t, *J* = 5.7 Hz, 1H), 6.08 (dd, *J* = 5.8, 3.1 Hz, 1H), 5.80 (dd, *J* = 5.8, 3.0 Hz, 1H), 3.62 (t,  
6 *J* = 6.6 Hz, 2H), 3.54 – 3.30 (m, 8H), 3.23 – 3.02 (m, 3H), 2.84 – 2.71 (m, 2H), 1.77 – 1.63 (m, 3H), 1.55 – 1.43 (m, 2H), 1.42 – 1.18  
7 (m, 7H).

8 **<sup>13</sup>C NMR** (101 MHz, DMSO-*d*<sub>6</sub>) δ [ppm] = 172.86, 136.76, 132.18, 70.18, 69.58, 69.45, 69.09, 49.35, 45.59, 45.37, 43.25, 42.08, 38.55,  
9 32.02, 29.09, 28.35, 26.13, 24.94.

10 **HRMS (ESI)** calc. for C<sub>18</sub>H<sub>31</sub>ClNO<sub>3</sub><sup>+</sup> [M+H]<sup>+</sup>: 344.1987; found 344.1989.

11

12 **1.3.3 2-((1S,4S)-bicyclo[2.2.1]hept-5-en-2-yl)-N-(2-(2-((6-chlorohexyl)oxy)ethoxy)ethyl)acetamide (CA-Nor2)**



13  
14 Reaction was conducted according to general procedure A using CA-NH<sub>2</sub> and 2-((1S,4S)-bicyclo[2.2.1]hept-5-en-2-yl)acetic acid  
15 (5.6 μL, 32.6 μmol) yielding 6.4 mg (17.9 μmol) of the desired product as a colorless oil in 60% yield.

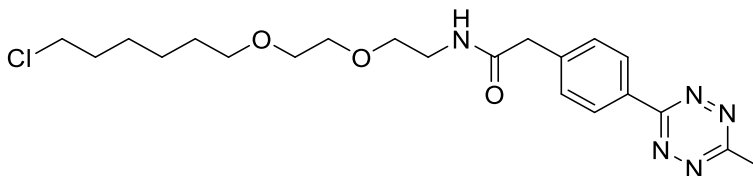
16 **<sup>1</sup>H NMR** (400 MHz, DMSO-*d*<sub>6</sub>) δ [ppm] = 7.73 (t, *J* = 5.7 Hz, 1H), 6.15 (dd, *J* = 5.8, 3.0 Hz, 1H), 5.95 (dd, *J* = 5.8, 2.9 Hz, 1H), 3.62 (t,  
17 *J* = 6.6 Hz, 2H), 3.47 – 3.36 (m, 8H), 3.23 – 3.09 (m, 2H), 2.76 – 2.68 (m, 2H), 2.40 – 2.29 (m, 1H), 1.89 – 1.74 (m, 3H), 1.74 – 1.65  
18 (m, 2H), 1.53 – 1.43 (m, 2H), 1.39 – 1.17 (m, 6H), 0.47 (m, *J* = 11.5, 4.4, 2.6 Hz, 1H).

19 **<sup>13</sup>C NMR** (101 MHz, DMSO-*d*<sub>6</sub>) δ [ppm] = 171.61, 136.88, 132.47, 70.15, 69.52, 69.42, 69.08, 49.03, 45.32, 45.13, 42.02, 40.58, 40.14,  
20 39.93, 39.73, 39.51, 39.31, 39.10, 38.89, 38.35, 35.06, 31.99, 31.37, 29.04, 26.08, 24.89.

21 **HRMS (ESI)** calc. for C<sub>19</sub>H<sub>32</sub>ClNNaO<sub>3</sub><sup>+</sup> [M+Na]<sup>+</sup>: 380.1963; found 380.1963.

22

23 **1.3.4 N-(2-(2-((6-chlorohexyl)oxy)ethoxy)ethyl)-2-(4-(6-methyl-1,2,4,5-tetrazin-3-yl)phenyl)acetamide (CA-Tz)**



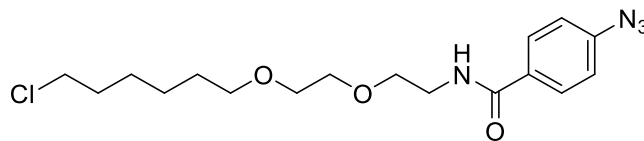
24  
25 Reaction was conducted according to general procedure A using CA-NH<sub>2</sub> and 2-(4-(6-methyl-1,2,4,5-tetrazin-3-yl)phenyl)acetic acid  
26 (7.5 mg, 32.6 μmol) yielding 7.4 mg (17.0 μmol) of the desired product as a rose solid in 57% yield.

27 **<sup>1</sup>H NMR** (400 MHz, DMSO-*d*<sub>6</sub>) δ [ppm] = 8.44 – 8.36 (m, 2H), 8.23 (t, *J* = 5.6 Hz, 1H), 7.58 – 7.50 (m, 2H), 3.61 (t, *J* = 6.6 Hz, 2H),  
28 3.56 (s, 2H), 3.53 – 3.40 (m, 6H), 3.36 (t, *J* = 6.6 Hz, 2H), 3.23 (q, *J* = 5.7 Hz, 2H), 2.99 (s, 3H), 1.75 – 1.62 (m, 2H), 1.53 – 1.42 (m,  
29 2H), 1.42 – 1.25 (m, 4H).

30 **<sup>13</sup>C NMR** (101 MHz, DMSO-*d*<sub>6</sub>) δ [ppm] = 169.58, 167.05, 163.22, 141.29, 130.05, 130.00, 127.28, 70.20, 69.60, 69.45, 69.05, 45.37,  
31 42.19, 38.79, 32.02, 29.07, 26.12, 24.93, 20.83.

32 **HRMS (ESI)** calc. for C<sub>21</sub>H<sub>31</sub>ClN<sub>5</sub>O<sub>3</sub><sup>+</sup> [M+H]<sup>+</sup>: 436.2110; found 436.2113.

1 **1.3.5 4-azido-N-(2-(2-((6-chlorohexyl)oxy)ethoxy)ethyl)benzamide (CA-PhN<sub>3</sub>)**



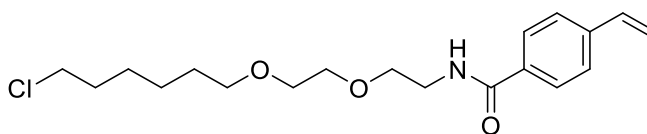
2  
3 Reaction was conducted according to general procedure A using CA-NH<sub>2</sub> and 4-azidobenzoic acid (5.3 mg, 32.6 μmol) to obtain 6.1 mg  
4 (15.5 μmol) of the desired product as a colorless oil in 56% yield.

5 <sup>1</sup>H NMR (400 MHz, DMSO-*d*<sub>6</sub>) δ [ppm] = 8.52 (t, *J* = 5.6 Hz, 1H), 7.90 (d, *J* = 8.6 Hz, 2H), 7.20 (d, *J* = 8.6 Hz, 2H), 3.60 (t, *J* = 6.6 Hz,  
6 2H), 3.56 – 3.49 (m, 4H), 3.50 – 3.44 (m, 2H), 3.44 – 3.30 (m, 4H), 1.74 – 1.61 (m, 2H), 1.51 – 1.39 (m, 2H), 1.40 – 1.20 (m, 4H).

7 <sup>13</sup>C NMR (101 MHz, DMSO-*d*<sub>6</sub>) δ [ppm] = 165.23, 142.19, 130.95, 129.06, 118.85, 70.17, 69.62, 69.40, 68.84, 45.35, 39.21, 32.00,  
8 29.07, 26.12, 24.91.

9 HRMS (ESI) calc. for C<sub>17</sub>H<sub>25</sub>ClN<sub>4</sub>NaO<sub>3</sub><sup>+</sup> [M+Na]<sup>+</sup>: 391.1507; found 391.1511.

10 **1.3.5.1 N-(2-(2-((6-chlorohexyl)oxy)ethoxy)ethyl)-4-vinylbenzamide (CA-Vbn)**



11  
12 Reaction was conducted according to general procedure A using CA-NH<sub>2</sub> and 4-vinylbenzoic acid (4.8 mg, 32.6 μmol) to obtain 7.5 mg  
13 (21.2 μmol) of the desired product as a colorless oil in 72% yield.

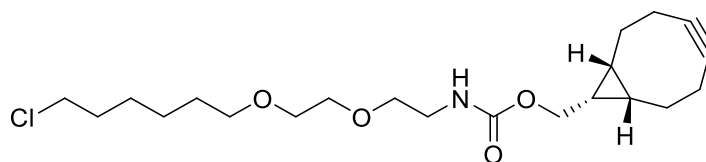
14 <sup>1</sup>H NMR (400 MHz, DMSO-*d*<sub>6</sub>) δ [ppm] = 8.49 (t, *J* = 5.6 Hz, 1H), 7.83 (d, *J* = 8.2 Hz, 2H), 7.55 (d, *J* = 8.2 Hz, 2H), 6.78 (dd, *J* = 17.7,  
15 10.9 Hz, 1H), 5.94 (d, *J* = 17.7 Hz, 1H), 5.36 (d, *J* = 10.9 Hz, 1H), 3.62 – 3.57 (m, 2H), 3.55 – 3.51 (m, 4H), 3.49 – 3.45 (m, 2H), 3.44  
16 – 3.37 (m, 4H), 1.73 – 1.59 (m, 2H), 1.50 – 1.40 (m, 2H), 1.40 – 1.24 (m, 4H).

17 <sup>13</sup>C NMR (101 MHz, DMSO-*d*<sub>6</sub>) δ [ppm] = 166.28, 140.15, 136.39, 134.03, 127.99, 126.41, 116.59, 70.66, 70.11, 69.88, 69.33, 45.84,  
18 39.67, 32.48, 29.55, 26.59, 25.39.

19 HRMS (ESI) calc. for C<sub>19</sub>H<sub>28</sub>ClNNaO<sub>3</sub><sup>+</sup> [M+Na]<sup>+</sup>: 376.1650; found 376.1640.

20

21 **1.3.6 ((1*R*,8*S*,9*S*)-bicyclo[6.1.0]non-4-yn-9-yl)methyl (2-(2-((6-chlorohexyl)oxy)ethoxy)ethyl)carbamate (CA-BCN)**



22  
23 BCN-NHS (14.0 mg, 47.6 μmol, 1.1 eq) was dissolved in 500 μL DMSO. DIPEA (71.4 μL, 432 μmol, 10 equiv.) was added followed by  
24 CA-NH<sub>2</sub> (14.0 mg, 43.2 μmol, 1.0 equiv.) solubilized in DMSO. The solution was stirred for 30 min. The crude product was purified by  
25 preparative HPLC eluted with MeCN / H<sub>2</sub>O (0.1% TFA) (50% - 90% MeCN over 60 min) to obtain 11.9 mg (29.8 μmol) of the product  
26 as a clear oil in 69% yield after lyophilization.

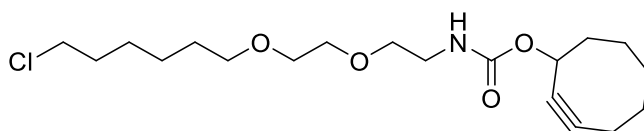
27 <sup>1</sup>H NMR (400 MHz, DMSO-*d*<sub>6</sub>): δ = 7.07 (t, *J*=5.7, 1H), 4.03 (d, *J*=8.0, 2H), 3.62 (t, *J*=6.6, 2H), 3.52 – 3.44 (m, 4H), 3.38 (dt, *J*=11.3,  
28 6.3, 4H), 3.11 (q, *J*=6.0, 2H), 2.30 – 2.06 (m, 6H), 1.78 – 1.64 (m, 2H), 1.59 – 1.42 (m, 4H), 1.41 – 1.19 (m, 4H), 0.95 – 0.78 (m, 2H).

29 <sup>13</sup>C NMR (100 MHz, DMSO-*d*<sub>6</sub>): δ = 156.4, 99.0, 70.2, 69.5, 69.4, 69.1, 61.3, 45.4, 40.1, 32.0, 29.1, 28.6, 26.1, 24.9, 20.8, 19.5, 17.6.

30 HRMS (ESI) calc. for [M+H]<sup>+</sup>: 400.2249, found 400.2250.

31

32 **1.3.6.1 Cyclooct-2-yn-1-yl (2-(2-((6-chlorohexyl)oxy)ethoxy)ethyl)carbamate (CA-SCO)**



33

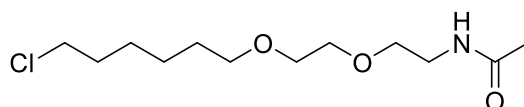
1 CA-NH<sub>2</sub> (15 mg, 44.4 μmol, 1.3 equiv.) was dissolved in dry DMSO (0.15 mL) and a solution of cyclooct-2-yn-1-yl (4-nitrophenyl)  
2 carbonate (10 mg, 34.2 μmol, 1.0 equiv.) in dry DMF (0.4 mL) was added followed by DIPEA (58 μL, 348 μmol: 10.2 equiv.). The  
3 reaction mixture was stirred at r.t. for 1 h. The resulted mixture was acidified with 50 μL of acetic acid and afterwards purified by semi-  
4 preparative HPLC eluted with MeCN / H<sub>2</sub>O (0.1% TFA) (15% MeCN for 2 min., then 15 - 100% MeCN over 25 min., followed by 100%  
5 MeCN for 15 min.) to give 8.7 mg (23.3 μmol) of the desired product as a colorless oil in 68% yield after lyophilization.

6 <sup>1</sup>H NMR (400 MHz, DMSO-*d*<sub>6</sub>) δ [ppm] = 7.18 (t, *J* = 5.9 Hz, 1H), 5.18 – 5.09 (m, 1H), 3.62 (t, *J* = 6.6 Hz, 2H), 3.50 – 3.43 (m, 4H),  
7 3.40 – 3.34 (m, 4H), 3.09 (q, *J* = 5.9 Hz, 2H), 2.30 – 2.00 (m, 3H), 1.93 – 1.78 (m, 3H), 1.76 – 1.65 (m, 3H), 1.64 – 1.54 (m, 2H), 1.53  
8 – 1.43 (m, 3H), 1.42 – 1.25 (m, 4H).

9 <sup>13</sup>C NMR (101 MHz, DMSO-*d*<sub>6</sub>) δ [ppm] = 155.29, 100.82, 91.79, 70.19, 69.53, 69.42, 68.99, 65.70, 45.38, 41.59, 40.07, 33.85, 32.03,  
10 29.21, 29.06, 26.13, 25.78, 24.94, 19.95.

11 HRMS (ESI) calc. for C<sub>19</sub>H<sub>32</sub>ClNNaO<sub>4</sub><sup>+</sup> [M+Na]<sup>+</sup>; 396.1912; found 396.1923.

### 13 1.3.7 *N*-(2-(2-((6-chlorohexyl)oxy)ethoxy)ethyl)acetamide (CA-Ac)



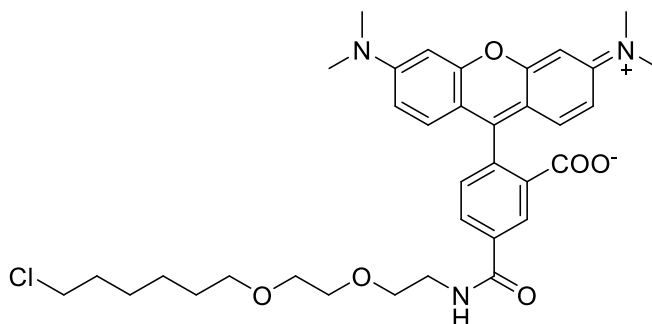
14 Tert-butyl (2-(2-((6-chlorohexyl)oxy)ethoxy)ethyl)carbamate (301 mg, 0.93 μmol, 1.0 equiv.) was deprotected by addition of TFA (2 mL)  
15 and afterwards dried under a stream of pressured air for 15 min. DIPEA (307 μL, 1.86 mmol, 2.0 equiv.) and DMSO (333 μL) were  
16 added followed by dropwise addition of acetic anhydride (131 μL, 1.39 mmol, 1.5 equiv.) while stirring. The reaction was stirred at r.t  
17 for 1 h. The mixture was quenched with saturated solution of NaHCO<sub>3</sub> (20 mL) and extracted with DCM (3 × 20 mL). The combined  
18 organic layers were washed with brine and dried over MgSO<sub>4</sub>. All volatiles were evaporated and the crude product was purified over  
19 normal phase flash chromatography (MeOH: DCM = 2% : 98% to 3% : 97%). The fractions containing the product were combined to  
20 give 238 mg (896 μmol) of the desired product as a colorless oil in 97% yield after evaporation.

21 <sup>1</sup>H NMR (400 MHz, CDCl<sub>3</sub>) δ [ppm] = 6.05 (s, 1H), 3.67 – 3.38 (m, 12H), 1.98 (s, 3H), 1.83 – 1.71 (m, 2H), 1.61 (p, *J* = 6.8 Hz, 2H),  
22 1.52 – 1.31 (m, 4H).

23 <sup>13</sup>C NMR (101 MHz, CDCl<sub>3</sub>) δ [ppm] = 169.92, 71.09, 70.07, 69.83, 69.60, 44.84, 39.10, 32.32, 29.28, 26.49, 25.24, 23.10.

24 HRMS (ESI) calc. for C<sub>12</sub>H<sub>25</sub>ClNO<sub>3</sub><sup>+</sup> [M+H]<sup>+</sup>: 266.1517; found 266.1518.

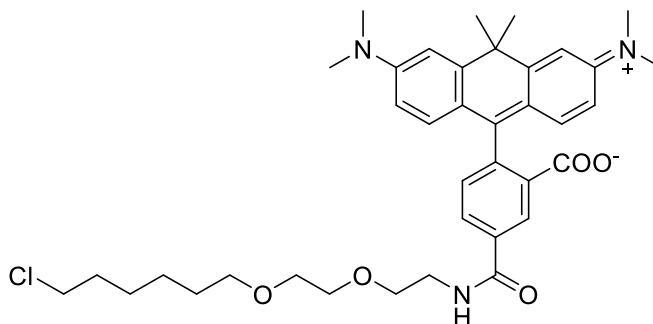
### 27 1.3.1 5-((2-(2-((6-chlorohexyl)oxy)ethoxy)ethyl)carbamoyl)-2-(6-(dimethylamino)-3-(dimethyliminio)-3H-xanthen-9- 28 yl)benzoate (CA-5-TMR)



29 To a solution of TMR-5-COOH (2.5 mg, 5.81 μmol, 1.0 equiv.) in dry DMSO (500 μL), benzotriazolylxytris(dimethylamino)-  
30 phosphonium hexafluorophosphat (BOP) (0.5 M in DMSO, 16.4 μL, 8.21 μmol, 1.5 equiv.) was added and the reaction was shaken at  
31 500 rpm and r.t. for 5 min. DIPEA (3.84 μL, 23.2 μmol, 4.0 equiv.) and CA-NH<sub>2</sub> (1 M in DMSO, 8.71 μL, 8.71 μmol, 1.5 equiv.) were  
32 added and the reaction was shaken at 500 rpm and r.t. for 4 h. The crude product was acidified with acetic acid and purified over  
33 preparative HPLC eluted with MeCN / H<sub>2</sub>O (0.1% FA) (10% - 90% MeCN over 50 min) to give 1.2 mg (1.89 μmol) of the desired product in  
34 33% yield after lyophilization.

35 HRMS (ESI): calc. for C<sub>36</sub>H<sub>44</sub>N<sub>2</sub>O<sub>6</sub>Cl<sup>+</sup> [M+H]<sup>+</sup>: 635.2887; found 635.2882.

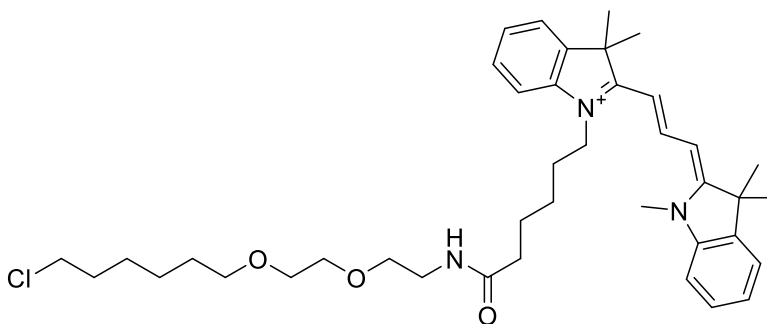
1 **1.3.2 5-((2-(2-((6-chlorohexyl)oxy)ethoxy)ethyl)carbamoyl)-2-(6-(dimethylamino)-3-(dimethyliminio)-10,10-dimethyl-3,10-**  
2 **dihydroanthracen-9-yl)benzoate (CA-5-CPY)**



3  
4 To a solution of CPY-5-COOH (2.5 mg, 5.48  $\mu\text{mol}$ , 1.0 equiv.) in dry DMSO (1 mL), BOP (0.5 M in DMSO, 16.4  $\mu\text{L}$ , 8.21  $\mu\text{mol}$ , 1.5  
5 equiv.) was added and the reaction was shaken at 500 rpm and r.t. for 5 min. DIPEA (3.62  $\mu\text{L}$ , 21.9  $\mu\text{mol}$ , 4.0 equiv.) and CA-NH<sub>2</sub> (1 M  
6 in DMSO, 8.21  $\mu\text{L}$ , 8.21  $\mu\text{mol}$ , 1.5 equiv.) were added and the reaction was shaken at 500 rpm and r.t. for 4 h. The crude product was  
7 acidified with acetic acid and purified over preparative HPLC eluted with MeCN / H<sub>2</sub>O (0.1% FA) (10% - 90% MeCN over 50 min) to  
8 give 0.38 mg (0.57  $\mu\text{mol}$ ) of the desired product in 10% yield after lyophilization.

9 **HRMS** (ESI): calc. for C<sub>38</sub>H<sub>49</sub>N<sub>3</sub>O<sub>5</sub>Cl<sup>+</sup> [M+H]<sup>+</sup>: 662.3360; found 662.3349.

10  
11 **1.3.3 1-(6-((2-(2-((6-chlorohexyl)oxy)ethoxy)ethyl)amino)-6-oxohexyl)-3,3-dimethyl-2-((E)-3-((Z)-1,3,3-trimethylindolin-2-**  
12 **ylidene)prop-1-en-1-yl)-3H-indol-1-ium (CA-Cy3)**



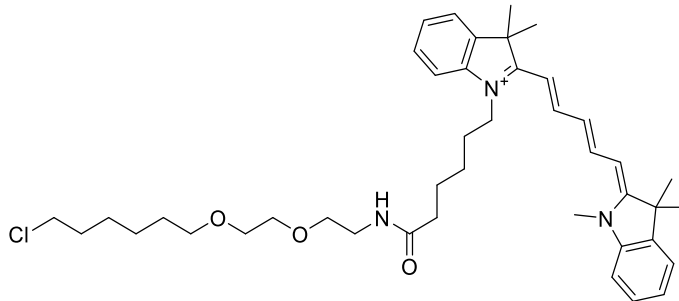
13  
14 Cy3-COOH was synthesized according to Ueno et al. 2010 (3). To a solution of Cy3-COOH (100 mg, 219  $\mu\text{mol}$ , 1.0 equiv.) in dry  
15 DMSO (2 mL), DIPEA (217  $\mu\text{L}$ , 1.3 mmol, 6.0 equiv.) and TSTU (92.1 mg, 306  $\mu\text{mol}$ , 1.4 equiv.) were added and the reaction mixture  
16 was stirred for 10 min. at r.t. CA-NH<sub>2</sub> (58 mg, 262  $\mu\text{mol}$ , 1.2 equiv.) in 0.5 mL DMSO was added and the reaction was stirred for 30  
17 min, at r.t. The reaction was quenched by addition of acetic acid (230  $\mu\text{L}$ ) and 10% H<sub>2</sub>O, followed by purification over preparative HPLC  
18 eluted with MeCN / H<sub>2</sub>O (0.1% FA) (10% - 90% MeCN over 60 min) to give 102 mg (154  $\mu\text{mol}$ ) of the desired product in 70% yield  
19 after lyophilization.

20 **HRMS** (ESI): calc. for C<sub>40</sub>H<sub>57</sub>N<sub>3</sub>O<sub>3</sub>Cl<sup>+</sup> [M]<sup>+</sup>: 662.4083; found 662.4084.

21



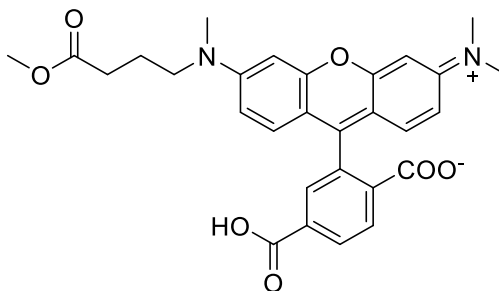
1 **1.3.4 1-(6-((2-(2-((6-chlorohexyl)oxy)ethoxy)ethyl)amino)-6-oxohexyl)-3,3-dimethyl-2-((1E,3E)-5-((Z)-1,3,3-**  
2 **trimethylindolin-2-ylidene)penta-1,3-dien-1-yl)-3H-indol-1-ium (CA-Cy5)**



3  
4 Cy5-COOH was synthesized according to Ueno et al. 2010 (3). To a solution of Cy5-COOH (100 mg, 207  $\mu\text{mol}$ , 1.0 equiv.) in dry  
5 DMSO (2 mL), DIPEA (205  $\mu\text{L}$ , 1.24 mmol, 6.0 equiv.) and TSTU (87.1 mg, 289  $\mu\text{mol}$ , 1.4 equiv.) were added and the reaction mixture  
6 was stirred for 10 min. at r.t. CA-NH<sub>2</sub> (55.5 mg, 248  $\mu\text{mol}$ , 1.2 equiv.) in 0.5 mL DMSO was added and the reaction was stirred for 30  
7 min, at r.t. The reaction was quenched by addition of acetic acid (291  $\mu\text{L}$ ) and 10% H<sub>2</sub>O, followed by purification over preparative HPLC  
8 eluted with MeCN / H<sub>2</sub>O (0.1% FA) (10% - 90% MeCN over 60 min) to give 98 mg (142  $\mu\text{mol}$ ) of the desired product in 69% yield after  
9 lyophilization.

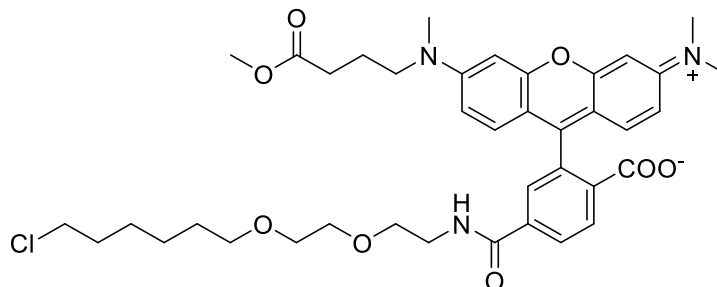
10 **HRMS** (ESI): calc. for C<sub>42</sub>H<sub>59</sub>N<sub>3</sub>O<sub>3</sub>Cl<sup>+</sup> [M]<sup>+</sup>: 688.4239; found 688.4239.

11  
12 **1.3.5 4-carboxy-2-(3-(dimethyliminio)-6-((4-methoxy-4-oxobutyl)(methyl)amino)-3H-xanthen-9-yl)benzoate (CA-TMR-**  
13 **biotin-1)**



14  
15 The compound was synthesized according to the procedure from Masharina et al. 2012 (15).

17 **1.3.6 4-((2-(2-((6-chlorohexyl)oxy)ethoxy)ethyl)carbamoyl)-2-(3-(dimethyliminio)-6-((4-methoxy-4-**  
18 **oxobutyl)(methyl)amino)-3H-xanthen-9-yl)benzoate (CA-TMR-biotin-2)**

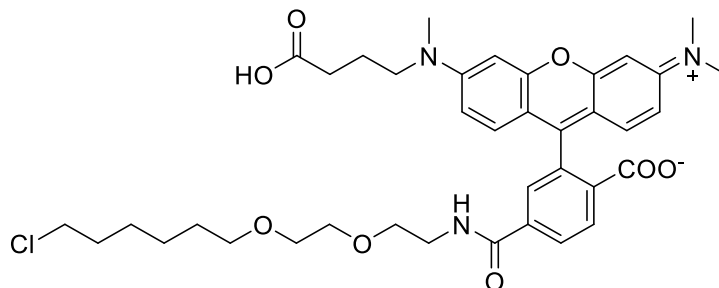


19  
20 To a solution of CA-TMR-biotin-1 (17.0 mg, 32.9  $\mu\text{mol}$ , 1.0 equiv.) in dry DMF, TSTU (11.9 mg, 39.5  $\mu\text{mol}$ , 1.2 equiv.) and DIPEA (32.6  
21  $\mu\text{L}$ , 197  $\mu\text{mol}$ , 6.0 equiv.) were added and the reaction was stirred at r.t. for 5 min. CA-NH<sub>2</sub> (14.7 mg, 65.8  $\mu\text{mol}$ , 2.0 equiv.) was added  
22 and the reaction was stirred at r.t. for 2 h. The crude product was acidified with acetic acid and purified via preparative eluted with  
23 MeCN / H<sub>2</sub>O (0.1% TFA) (10% - 90% MeCN over 50 min) to give 10 mg (13.8  $\mu\text{mol}$ ) of the desired product in 42% yield after  
24 lyophilization.

1 **HRMS** (ESI): calc. for  $C_{39}H_{49}N_3O_8Cl^+$   $[M+H]^+$ : 722.3208; found 722.3202.

2

3 **1.3.7 2-(6-((3-carboxypropyl)(methyl)amino)-3-(dimethyliminio)-3H-xanthen-9-yl)-4-((2-(2-((6-**  
4 **chlorohexyl)oxy)ethoxy)ethyl)carbamoyl)benzoate (CA-TMR-biotin-3)**



5

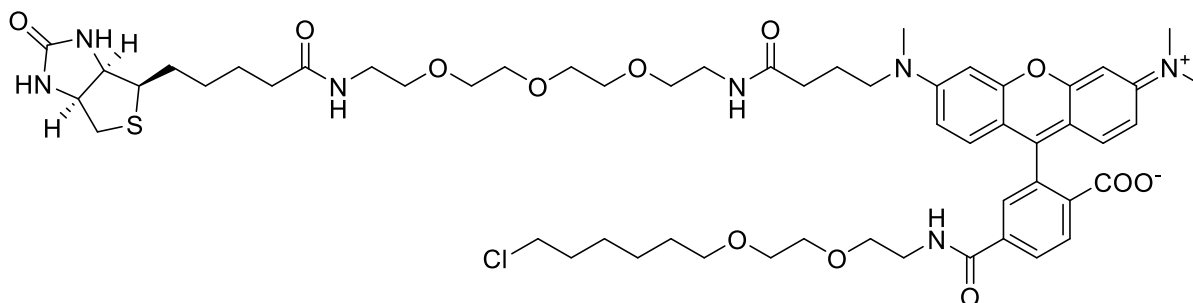
6

7 To a solution of CA-TMR-biotin-2 (8.0 mg, 11.1  $\mu$ mol, 1.0 equiv.) in THF:H<sub>2</sub>O (4:1), lithium hydroxide (1M in H<sub>2</sub>O, 22.2  $\mu$ L, 22.2  $\mu$ mol,  
8 2.0 equiv.) was added and the reaction was stirred at r.t. for 6 h. The crude product was acidified with acetic acid and purified via  
9 preparative HPLC eluted with MeCN / H<sub>2</sub>O (0.1% TFA) (10% - 90% MeCN over 50 min) to give 6.3 mg (8.9  $\mu$ mol) of the desired product  
10 in 80% yield after lyophilization.

11 **HRMS** (ESI): calc. for  $C_{39}H_{49}N_3O_8Cl^+$   $[M+H]^+$ : 708.3051; found 708.3049.

12

13 **1.3.8 4-((2-(2-((6-chlorohexyl)oxy)ethoxy)ethyl)carbamoyl)-2-(3-(dimethyliminio)-6-((4,18-dioxo-22-((3aR,4R,6aS)-2-**  
14 **oxohexahydro-1H-thieno[3,4-d]imidazol-4-yl)-8,11,14-trioxa-5,17-diazadocosyl)(methyl)amino)-3H-xanthen-9-**  
15 **yl)benzoate (CA-TMR-biotin)**



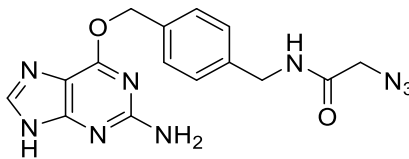
16

17 To a solution of CA-TMR-biotin-3 (6.0 mg, 8.47  $\mu$ mol, 1.0 equiv.) in dry DMF, TSTU (3.06 mg, 10.2  $\mu$ mol, 1.2 equiv.) and DIPEA (8.4  
18  $\mu$ L, 50.8  $\mu$ mol, 6.0 equiv.) were added and the reaction was stirred at r.t. for 5 min. Biotin-PEG3-NH<sub>2</sub> (7.09 mg, 16.9  $\mu$ mol, 2.0 equiv.)  
19 was added and the reaction was stirred at r.t. for another 2 h. The crude product was acidified with acetic acid and purified via  
20 preparative HPLC eluted with MeCN / H<sub>2</sub>O (0.1% TFA) (10% - 90% MeCN over 50 min) to give 6.2 mg (5.6  $\mu$ mol) of the desired product  
21 in 66% yield after lyophilization.

22 **HRMS** (ESI): calc. for  $C_{56}H_{80}N_7O_{12}ClS^{2+}$   $[M+2H]^{2+}$ : 554.7628; found 554.7632.

## 23 **1.4 SNAP substrates based on benzylguanine (BG)**

24 **1.4.1 N-(4-(((2-amino-9H-purin-6-yl)oxy)methyl)benzyl)-2-azidoacetamide (BG-N<sub>3</sub>)**



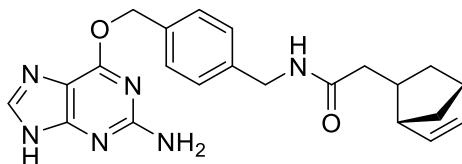
25

1 Reaction was conducted according to general procedure A using BG-NH<sub>2</sub> and 2-azidoacetic acid (40.7 μmol; 5.7 μL) and 11.1 mg  
2 (23.8 μmol) of the desired product were obtained as a colorless TFA-salt in 64% yield.

3 <sup>1</sup>H NMR (400 MHz, DMSO-*d*<sub>6</sub>) δ [ppm] = 8.65 (t, *J* = 5.9 Hz, 1H), 8.34 (s, 1H), 7.55 – 7.44 (m, 2H), 7.36 – 7.28 (m, 2H), 5.52 (s, 2H),  
4 4.31 (d, *J* = 5.9 Hz, 2H), 3.89 (s, 2H).

5 HRMS (ESI) calc. for C<sub>15</sub>H<sub>16</sub>N<sub>9</sub>O<sub>2</sub><sup>+</sup> [M+H]<sup>+</sup>: 354.1421; found 354.1423.

#### 7 1.4.2 *N*-(4-(((2-amino-9*H*-purin-6-yl)oxy)methyl)benzyl)-2-((1*S*,4*S*)-bicyclo[2.2.1]hept-5-en-2-yl)acetamide (BG-Nor2)



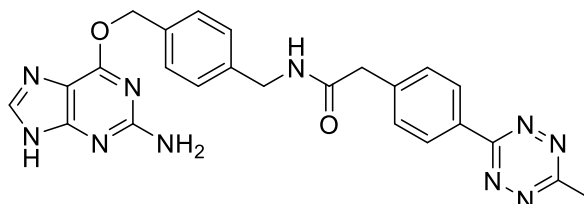
8  
9 Reaction was conducted according to general procedure A with a reduced reaction time of 15 min. using BG-NH<sub>2</sub> and 2-((1*S*,4*S*)-  
10 bicyclo[2.2.1]hept-5-en-2-yl)acetic acid (40.7 μmol; 7.0 μL) resulting in 15.9 mg (30.7 μmol) of the desired product as a colorless TFA-  
11 salt in 83% yield.

12 <sup>1</sup>H NMR (400 MHz, DMSO-*d*<sub>6</sub>) δ [ppm] = 8.47 (s, 1H), 8.29 (t, *J* = 6.0 Hz, 1H), 7.49 (d, *J* = 8.1 Hz, 2H), 7.27 (d, *J* = 8.1 Hz, 2H), 6.16  
13 (dd, *J* = 5.7, 3.0 Hz, 1H), 5.96 (dd, *J* = 5.7, 2.9 Hz, 1H), 5.53 (s, 2H), 4.25 (d, *J* = 6.0 Hz, 2H), 2.77 – 2.69 (m, 2H), 2.45 – 2.34 (m, 1H),  
14 1.95 (dd, *J* = 13.8, 7.6 Hz, 1H), 1.90 – 1.77 (m, 2H), 1.33 – 1.26 (m, 1H), 1.25 – 1.19 (m, 1H), 0.50 (m, *J* = 11.4, 4.5, 2.5 Hz, 1H).

15 <sup>13</sup>C NMR (101 MHz, DMSO-*d*<sub>6</sub>) δ [ppm] = 171.71, 158.83, 158.03, 153.44, 140.89, 140.30, 137.07, 133.90, 132.45, 128.84, 127.13,  
16 68.12, 49.10, 45.26, 42.09, 41.71, 40.67, 35.15, 31.47.

17 HRMS (ESI) calc. for C<sub>22</sub>H<sub>25</sub>N<sub>6</sub>O<sub>2</sub><sup>+</sup> [M+H]<sup>+</sup>: 405.2034; found 405.2034.

#### 19 1.4.3 *N*-(4-(((2-amino-9*H*-purin-6-yl)oxy)methyl)benzyl)-2-(4-(6-methyl-1,2,4,5-tetrazin-3-yl)phenyl)acetamide (BG-Tz)



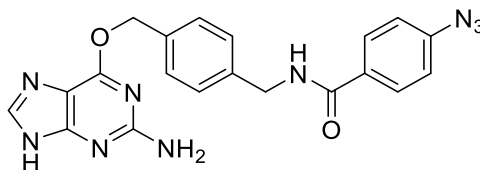
21 Reaction was conducted according to general procedure A using BG-NH<sub>2</sub> and 2-(4-(6-methyl-1,2,4,5-tetrazin-3-yl)phenyl)acetic acid  
22 (40.7 μmol, 9.4 mg) to give 12.4 mg (17.0 μmol) of the desired product as a rose TFA-salt in 56% yield.

23 <sup>1</sup>H NMR (400 MHz, DMSO-*d*<sub>6</sub>) δ [ppm] = 8.70 (t, *J* = 5.9 Hz, 1H), 8.45 – 8.39 (m, 2H), 8.37 (s, 1H), 7.60 – 7.53 (m, 2H), 7.52 – 7.44  
24 (m, 2H), 7.33 – 7.26 (m, 2H), 5.51 (s, 2H), 4.31 (d, *J* = 5.9 Hz, 2H), 3.64 (s, 2H), 2.99 (s, 3H), 2.54 (s, 3H).

25 <sup>13</sup>C NMR (101 MHz, DMSO-*d*<sub>6</sub>) δ [ppm] = 170.04, 167.53, 163.69, 159.37, 158.85, 158.53, 154.36, 141.59, 140.96, 140.84, 140.19,  
26 134.78, 130.62, 130.61, 129.34, 127.81, 68.28, 42.69, 40.90, 21.31.

27 HRMS (ESI) calc. for C<sub>24</sub>H<sub>23</sub>N<sub>10</sub>O<sub>2</sub><sup>+</sup> [M+H]<sup>+</sup>: 483.2000; found 483.2006.

#### 29 1.4.4 *N*-(4-(((2-amino-9*H*-purin-6-yl)oxy)methyl)benzyl)-4-azidobenzamide (BG-PhN<sub>3</sub>)



31 Reaction was conducted according to general procedure A with a reduced reaction time of 15 min. using BG-NH<sub>2</sub> and 4-azidobenzoic  
32 acid (6.6 mg, 40.7 μmol) to obtain 15.5 mg (29.3 μmol) of the desired product as a colorless TFA-salt in 79% yield.

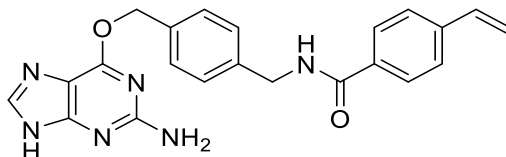
1 <sup>1</sup>H NMR (400 MHz, DMSO-*d*<sub>6</sub>) δ [ppm] = 9.10 (t, *J* = 5.9 Hz, 1H), 8.38 (s, 1H), 7.99 – 7.89 (m, 2H), 7.55 – 7.46 (m, 2H), 7.38 – 7.33  
2 (m, 2H), 7.25 – 7.16 (m, 2H), 5.52 (s, 2H), 4.48 (d, *J* = 5.9 Hz, 2H).

3 <sup>13</sup>C NMR (101 MHz, DMSO-*d*<sub>6</sub>) δ [ppm] = 165.27, 158.91, 158.61, 158.26, 153.77, 142.36, 140.57, 140.02, 134.19, 130.81, 129.15,  
4 128.89, 127.36, 118.96, 67.94, 42.48.

5 HRMS (ESI) calc. for C<sub>20</sub>H<sub>18</sub>N<sub>6</sub>O<sub>2</sub><sup>+</sup> [M+H]<sup>+</sup> : 416.1578; found 416.1577.

6

#### 7 1.4.5 *N*-(4-(((2-amino-9*H*-purin-6-yl)oxy)methyl)benzyl)-4-vinylbenzamide (BG-VBn)



8  
9 Reaction was conducted according to general procedure A with a reduced reaction time of 15 min. using BG-NH<sub>2</sub> and 4-vinylbenzoic  
10 acid (40.7 μmol; 6.5 mg) to obtain 14.7 mg (28.6 μmol) of the desired product as a colorless TFA-salt in 77% yield.

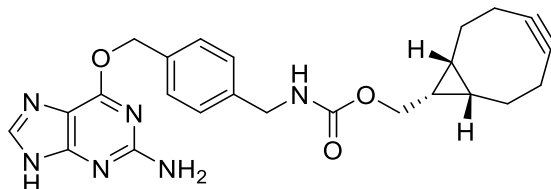
11 <sup>1</sup>H NMR (400 MHz, DMSO-*d*<sub>6</sub>) δ [ppm] = 9.09 (t, *J* = 6.0 Hz, 1H), 8.44 (s, 1H), 7.87 (d, *J* = 8.3 Hz, 2H), 7.57 (d, *J* = 8.3 Hz, 2H), 7.51  
12 (d, *J* = 7.9 Hz, 2H), 7.36 (d, *J* = 7.9 Hz, 2H), 6.79 (dd, *J* = 17.7, 11.0 Hz, 1H), 5.95 (d, *J* = 17.7 Hz, 1H), 5.53 (s, 2H), 5.37 (d, *J* = 11.0  
13 Hz, 1H), 4.49 (d, *J* = 6.0 Hz, 2H).

14 <sup>13</sup>C NMR (101 MHz, DMSO-*d*<sub>6</sub>) δ [ppm] = 165.81, 158.85, 158.62, 158.28, 153.55, 140.79, 140.13, 139.84, 135.91, 134.06, 133.43,  
15 128.92, 127.61, 127.35, 126.03, 116.24, 68.09, 42.46.

16 HRMS (ESI) calc. for C<sub>22</sub>H<sub>21</sub>N<sub>6</sub>O<sub>2</sub><sup>+</sup> [M+H]<sup>+</sup>: 401.1721; found 401.1707.

17

#### 18 1.4.6 ((1*R*,8*S*,9*S*)-bicyclo[6.1.0]non-4-yn-9-yl)methyl 4-(((2-amino-9*H*-purin-6-yl)oxy)methyl)benzyl)carbamate (BG-BCN)



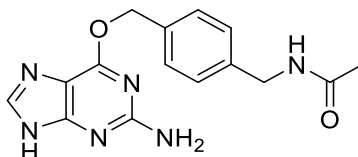
19  
20 A solution of ((1*R*,8*S*,9*S*)-bicyclo[6.1.0]non-4-yn-9-yl)methyl (2,5-dioxopyrrolidin-1-yl) carbonate (10 mg, 34.3 μmol, 1.0 equiv.) in dry  
21 DMSO (0.4 mL) was added to a solution of 10.2 mg BG-NH<sub>2</sub> (37.8 μmol, 1.1 equiv.) in dry DMSO (0.1 mL) followed by 28.4 μL of  
22 DIPEA (172 μmol, 5 equiv.). The reaction was stirred at r.t. for 30 min. The resulted mixture was acidified with acetic acid (3 μL) and  
23 H<sub>2</sub>O (53 μL), then purified by semi-preparative HPLC eluted with MeCN / H<sub>2</sub>O (0.1% TFA) (10% MeCN for 10 min., then 10 - 90%  
24 MeCN over 55 min. followed by 99% MeCN for 5 min.) to give 14.0 mg (31.4 μmol) of the desired product as a colorless solid in 91%  
25 yield after lyophilization.

26 <sup>1</sup>H NMR (400 MHz, DMSO-*d*<sub>6</sub>) δ [ppm] = 8.36 (s, 1H), 7.70 (t, *J* = 6.2 Hz, 1H), 7.52 – 7.46 (m, 2H), 7.28 (d, *J* = 8.0 Hz, 2H), 5.51 (s,  
27 2H), 4.18 (d, *J* = 6.0 Hz, 2H), 4.06 (d, *J* = 8.0 Hz, 2H), 2.28 – 2.07 (m, 6H), 1.52 (d, *J* = 12.4 Hz, 2H), 1.28 (dt, *J* = 18.3, 9.1 Hz, 1H),  
28 0.86 (t, *J* = 9.8 Hz, 2H).

29 HRMS (ESI) calc. for C<sub>24</sub>H<sub>27</sub>N<sub>6</sub>O<sub>3</sub><sup>+</sup> [M+H]<sup>+</sup>: 447.2139; found 447.2135.

30

#### 31 1.4.6.1 *N*-(4-(((2-amino-9*H*-purin-6-yl)oxy)methyl)benzyl)acetamide (BG-Ac)



32  
33 BG-NH<sub>2</sub> (300 mg, 1.11 mmol, 1.0 equiv.) was dissolved in dry DMSO (2.5 mL) and 367 μL of DIPEA (2.22 mmol, 2.0 equiv.) was added  
34 followed by dropwise addition of acetic anhydride (156 μL, 1.66 mmol, 1.5 equiv.) while stirring. The reaction mixture was stirred at r.t.

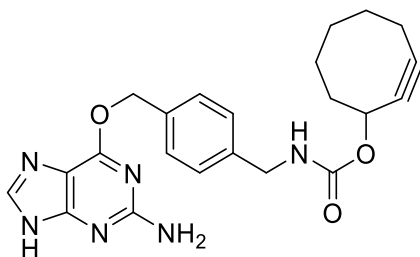
1 for 1 h. Afterwards, the reaction was quenched with acetic acid (387  $\mu$ L) and H<sub>2</sub>O (341  $\mu$ L) followed by centrifugation at 3'000 rpm for  
2 3 min. The pellet was washed twice with H<sub>2</sub>O and afterwards lyophilized to obtain 190 mg (608  $\mu$ mol) of the desired product as a  
3 colorless solid in 55% yield.

4 **<sup>1</sup>H NMR** (400 MHz, DMSO-*d*<sub>6</sub>)  $\delta$  [ppm] = 8.30 (s, 1H), 7.45 (d, *J* = 8.1 Hz, 2H), 7.27 (d, *J* = 7.9 Hz, 2H), 6.82 (s, 2H), 5.48 (s, 2H), 4.24  
5 (d, *J* = 5.9 Hz, 2H), 1.86 (s, 3H).

6 **HRMS** (ESI) calc. for C<sub>15</sub>H<sub>17</sub>N<sub>6</sub>O<sub>2</sub><sup>+</sup> [M+H]<sup>+</sup>: 313.1408; found 313.1406.

7

#### 8 1.4.7 Cyclooct-2-yn-1-yl 4-(((2-amino-9H-purin-6-yl)oxy)methyl)benzyl)carbamate (BG-SCO)



9  
10 BG-NH<sub>2</sub> (10 mg, 37.0  $\mu$ mol, 1.0 equiv.) was dissolved in dry DMSO (0.5 mL) and a solution of cyclooct-2-yn-1-yl (4-nitrophenyl)  
11 carbonate (10.7 mg, 37  $\mu$ mol, 1.0 equiv.) in dry DMF (0.4 mL) was added followed by DIPEA (30.6  $\mu$ L, 142  $\mu$ mol: 5.0 equiv.). The  
12 reaction mixture was stirred at r.t. for 1 h. The resulted mixture was acidified with acetic acid (25  $\mu$ L) and afterwards purified by semi-  
13 preparative HPLC eluted with MeCN / H<sub>2</sub>O (0.1% TFA) (15% MeCN for 5 min., then 15 - 100% MeCN over 25 min., followed by 100%  
14 MeCN for 15 min.) to give 16 mg (23.3  $\mu$ mol) of the desired product as a colorless TFA-salt in 81% yield after lyophilization.

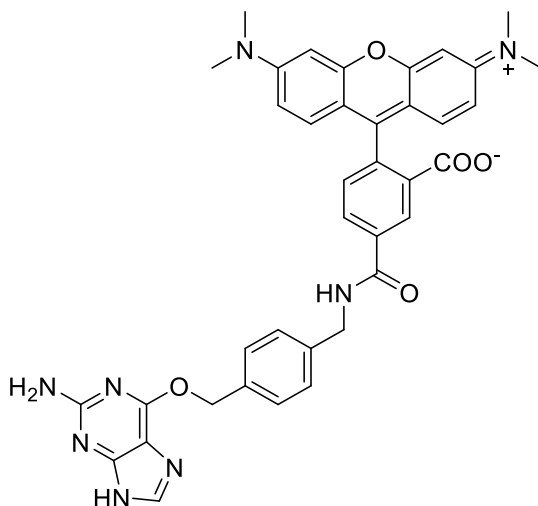
15 **<sup>1</sup>H NMR** (400 MHz, DMSO-*d*<sub>6</sub>)  $\delta$  [ppm] = 8.44 (s, 1H), 7.81 (t, *J* = 6.1 Hz, 1H), 7.50 (d, *J* = 8.0 Hz, 2H), 7.28 (d, *J* = 8.0 Hz, 2H), 5.52  
16 (s, 2H), 5.20 – 5.11 (m, 1H), 4.17 (d, *J* = 6.1 Hz, 2H), 2.30 – 2.02 (m, 3H), 1.96 – 1.85 (m, 1H), 1.89 – 1.76 (m, 2H), 1.76 – 1.64 (m,  
17 1H), 1.64 – 1.53 (m, 2H), 1.55 – 1.41 (m, 1H).

18 **<sup>13</sup>C NMR** (101 MHz, DMSO-*d*<sub>6</sub>)  $\delta$  [ppm] = 158.86, 158.10, 155.53, 153.58, 140.80, 140.06, 134.15, 128.90, 127.16, 107.66, 100.97,  
19 91.76, 68.06, 65.95, 43.50, 41.58, 33.85, 29.21, 25.79, 19.95.

20 **HRMS** (ESI) calc. for C<sub>22</sub>H<sub>24</sub>N<sub>6</sub>NaO<sub>3</sub><sup>+</sup> [M+Na]<sup>+</sup>: 443.1802; found 443.1797.

21

#### 22 1.4.8 5-(((4-(((2-amino-9H-purin-6-yl)oxy)methyl)benzyl)carbamoyl)-2-(6-(dimethylamino)-3-(dimethyliminio)-2,3,4,4a- 23 tetrahydro-1H-xanthen-9-yl)benzoate (BG-5-TMR)



24  
25 TSTU (1.45 mg, 4.82  $\mu$ mol, 1.2 equiv.) was dissolved in dry DMSO-*d*<sub>6</sub> (500  $\mu$ L). TMR-5-COOH (1.15 mg, 2.68  $\mu$ mol, 1.0 equiv.) was  
26 dissolved in the TSTU solution and DIPEA (1.77  $\mu$ L, 10.7  $\mu$ mol, 4.0 equiv.) was added. The mixture was stirred at r.t. for 10 min. BG-  
27 NH<sub>2</sub> (1.08 mg, 4.01  $\mu$ mol, 1.5 equiv.) was dissolved in dry DMSO-*d*<sub>6</sub> (200  $\mu$ L) and added to the reaction. The reaction mixture was

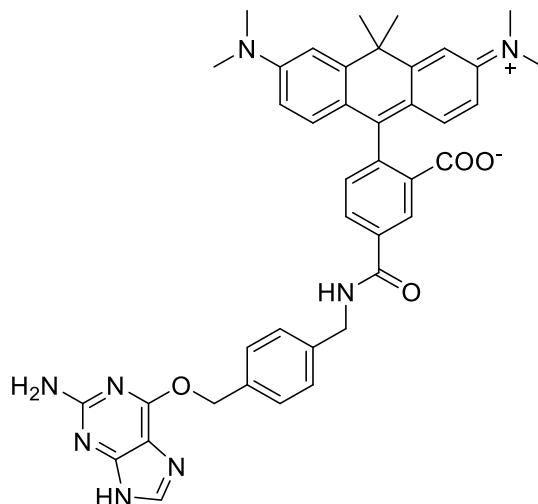
1 stirred at r.t. for 1 h. The compound was purified over preparative HPLC eluted with MeCN / H<sub>2</sub>O (0.1% TFA) (10% MeCN for 10 min.,  
2 then 10 - 90% MeCN over 40 min., followed by 90% MeCN for 5 min.) to give after lyophilization 378 μg (554 nmol) of the desired  
3 product in 21% yield.

4 **HRMS** (ESI): calc. for C<sub>38</sub>H<sub>37</sub>N<sub>6</sub>O<sub>5</sub> [M+2H]<sup>2+</sup> : 342.1399; found 342.1394.

5 **<sup>1</sup>H NMR** (TMR-5-COOH) (400 MHz, DMSO-*d*<sub>6</sub>) δ [ppm] = 8.39 (s, *J* = 1.5 Hz, 1H), 8.28 (dd, *J* = 8.1, 1.5 Hz, 1H), 7.33 (d, *J* = 8.0 Hz,  
6 1H), 6.58 – 6.45 (m, 6H), 2.95 (s, 12H).

7 **<sup>13</sup>C NMR** (TMR-5-COOH) (101 MHz, DMSO-*d*<sub>6</sub>) δ [ppm] = 168.31, 166.09, 152.03, 135.96, 132.76, 128.50, 109.05, 97.95, 40.15,  
8 39.99, 39.79.

9 **1.4.9 5-((4-(((2-amino-9H-purin-6-yl)oxy)methyl)benzyl)carbamoyl)-2-(6-(dimethylamino)-3-(dimethyliminio)-10,10-**  
10 **dimethyl-1,2,3,4,4a,10-hexahydroanthracen-9-yl)benzoate (BG-5-CPY)**

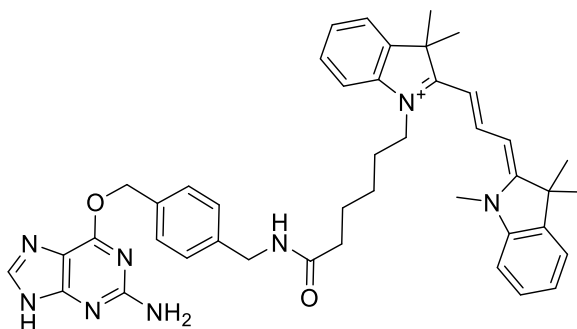


11  
12 TSTU (1.44 mg, 4.78 μmol, 1.2 equiv.) was dissolved in dry DMSO-*d*<sub>6</sub> (500 μL). CPY-5-COOH (2.0 mg, 4.38 μmol, 1.1 equiv.) was  
13 dissolved in the TSTU solution and DIPEA (2.63 μL, 15.9 μmol, 4 equiv.) was added. The mixture was stirred at r.t. for 10 min. BG-  
14 NH<sub>2</sub> (1.08 mg, 3.98 μmol, 1.5 equiv.) was dissolved in dry DMSO-*d*<sub>6</sub> (200 μL) and added to the reaction. The reaction mixture was  
15 stirred at r.t. for 1 h. The compound was purified over preparative HPLC eluted with MeCN / H<sub>2</sub>O (0.1% TFA) (10% MeCN for 10 min.,  
16 then 10 - 90% MeCN over 40 min., followed by 90% MeCN for 5 min.) to give 346 μg (488 nmol) of the desired product in 18% yield  
17 after lyophilization.

18 **HRMS** (ESI): calc. for C<sub>41</sub>H<sub>42</sub>N<sub>8</sub>O<sub>4</sub> [M+2H]<sup>2+</sup>: 355.1659; found 355.1659.

19

20 **1.4.9.1 1-(6-((4-(((2-amino-9H-purin-6-yl)oxy)methyl)benzyl)amino)-6-oxohexyl)-3,3-dimethyl-2-((E)-3-(Z)-1,3,3-**  
21 **trimethylindolin-2-ylidene)prop-1-en-1-yl)-3H-indol-1-ium (BG-Cy3)**



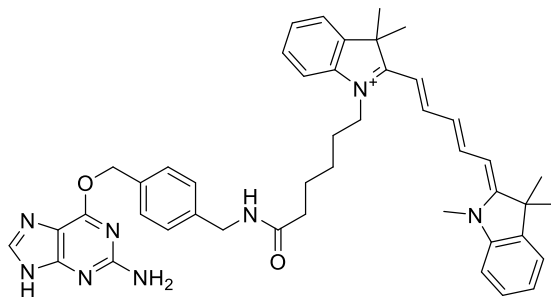
22  
23 Cy3-COOH was synthesized according to Ueno et al. 2010 (3). To a solution of Cy3-COOH (100 mg, 219 μmol, 1.0 equiv.) in dry  
24 DMSO (1.5 mL), DIPEA (217 μL, 1.3 mmol, 6.0 equiv.) and TSTU (92.1 mg, 306 μmol, 1.4 equiv.) were added and the reaction mixture  
25 was stirred for 10 min. at r.t. BG-NH<sub>2</sub> (70.9 mg, 262 μmol, 1.2 equiv.) was added and the reaction was stirred for 30 min. at r.t. The

1 reaction was quenched by addition of acetic acid (230  $\mu\text{L}$ ) and 10%  $\text{H}_2\text{O}$ , followed by purification over preparative HPLC eluted with  
2 MeCN /  $\text{H}_2\text{O}$  (0.1% FA) (10% - 90% MeCN over 60 min.) to give 28.5 mg (40.1  $\mu\text{mol}$ ) of the desired product in 18% yield after  
3 lyophilization.

4 **HRMS** (ESI): calc. for  $\text{C}_{43}\text{H}_{50}\text{N}_6\text{O}_2^{2+}$   $[\text{M}+\text{H}]^{2+}$ : 355.2023; found 355.2022.

5

6 **1.4.10 1-(6-(((4-(((2-amino-9H-purin-6-yl)oxy)methyl)benzyl)amino)-6-oxohexyl)-3,3-dimethyl-2-((1E,3E)-5-((Z)-1,3,3-**  
7 **trimethylindolin-2-ylidene)penta-1,3-dien-1-yl)-3H-indol-1-ium (BG-Cy5)**

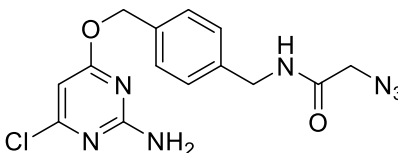


8  
9 Cy5-COOH was synthesized according to Ueno et al. 2010(3). To a solution of Cy5-COOH (50.0 mg, 103  $\mu\text{mol}$ , 1.0 equiv.) in dry  
10 DMSO (1.5 mL), DIPEA (103  $\mu\text{L}$ , 620  $\mu\text{mol}$ , 6.0 equiv.) and TSTU (43.6 mg, 145  $\mu\text{mol}$ , 1.4 equiv.) were added and the reaction mixture  
11 was stirred for 10 min. at r.t. BG-NH<sub>2</sub> (33.5 mg, 124  $\mu\text{mol}$ , 1.2 equiv.) was added and the reaction was stirred for 30 min. at r.t. The  
12 reaction was quenched by addition of acetic acid (109  $\mu\text{L}$ ) and 10%  $\text{H}_2\text{O}$ , followed by purification over preparative HPLC eluted with  
13 MeCN /  $\text{H}_2\text{O}$  (0.1% FA) (10% - 90% MeCN over 60 min.) to give 45 mg (61.1  $\mu\text{mol}$ ) of the desired product in 59% yield after  
14 lyophilization.

15 **HRMS** (ESI): calc. for  $\text{C}_{45}\text{H}_{52}\text{N}_8\text{O}_2^{2+}$   $[\text{M}+\text{H}]^{2+}$ : 368.2101; found 368.2102.

16 **1.5 SNAP substrates based on chloropyrimidine (CP)**

17 **1.5.1 N-(4-(((2-amino-6-chloropyrimidin-4-yl)oxy)methyl)benzyl)-2-azidoacetamide (CP-N<sub>3</sub>)**



18  
19 Reaction was conducted according to general procedure A using CP-NH<sub>2</sub> and 2-azidoacetic acid (5.8  $\mu\text{L}$ , 41.6  $\mu\text{mol}$ ) to obtain 10.1 mg  
20 (21.9  $\mu\text{mol}$ ) of the desired product as a colorless TFA-salt in 58% yield.

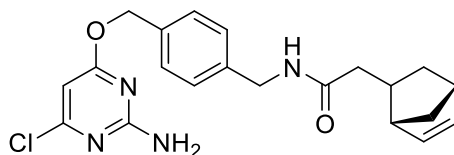
21 **<sup>1</sup>H NMR** (400 MHz, DMSO-*d*<sub>6</sub>)  $\delta$  [ppm] = 8.62 (t, *J* = 5.8 Hz, 1H), 7.40 (d, *J* = 7.7 Hz, 2H), 7.28 (d, *J* = 7.7 Hz, 2H), 6.13 (s, 1H), 5.29  
22 (s, 2H), 4.30 (d, *J* = 5.8 Hz, 2H), 3.88 (s, 2H).

23 **<sup>13</sup>C NMR** (101 MHz, DMSO-*d*<sub>6</sub>)  $\delta$  [ppm] = 170.28, 167.32, 162.77, 160.01, 138.90, 134.90, 128.44, 127.46, 94.42, 67.21, 50.78, 42.01.

24 **HRMS** (ESI) calc. for  $\text{C}_{14}\text{H}_{15}\text{ClN}_7\text{O}_2^+$   $[\text{M}+\text{H}]^+$ : 348.0970; found 348.0971.

25

26 **1.5.2 N-(4-(((2-amino-6-chloropyrimidin-4-yl)oxy)methyl)benzyl)-2-((1S,4S)-bicyclo[2.2.1]hept-5-en-2-yl)acetamide (CP-**  
27 **Nor2)**



28  
29 Reaction was conducted according to general procedure A with a reduced reaction time of 15 min. using CP-NH<sub>2</sub> and 2-((1S,4S)-  
30 bicyclo[2.2.1]hept-5-en-2-yl)acetic acid (7.1  $\mu\text{L}$ , 41.6  $\mu\text{mol}$ ) resulting in 14.5 mg (28.3  $\mu\text{mol}$ ) of the desired product as a colorless TFA-  
31 salt in 75% yield.

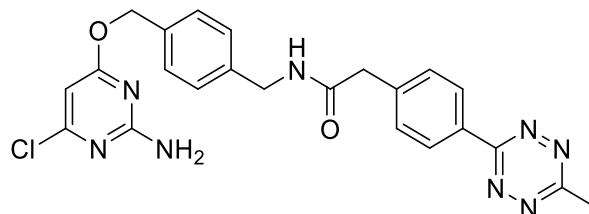
1 <sup>1</sup>H NMR (400 MHz, DMSO-*d*<sub>6</sub>) δ [ppm] = 8.25 (t, *J* = 5.9 Hz, 1H), 7.38 (d, *J* = 8.1 Hz, 2H), 7.23 (d, *J* = 8.1 Hz, 2H), 7.10 (brs, 2H), 6.16  
2 (dd, *J* = 5.7, 3.0 Hz, 1H), 6.13 (s, 1H), 5.96 (dd, *J* = 5.7, 2.9 Hz, 1H), 5.28 (s, 2H), 4.24 (d, *J* = 5.9 Hz, 2H), 2.77 – 2.69 (m, 2H), 2.46 –  
3 2.35 (m, 1H), 1.94 (dd, *J* = 13.8, 7.6 Hz, 1H), 1.90 – 1.76 (m, 2H), 1.35 – 1.26 (m, 1H), 1.26 – 1.18 (m, 1H), 0.50 (m, *J* = 11.4, 4.3, 2.5  
4 Hz, 1H).

5 <sup>13</sup>C NMR (101 MHz, DMSO-*d*<sub>6</sub>) δ [ppm] = 171.61, 170.28, 162.75, 159.97, 139.81, 137.01, 134.53, 132.42, 128.31, 127.11, 94.39,  
6 67.23, 49.07, 45.24, 42.06, 41.69, 40.64, 35.11, 31.45.

7 HRMS (ESI) calc. for C<sub>21</sub>H<sub>23</sub>ClN<sub>4</sub>NaO<sub>2</sub><sup>+</sup> [M+Na]<sup>+</sup>; 421.1402; found 421.1403.

8

9 **1.5.3 N-(4-(((2-amino-6-chloropyrimidin-4-yl)oxy)methyl)benzyl)-2-(4-(6-methyl-1,2,4,5-tetrazin-3-yl)phenyl)acetamide**  
10 **(CP-Tz)**



11  
12 Reaction was conducted according to general procedure A using CP-NH<sub>2</sub> and 2-(4-(6-methyl-1,2,4,5-tetrazin-3-yl)phenyl)acetic acid  
13 (9.6 mg, 41.6 μmol). The product was purified by preparative HPLC eluted with MeCN / H<sub>2</sub>O (0.1% TFA) (10% MeCN for 10 min., then  
14 10 - 90% MeCN over 40 min., followed by 90% MeCN for 10 min.) to give 2.6 mg (4.4 μmol) of the desired product as a rose TFA-salt  
15 in 12% yield after lyophilization.

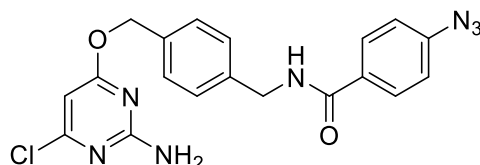
16 <sup>1</sup>H NMR (400 MHz, DMSO-*d*<sub>6</sub>) δ [ppm] = 8.66 (t, *J* = 5.9 Hz, 1H), 8.41 (d, *J* = 8.3 Hz, 2H), 7.56 (d, *J* = 8.3 Hz, 2H), 7.38 (d, *J* = 7.9 Hz,  
17 2H), 7.26 (d, *J* = 7.9 Hz, 2H), 7.10 (s, 2H), 6.13 (s, 1H), 5.28 (s, 2H), 4.29 (d, *J* = 5.9 Hz, 2H), 3.63 (s, 2H), 2.99 (s, 3H).

18 <sup>13</sup>C NMR (101 MHz, DMSO-*d*<sub>6</sub>) δ [ppm] = 170.28, 169.51, 167.04, 163.21, 162.76, 159.99, 141.13, 139.32, 134.75, 130.14, 130.07,  
19 128.42, 127.34, 94.40, 67.22, 42.21, 42.09, 20.83.

20 HRMS (ESI) calc. for C<sub>23</sub>H<sub>22</sub>ClN<sub>8</sub>O<sub>2</sub><sup>+</sup> [M+H]<sup>+</sup>: 477.1549; found 477.1553.

21

22 **1.5.4 N-(4-(((2-amino-6-chloropyrimidin-4-yl)oxy)methyl)benzyl)-4-azidobenzamide (CP-PhN<sub>3</sub>)**



23  
24 Reaction was conducted according to general procedure A with a reduced reaction time of 15 min. using BG-NH<sub>2</sub> and 4-azidobenzoic  
25 acid (6.8 mg, 41.6 μmol) to obtain 12.0 mg (22.9 μmol) of the desired product as a colorless TFA-salt in 61% yield.

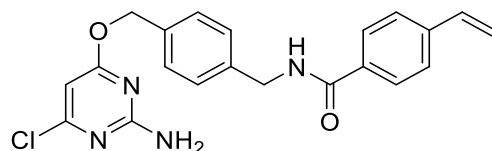
26 <sup>1</sup>H NMR (400 MHz, DMSO-*d*<sub>6</sub>) δ [ppm] = 9.06 (t, *J* = 5.9 Hz, 1H), 7.94 (d, *J* = 8.4 Hz, 2H), 7.39 (d, *J* = 7.9 Hz, 2H), 7.32 (d, *J* = 7.9 Hz,  
27 2H), 7.21 (d, *J* = 8.4 Hz, 2H), 7.10 (s, 2H), 5.29 (s, 2H), 4.47 (d, *J* = 5.9 Hz, 2H).

28 <sup>13</sup>C NMR (101 MHz, DMSO-*d*<sub>6</sub>) δ [ppm] = 170.27, 165.20, 162.75, 159.97, 142.30, 139.59, 134.66, 130.83, 129.12, 128.36, 127.29,  
29 118.90, 94.38, 67.23, 42.44.

30 HRMS (ESI) calc. for C<sub>19</sub>H<sub>16</sub>ClN<sub>7</sub>NaO<sub>2</sub><sup>+</sup> [M+Na]<sup>+</sup>: 432.0946; found 432.0942.

31

32 **1.5.5 N-(4-(((2-amino-6-chloropyrimidin-4-yl)oxy)methyl)benzyl)-4-vinylbenzamide (CP-Vbn)**



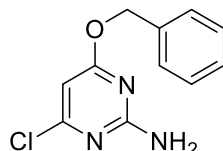
33



1 Reaction was conducted according to general procedure A with a reduced reaction time of 15 min. using CP-NH<sub>2</sub> and 4-vinylbenzoic  
2 acid (41.6 μmol; 6.2 mg) to obtain 11.6 mg (22.8 μmol) of the desired product as a colorless TFA-salt in 60% yield.  
3 **<sup>1</sup>H NMR** (400 MHz, DMSO-*d*<sub>6</sub>) δ [ppm] = 9.04 (t, *J* = 6.0 Hz, 1H), 7.87 (d, *J* = 8.3 Hz, 2H), 7.57 (d, *J* = 8.3 Hz, 2H), 7.40 (d, *J* = 8.1 Hz,  
4 2H), 7.34 (d, *J* = 8.1 Hz, 2H), 6.79 (dd, *J* = 17.7, 10.9 Hz, 1H), 7.10 (brs, 2H), 6.12 (s, 1H), 5.95 (d, *J* = 17.7 Hz, 1H), 5.37 (d, *J* = 10.9  
5 Hz, 1H), 5.29 (s, 2H), 4.47 (d, *J* = 6.0 Hz, 2H).  
6 **<sup>13</sup>C NMR** (101 MHz, DMSO-*d*<sub>6</sub>) δ [ppm] = 170.29, 165.77, 162.77, 159.99, 139.80, 139.68, 135.91, 134.66, 133.45, 128.41, 127.61,  
7 127.31, 126.00, 116.20, 94.40, 67.27, 42.43.  
8 **HRMS** (ESI) calc. for C<sub>21</sub>H<sub>20</sub>ClN<sub>4</sub>O<sub>2</sub><sup>+</sup> [M+H]<sup>+</sup>: 395.1269; found 395.1258.

9

#### 10 1.5.6 4-(Benzyloxy)-6-chloropyrimidin-2-amine (CP)



11  
12 2-Amino-4,6-dichloropyrimidine (200 mg, 1.22 mmol, 1.0 equiv.) was dissolved in dry DMF (2 mL). Benzyl alcohol (63 μL, 1.22 mmol,  
13 1.0 equiv.), KO<sup>t</sup>Bu (342.2 mg, 3.04 mmol, 2.5 equiv.) and KI (20.2 mg, 0.122 mmol, 0.1 equiv.) were added and the reaction mixture  
14 was stirred at room temperature for 4 h. Afterwards, the reaction was quenched with water and extracted with EtOAc (3 x). The  
15 combined organic layers were washed with brine and dried over MgSO<sub>4</sub>. The volatiles were evaporated and the crude product was  
16 purified over normal phase flash chromatography (hexane:DCM = 50% : 50% to 100% DCM). The fractions containing the product  
17 were combined, volatiles were evaporated and 134 mg (0.569 mmol) of the desired product was obtained as a yellowish solid in 47%  
18 yield.

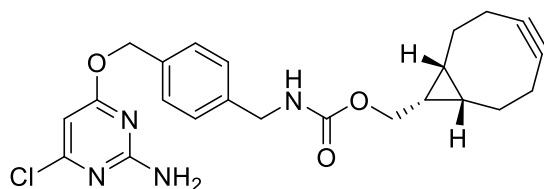
19 **<sup>1</sup>H NMR** (400 MHz, CDCl<sub>3</sub>): δ = 7.43–7.30 (m, 5H), 6.01 (d, *J* = 0.7 Hz, 1H), 5.31 (s, 2H), 2.26 (s, 3H) ppm.

20 **<sup>13</sup>C NMR** (101 MHz, CDCl<sub>3</sub>): δ = 170.6, 168.4, 162.6, 136.7, 128.7, 128.5, 128.0, 127.4, 97.2, 93.0, 77.4, 77.1, 76.7, 67.5, 123.7 ppm.

21 **HRMS** (ESI) calc. for C<sub>11</sub>H<sub>11</sub>ClN<sub>3</sub>O<sup>+</sup> [M+H]<sup>+</sup>: 236.0585; found 236.0583.

22

#### 23 1.5.7 ((1*R*,8*S*,9*S*)-bicyclo[6.1.0]non-4-yn-9-yl)methyl(4-(((2-amino-6-chloropyrimidin-4-yl)oxy)methyl)benzyl)carbamate 24 (CP-BCN)



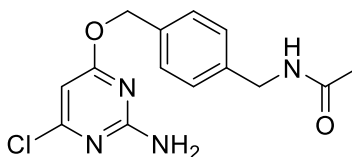
25  
26 ((1*R*,8*S*,9*S*)-bicyclo[6.1.0]non-4-yn-9-yl)methyl (2,5-dioxopyrrolidin-1-yl) carbonate (10.0 mg, 34.3 μmol; 1.0 equiv.) was dissolved in  
27 dry DMSO (0.5 mL) and DIPEA (28.4 μL, 172 μmol, 5 equiv.) followed by CP-NH<sub>2</sub> (10.0 mg, 37.8 μmol, 1.1 equiv.) were added. The  
28 reaction was stirred at r.t. for 30 min. The resulted mixture was acidified with acetic acid (3 μL) and H<sub>2</sub>O (53 μL), then purified by  
29 preparative HPLC eluted with MeCN / H<sub>2</sub>O (0.1% TFA) (10% MeCN for 10 min., then 10 - 90% MeCN over 55 min., followed by 99%  
30 MeCN for 5 min.) to give 1.4 mg (3.11 μmol) of the desired product as a colorless solid in 9% yield after lyophilization.

31 **<sup>1</sup>H NMR** (400 MHz, DMSO-*d*<sub>6</sub>) δ [ppm] = 7.68 (q, *J* = 6.4 Hz, 1H), 7.38 (d, *J* = 8.0 Hz, 2H), 7.25 (d, *J* = 7.8 Hz, 2H), 6.12 (s, 1H), 5.28  
32 (s, 2H), 4.17 (d, *J* = 6.1 Hz, 2H), 4.06 (d, *J* = 8.0 Hz, 2H), 2.29 – 1.72 (m, 6H), 1.71 – 1.38 (m, 2H), 1.35 – 0.60 (m, 3H).

33 **HRMS** (ESI) calc. for C<sub>23</sub>H<sub>26</sub>ClN<sub>4</sub>O<sub>3</sub><sup>+</sup> [M+H]<sup>+</sup>: 441.1688; found 441.1688.

34

1 **1.5.8 N-(4-(((2-amino-6-chloropyrimidin-4-yl)oxy)methyl)benzyl)acetamide (CP-Ac)**



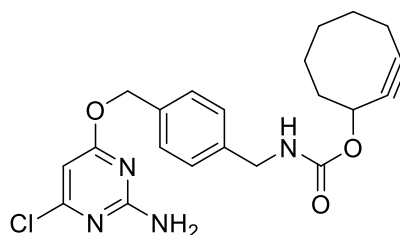
2  
3 CP-NH<sub>2</sub> (300 mg, 1.13 mmol, 1.0 equiv.) was dissolved in dry DMSO (1.5 mL) and DIPEA (375  $\mu$ L, 2.27 mmol, 2.0 equiv.) was added  
4 followed by dropwise addition of acetic anhydride (160  $\mu$ L, 1.70 mmol, 1.5 equiv.) while stirring. The reaction mixture was stirred at r.t.  
5 for 1 h. Afterwards, the reaction was quenched with acetic acid (387  $\mu$ L) and H<sub>2</sub>O (341  $\mu$ L) followed by purification over preparative  
6 HPLC eluted with MeCN / H<sub>2</sub>O (0.1% TFA) (30% MeCN for 10 min., then 30 - 90% MeCN over 55 min., followed by 99% MeCN for 5  
7 min.) to give 201 mg (655  $\mu$ mol) of the desired product as a colorless solid in 58% yield after lyophilization.

8 **<sup>1</sup>H NMR** (400 MHz, DMSO-*d*<sub>6</sub>)  $\delta$  [ppm] = 8.33 (t, *J* = 6.0 Hz, 1H), 7.41 – 7.35 (m, 2H), 7.28 – 7.22 (m, 2H), 7.09 (s, 2H), 6.13 (s, 1H),  
9 5.29 (s, 2H), 4.24 (d, *J* = 5.9 Hz, 2H), 1.86 (s, 3H).

10 **HRMS** (ESI) calc. for C<sub>14</sub>H<sub>16</sub>ClN<sub>4</sub>O<sub>2</sub><sup>+</sup> [M+H]<sup>+</sup>: 307.0956; found 307.0957.

11

12 **1.5.9 Cyclooct-2-yn-1-yl (4-(((2-amino-6-chloropyrimidin-4-yl)oxy)methyl)benzyl)carbamate (CP-SCO)**



13  
14 CP-NH<sub>2</sub> (10 mg; 37.8  $\mu$ mol, 1.3 equiv.) was dissolved in dry DMF (0.3 mL) and a solution of 8.4 mg cyclooct-2-yn-1-yl (4-nitrophenyl)  
15 carbonate (29.1  $\mu$ mol, 1.0 equiv.) in dry DMF (0.2 mL) was added followed by DIPEA (24.0  $\mu$ L, 145  $\mu$ mol: 5.0 equiv.). The reaction  
16 mixture was stirred at r.t. for 2 h. The resulted mixture was acidified with acetic acid (25  $\mu$ L) and afterwards purified by semi-preparative  
17 HPLC eluted with MeCN / H<sub>2</sub>O (0.1% TFA) (15% MeCN for 2 min., then 15 - 100% MeCN over 25 min., followed by 100% MeCN for  
18 15 min.) to give 12.0 mg (22.7  $\mu$ mol) of the desired product as a colorless TFA-salt in 78% yield after lyophilization.

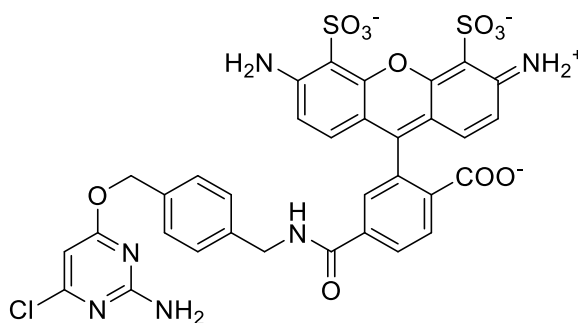
19 **<sup>1</sup>H NMR** (400 MHz, DMSO-*d*<sub>6</sub>)  $\delta$  [ppm] = 7.78 (t, *J* = 6.2 Hz, 1H), 7.38 (d, *J* = 8.1 Hz, 2H), 7.24 (d, *J* = 8.1 Hz, 2H), 6.13 (s, 1H), 5.28  
20 (s, 2H), 5.21 – 5.11 (m, 1H), 4.15 (d, *J* = 6.2 Hz, 2H), 2.29 – 2.02 (m, 3H), 1.95 – 1.85 (m, 1H), 1.85 – 1.78 (m, 2H), 1.76 – 1.65 (m,  
21 1H), 1.65 – 1.54 (m, 2H), 1.54 – 1.42 (m, 1H).

22 **<sup>13</sup>C NMR** (101 MHz, DMSO-*d*<sub>6</sub>)  $\delta$  [ppm] = 170.30, 162.78, 159.99, 155.51, 139.64, 134.73, 128.40, 127.11, 100.94, 94.41, 91.76,  
23 67.25, 65.93, 43.50, 41.58, 33.84, 29.21, 25.79, 19.96.

24 **HRMS** (ESI) calc. for C<sub>21</sub>H<sub>23</sub>ClN<sub>4</sub>NaO<sub>3</sub><sup>+</sup> [M+Na]<sup>+</sup>: 437.1351; found 437.1358.

25

26 **1.5.10 2-(6-amino-3-iminio-4,5-disulfonato-3H-xanthen-9-yl)-4-(((2-amino-6-chloropyrimidin-4-yl)oxy)methyl)benzyl)carbamoyl)benzoate (CP-Alexa488)**

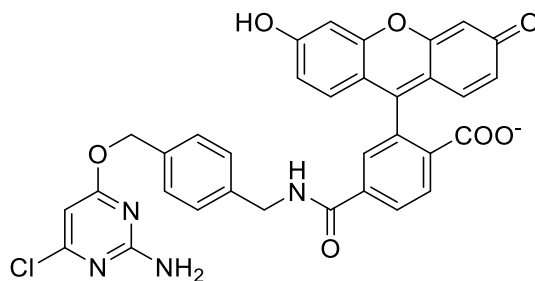


28

1 In an Eppendorf tube, CP-NH<sub>2</sub> (0.34 μg, 1.27 μmol, 2.0 equiv.) was dissolved in dry DMSO (100 μL) followed by addition of DIPEA  
2 (885 μL, 5.1 μmol, 8.0 equiv.) and a solution of 2-(6-amino-3-imino-4,5-disulfonato-3H-xanthen-9-yl)-4-(((2,5-dioxopyrrolidin-1-  
3 yl)oxy)carbonyl)benzoate (0.4 mg, 0.64 μmol, 1.0 equiv.) in dry DMSO (100 μL). The reaction was kept at r.t. for 1 h. The compound  
4 was purified over preparative HPLC eluted with MeCN / H<sub>2</sub>O (0.1% TFA) (10% MeCN for 10 min., then 10 - 90% MeCN over 40 min.,  
5 followed by 90% MeCN for 5 min.) to give 195 μg (252 nmol) of the desired product as a yellow solid in 79% yield after lyophilization.  
6 **HRMS** (ESI) calc. for C<sub>33</sub>H<sub>25</sub>ClN<sub>6</sub>O<sub>11</sub>S<sub>2</sub> [M+3H]<sup>+</sup>: 781.0784; found 781.0772.

7

8 **1.5.11 4-(((2-amino-6-chloropyrimidin-4-yl)oxy)methyl)benzyl)carbamoyl)-2-(6-hydroxy-3-oxo-3H-xanthen-9-  
9 yl)benzoate (CP-Fluorescein)**

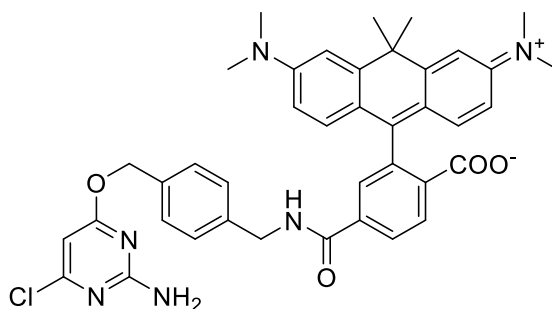


10  
11 Fluorescein-6-COOH (25.0 mg, 66.4 μmol, 1.0 equiv.) was dissolved in dry DMSO (1.25 mL) and DIPEA (22.0 μL, 133 μmol, 2.0  
12 equiv.) as well as TSTU (24.0 mg, 79.7 μmol, 1.2 equiv.) were added and the mixture was stirred at r.t. for 30 min. Afterwards, CP-  
13 NH<sub>2</sub> (26.4 mg, 99.7 μmol, 1.5 equiv.) was added and the reaction mixture was stirred at r.t. for 1 h. The resulted mixture was quenched  
14 with acetic acid (22.0 μL) and 10% H<sub>2</sub>O, then the compound was purified over preparative HPLC eluted with MeCN / H<sub>2</sub>O (0.1% TFA)  
15 (10% MeCN for 10 min., then 10 - 90% MeCN over 40 min., followed by 90% MeCN for 5 min.) to give 31 mg (49.8 μmol) of the desired  
16 product in 75% yield after lyophilization.

17 **HRMS** (ESI) calc. for C<sub>33</sub>H<sub>24</sub>ClN<sub>4</sub>O<sub>7</sub><sup>+</sup> [M+H]<sup>+</sup>: 623.1328; found 623.1327.

18

19 **1.5.12 4-(((2-amino-6-chloropyrimidin-4-yl)oxy)methyl)benzyl)carbamoyl)-2-(6-(dimethylamino)-3-(dimethyliminio)-  
20 10,10-dimethyl-3,10-dihydroanthracen-9-yl)benzoate (CP-CPY)**



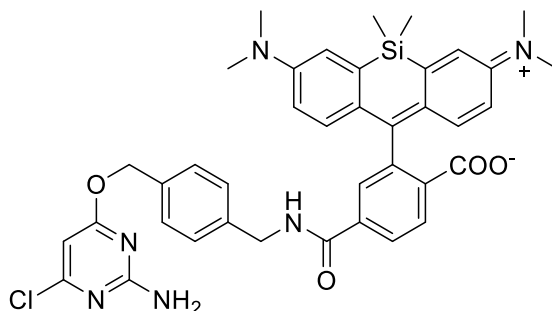
21  
22 CPY-6-COOH(1) (250 mg, 530 μmol, 1.0 equiv.) was dissolved in dry DMSO (2 mL) and DIPEA (362 μL, 2.19 mmol, 4.0 equiv.) as  
23 well as TSTU (231 mg, 767 μmol, 1.4 equiv.) were added and the mixture was stirred at r.t. for 5 min. Afterwards, CP-NH<sub>2</sub> (217 mg,  
24 821 μmol, 1.5 equiv.) was added and the reaction mixture was stirred at r.t. for 35 min. The resulted mixture was acidified with acetic  
25 acid (362 μL) and H<sub>2</sub>O (500 μL), then the compound was purified over preparative HPLC eluted with MeCN / H<sub>2</sub>O (0.1% TFA) (10%  
26 MeCN for 10 min., then 10 - 90% MeCN over 40 min., followed by 90% MeCN for 5 min.) to give 130 mg (184.9 μmol) of the desired  
27 product in 34% yield after lyophilization.

28 **<sup>1</sup>H NMR** (400 MHz, acetone-*d*<sub>6</sub>) δ [ppm] = 8.51 (t, J = 6.4 Hz, 1H), 8.23 (d, J = 8.1 Hz, 1H), 8.12 (d, J = 8.7 Hz, 1H), 7.67 (s, 1H), 7.39  
29 - 7.30 (m, 4H), 7.11 (s, 2H), 6.67 (s, 4H), 6.36 (s, 1H), 6.07 (m, J = 10.7, 2.5 Hz, 1H), 5.30 (m, J = 11.2, 2.5 Hz, 2H), 4.55 (d, J = 5.9  
30 Hz, 2H), 3.11 (s, 12H), 1.89 (d, J = 2.5 Hz, 3H), 1.76 (d, J = 2.4 Hz, 3H).

31 **<sup>13</sup>C NMR** (101 MHz, acetone-*d*<sub>6</sub>) δ [ppm] = 171.72, 165.87, 161.60, 140.12, 136.37, 134.01, 129.34, 129.25, 128.85, 120.23, 113.03,  
32 110.69, 96.16, 68.31, 44.02, 40.62, 35.59, 33.04, 30.42, 30.22, 30.03, 29.84, 29.65, 29.45, 29.26, 26.13.

1 **HRMS** (ESI) calc. for  $C_{40}H_{39}ClN_6O_4^+$   $[M+H]^+$ : 703.2794; found 703.2792.

2  
3 **1.5.13 4-((4-(((2-amino-6-chloropyrimidin-4-yl)oxy)methyl)benzyl)carbamoyl)-2-(7-(dimethylamino)-3-(dimethyliminio)-5,5-**  
4 **dimethyl-3,5-dihydrodibenzo[b,e]silin-10-yl)benzoate (CP-SiR)**

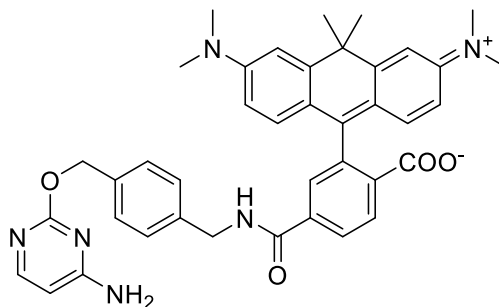


5  
6 SiR-6-COOH(4) (481 mg, 1.02 mmol, 1.1 equiv.) was dissolved in dry DMSO (4 mL) and DIPEA (919  $\mu$ L, 5.56 mmol, 6.0 equiv.) was  
7 added. The mixture was sonicated until complete solution and TSTU (391 mg, 1.30 mmol, 1.4 equiv.) were added and the mixture was  
8 stirred at r.t. for 5 min. Afterwards, CP-NH<sub>2</sub> (294 mg, 1.11 mmol, 1.2 equiv.) was added and the reaction mixture was stirred at r.t. for  
9 2h. The resulted mixture was quenched by addition of acetic acid (973  $\mu$ L) and 10% H<sub>2</sub>O, followed by purification over preparative  
10 HPLC eluted with MeCN / H<sub>2</sub>O (0.1% FA) (10% - 90% MeCN over 60 min) to give 355 mg (494  $\mu$ mol) of the desired product in 53%  
11 yield after lyophilization.

12 **HRMS** (ESI): calc. for  $C_{39}H_{39}N_6O_4Si^+$   $[M+H]^+$ : 719.2563; found 719.2561.

## 13 **1.6 CLIP substrates**

14 **1.6.1 4-((4-(((4-aminopyrimidin-2-yl)oxy)methyl)benzyl)carbamoyl)-2-(6-(dimethylamino)-3-(dimethyliminio)-10,10-**  
15 **dimethyl-3,10-dihydroanthracen-9-yl)benzoate (BC-CPY)**



16  
17 CPY-6-COOH(1) (250 mg, 530  $\mu$ mol, 1.0 equiv.) was dissolved in dry DMSO (2 mL). DIPEA (362  $\mu$ L, 2.19 mmol, 4.0 equiv.) and TSTU  
18 (231 mg, 767  $\mu$ mol, 1.4 equiv.) were added and the mixture was stirred at r.t. for 5 min. Afterwards, BC-NH<sub>2</sub> (189 mg, 821  $\mu$ mol, 1.5  
19 equiv.) was added and the reaction mixture was stirred at r.t. for 35 min. The resulted mixture was acidified with acetic acid (362  $\mu$ L)  
20 and H<sub>2</sub>O (500  $\mu$ L), then compound was purified over preparative HPLC eluted with MeCN / H<sub>2</sub>O (0.1% TFA) (10% MeCN for 10 min.,  
21 then 10 - 90% MeCN over 40 min., followed by 90% MeCN for 5 min.) to give 180 mg (269.1  $\mu$ mol) of the desired product in 49% yield  
22 after lyophilization.

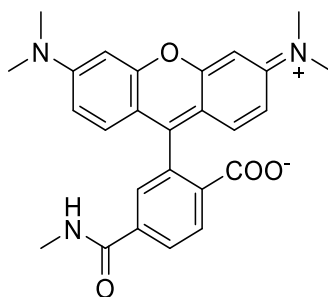
23 **<sup>1</sup>H NMR** (400 MHz, acetone-*d*<sub>6</sub>)  $\delta$  [ppm] = 8.51 (t,  $J$  = 6.9 Hz, 1H), 8.21 (d,  $J$  = 8.1 Hz, 1H), 8.10 – 8.01 (m, 2H), 7.61 (s, 1H), 7.38 (d,  
24  $J$  = 7.4 Hz, 2H), 7.32 (d,  $J$  = 7.8 Hz, 2H), 7.27 (s, 1H), 7.05 (s, 2H), 6.61 (s, 4H), 6.40 (d,  $J$  = 6.6, 2.4 Hz, 1H), 5.36 (s, 2H), 4.56 – 4.50  
25 (m, 2H), 3.04 (s, 12H), 1.88 (d,  $J$  = 2.5 Hz, 3H), 1.76 (d,  $J$  = 2.6 Hz, 3H).

26 **<sup>13</sup>C NMR** (101 MHz, acetone-*d*<sub>6</sub>)  $\delta$  [ppm] = 169.57, 165.97, 162.80, 152.54, 152.01, 148.78, 141.22, 140.20, 136.01, 130.47, 129.26,  
27 128.83, 126.23, 124.12, 120.13, 112.83, 110.38, 100.42, 69.65, 44.02, 43.89, 40.54, 39.65, 35.58, 33.19, 30.42, 30.23, 30.03, 29.84,  
28 29.65, 29.46, 29.26.

29 **HRMS** (ESI): calc. for  $C_{40}H_{42}N_6O_4^{2+}$   $[M+2H]^{2+}$ : 335.1628; found 335.1629.

## 1 1.7 Additional substrates

### 2 1.7.1 2-(6-(dimethylamino)-3-(dimethyliminio)-3H-xanthen-9-yl)-4-(methylcarbamoyl)benzoate (meAm-6-TMR)



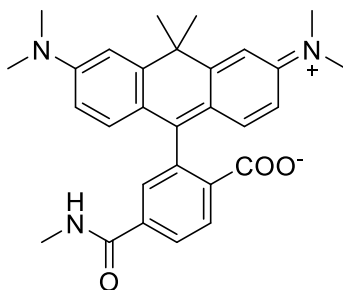
3  
4 To a solution of TMR-6-COOH (1.0 mg, 2.32 μmol, 1.1 equiv.) in dry DMSO (500 μL), TSTU (763 μg, 2.53 μmol, 1.2 equiv.) was added  
5 and the mixture was stirred at r.t. for 5 min. Afterwards, DIPEA (1.4 μL, 8.45 μmol, 4 equiv.) and methylamine (2 M, 1.06 μL, 2.11 μmol,  
6 1 equiv.) were added and the reaction mixture was stirred at r.t. overnight. The compound was purified over preparative HPLC eluted  
7 with MeCN / H<sub>2</sub>O (0.1% TFA) (10% MeCN for 10 min., then 10 - 90% MeCN over 40 min., followed by 90% MeCN for 5 min.) to give  
8 91.1 μg (205.4 nmol) of the desired product in 10% yield after lyophilization.

9 <sup>1</sup>H NMR (TMR-6-COOH) (400 MHz, DMSO-*d*<sub>6</sub>) δ [ppm] = 8.21 (dd, *J* = 8.0, 1.4 Hz, 1H), 8.17 – 7.99 (m, 1H), 7.61 – 7.56 (m, 1H), 6.58  
10 – 6.45 (m, 6H), 2.95 (s, 12H).

11 <sup>13</sup>C NMR (TMR-6-COOH) (101 MHz, DMSO-*d*<sub>6</sub>) δ [ppm] = 168.56, 166.53, 152.67, 152.47, 131.16, 128.91, 109.56, 105.91, 98.43,  
12 40.46, 40.26.

13 HRMS (ESI): calc. for C<sub>26</sub>H<sub>26</sub>N<sub>3</sub>O<sub>4</sub><sup>+</sup> [M+H]<sup>+</sup>: 444.1918; found 444.1914.

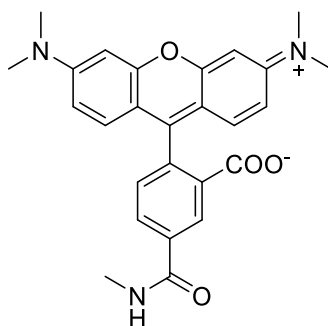
### 15 1.7.2 2-(6-(dimethylamino)-3-(dimethyliminio)-10,10-dimethyl-3,10-dihydroanthracen-9-yl)-4-(methylcarbamoyl)benzoate (meAm-6-CPY)



17  
18 To a solution of CPY-6-COOH (1.0 mg, 2.19 μmol, 1.1 equiv.) in dry DMSO (500 μL), TSTU (719 μg, 2.39 μmol, 1.2 equiv.) was added  
19 and the mixture was stirred at r.t. for 5 min. Afterwards, DIPEA (1.32 μL, 7.97 μmol, 4.0 equiv.) and methylamine (2 M, 0.996 μL, 1.99  
20 μmol, 1.0 equiv.) were added and the reaction mixture was stirred at r.t. overnight. The compound was purified over preparative HPLC  
21 eluted with MeCN / H<sub>2</sub>O (0.1% TFA) (10% MeCN for 10 min., then 10 - 90% MeCN over 40 min., followed by 90% MeCN for 5 min.)  
22 to give 97.7 μg (208.1 nmol) of the desired product in 10% yield after lyophilization.

23 HRMS (ESI): calc. for C<sub>29</sub>H<sub>32</sub>N<sub>3</sub>O<sub>3</sub> [M+H]<sup>+</sup>: 470.2438; found 470.2434.

1 **1.7.3 2-(6-(dimethylamino)-3-(dimethyliminio)-3H-xanthen-9-yl)-5-(methylcarbamoyl)benzoate (meAm-5-TMR)**



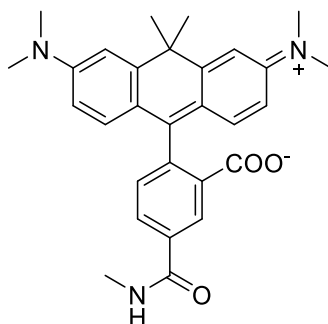
2  
3 To a solution of TMR-5-COOH (2.5 mg, 5.81  $\mu\text{mol}$ , 1.0 equiv.) in dry DMSO (500  $\mu\text{L}$ ), BOP (2.59 mg, 8.71  $\mu\text{mol}$ , 1.5 equiv.) was added  
4 and the reaction was shaken at r.t. and 500 rpm for 5 min. DIPEA (3.84  $\mu\text{L}$ , 23.2  $\mu\text{mol}$ , 4.0 equiv.) and methylamine (2M in THF, 4.36  
5  $\mu\text{L}$ , 8.71  $\mu\text{mol}$ , 1.5 equiv.) were added and the reaction was shaken at r.t. and 500 rpm for 4 h. The crude product was acidified with  
6 acetic acid and purified over preparative HPLC eluted with MeCN / H<sub>2</sub>O (0.1% FA) (10% - 90% MeCN over 50 min) to give 0.97 mg  
7 (2.19  $\mu\text{mol}$ ) of the desired product in 38% yield after lyophilization.

8 **<sup>1</sup>H NMR** (TMR-5-COOH) (400 MHz, DMSO-*d*<sub>6</sub>)  $\delta$  [ppm] = 8.39 (s, *J* = 1.5 Hz, 1H), 8.28 (dd, *J* = 8.1, 1.5 Hz, 1H), 7.33 (d, *J* = 8.0 Hz,  
9 1H), 6.58 – 6.45 (m, 6H), 2.95 (s, 12H).

10 **<sup>13</sup>C NMR** (TMR-5-COOH) (101 MHz, DMSO-*d*<sub>6</sub>)  $\delta$  [ppm] = 168.31, 166.09, 152.03, 135.96, 132.76, 128.50, 109.05, 97.95, 40.15,  
11 39.99, 39.79.

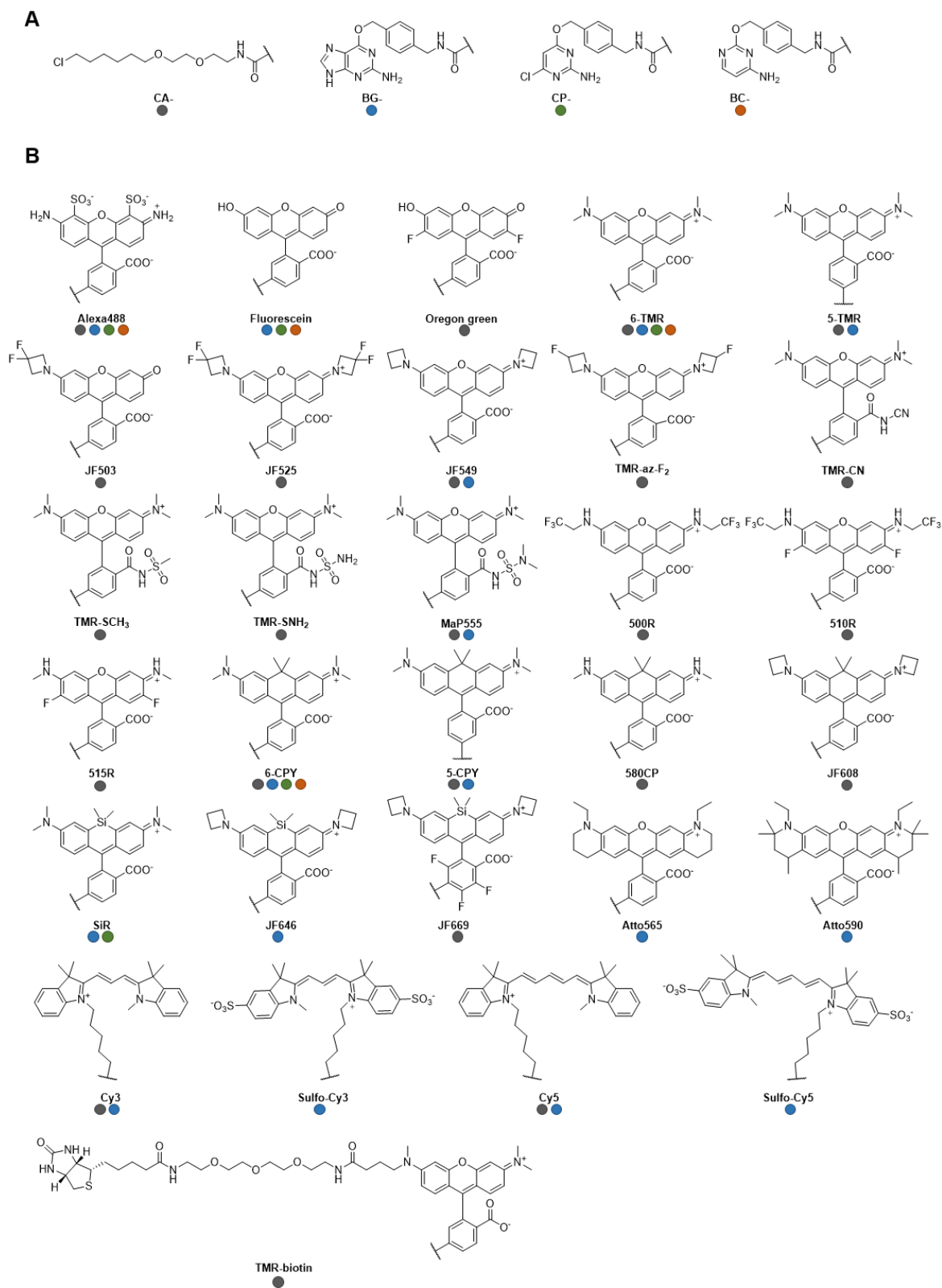
12 **HRMS** (ESI): calc. for C<sub>26</sub>H<sub>26</sub>N<sub>3</sub>O<sub>4</sub><sup>+</sup> [M+H]<sup>+</sup>: 444.1923; found 444.1914.

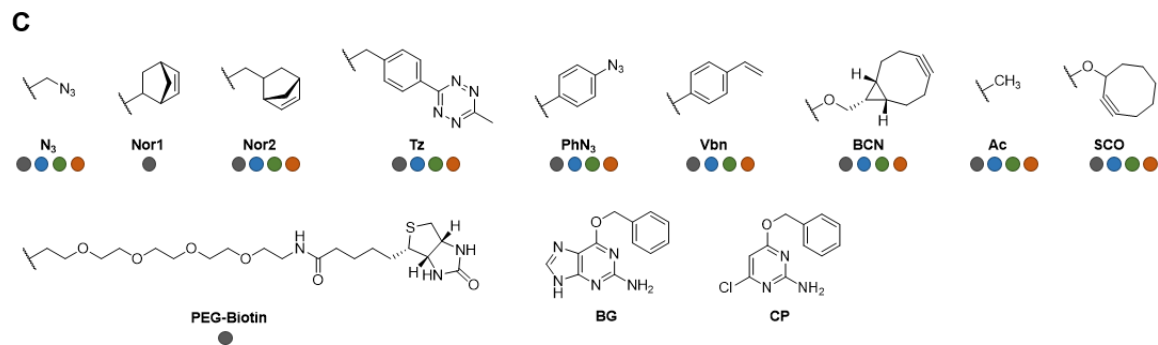
13  
14 **1.7.4 2-(6-(dimethylamino)-3-(dimethyliminio)-10,10-dimethyl-3,10-dihydroanthracen-9-yl)-5-(methylcarbamoyl)benzoate**  
15 **(meAm-5-CPY)**



16  
17 To a solution of CPY-5-COOH (2.5 mg, 5.48  $\mu\text{mol}$ , 1.0 equiv.) in dry DMSO (1 mL), BOP (0.5 M in DMSO, 17.4  $\mu\text{L}$ , 8.71  $\mu\text{mol}$ , 1.5  
18 equiv.) was added and the reaction was shaken at r.t. and 500 rpm for 5 min. DIPEA (3.62  $\mu\text{L}$ , 21.9  $\mu\text{mol}$ , 4.0 equiv.) and methylamine  
19 (2 M in THF, 4.11  $\mu\text{L}$ , 8.21  $\mu\text{mol}$ , 1.5 equiv.) were added and the reaction was shaken at 500 rpm, r.t. for 4 h. The crude product was  
20 acidified with acetic acid and purified over preparative HPLC eluted with MeCN / H<sub>2</sub>O (0.1% FA) (10% - 90% MeCN over 50 min) to  
21 give 0.77 mg (1.64  $\mu\text{mol}$ ) of the desired product in 30% yield after lyophilization.

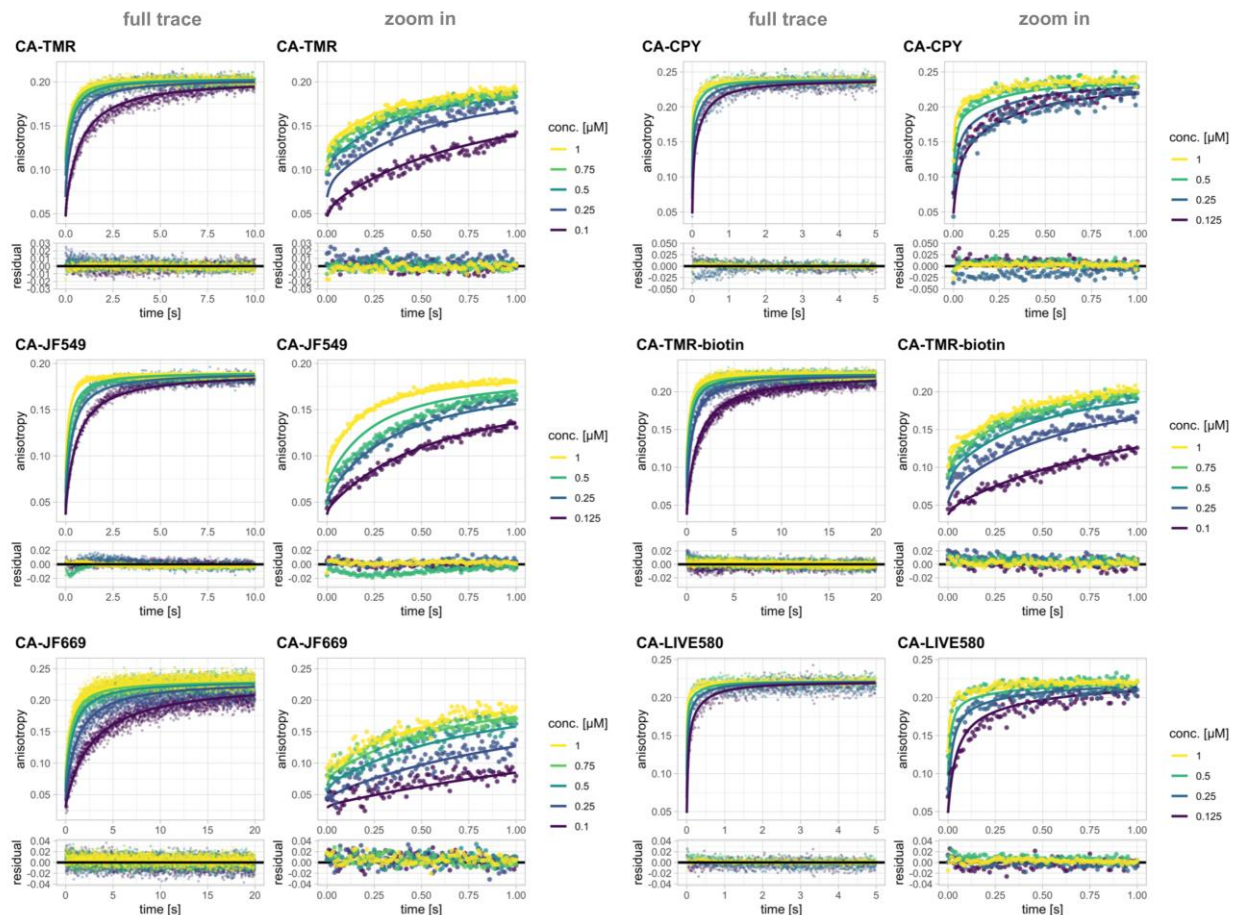
22 **HRMS** (ESI): calc. for C<sub>29</sub>H<sub>32</sub>N<sub>3</sub>O<sub>3</sub><sup>+</sup> [M+H]<sup>+</sup>: 470.2443; found 470.2437.



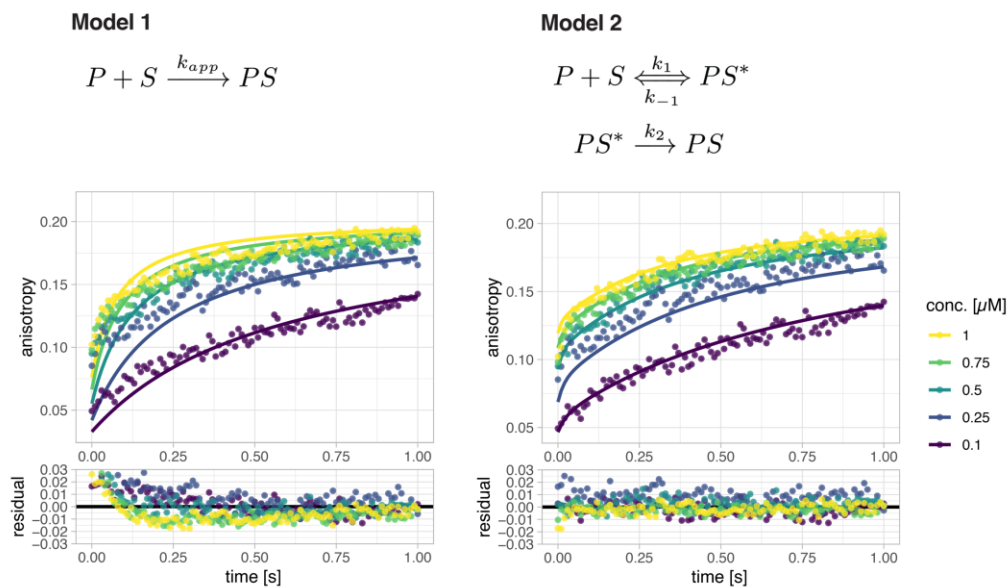


- 1
- 2 **Figure S1 (continued):** Chemical structures of SLP substrates.
- 3 **A.** Chemical structures of HT7 (CA), SNAP (BG and CP) and CLIP (BC) core substrates. **B.** Chemical structures of fluorescent
- 4 substituents. **C.** Chemical structures of non-fluorescent substituents. Colored dots indicate the tested substrates for the corresponding
- 5 SLPs (grey = CA, blue = BG, green = CP and orange = BC).



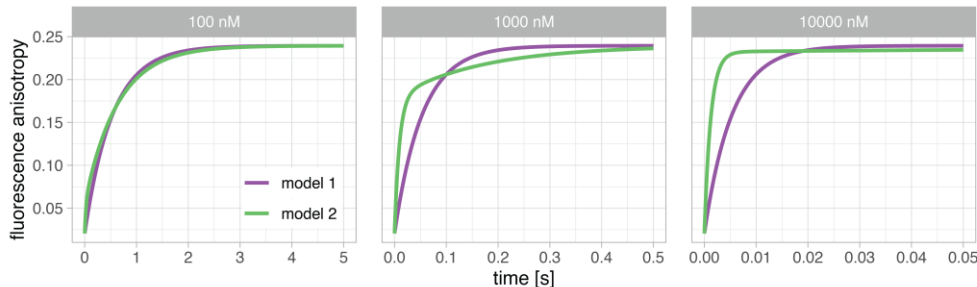


1  
2 **Figure S2:** Labeling kinetics of HT7 with fluorescent CA substrates.  
3 Full anisotropy traces (points) and predications of fits based on model 2 (lines) along with zoom on the first second are represented  
4 on the top panels. Residuals from the fits are depicted in the bottom panels. Kinetics were recorded by following fluorescence  
5 anisotropy changes over time using a stopped flow device. All conditions are 1:1 mixtures of protein and substrate at the given  
6 concentrations (conc.). For structures of CA substrates see **Fig. S1**.

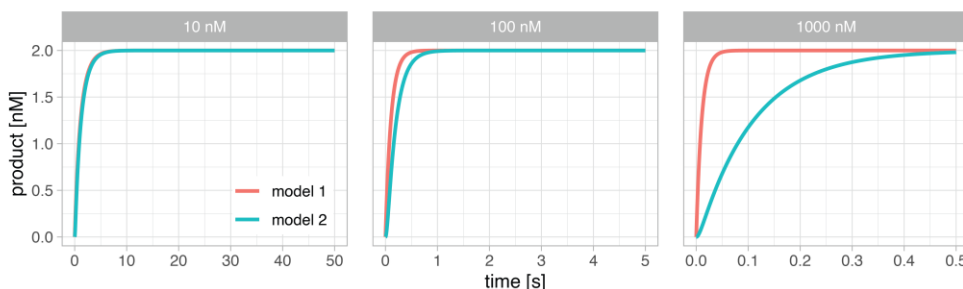


- 1
- 2 **Figure S3:** Comparison of model 1 and model 2 fitted to HT7 labeling kinetics.
- 3 Anisotropy traces (points) and predictions of fits based on either model 1 or model 2 (lines) of the labeling reaction between HT7 and
- 4 CA-TMR are represented in the top panels. Residuals from the fits are depicted in the bottom panels. Kinetics were recorded by
- 5 following fluorescence anisotropy changes over time using a stopped flow device. All conditions are 1:1 mixtures of protein and
- 6 substrate at the given concentrations (conc.). Model 2 describes the data better than the simplified model 1. For structures of CA
- 7 substrates see **Fig. S1**.
- 8

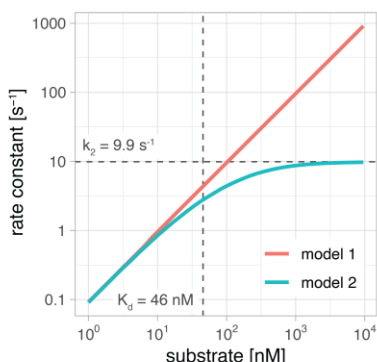
## A modeling anisotropy response for model 1 & 2



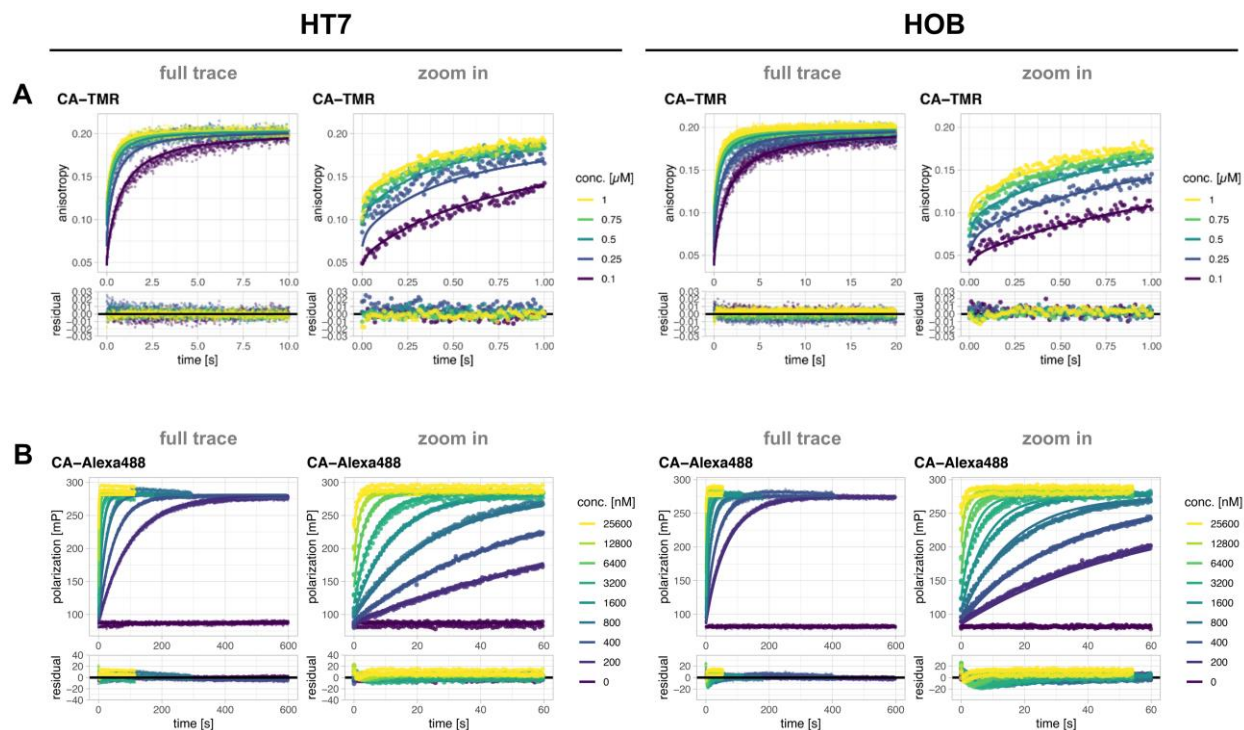
## B modeling covalent product formation for model 1 & 2



## C modeling reaction rate constants for model 1 & 2 vs substrate concentration



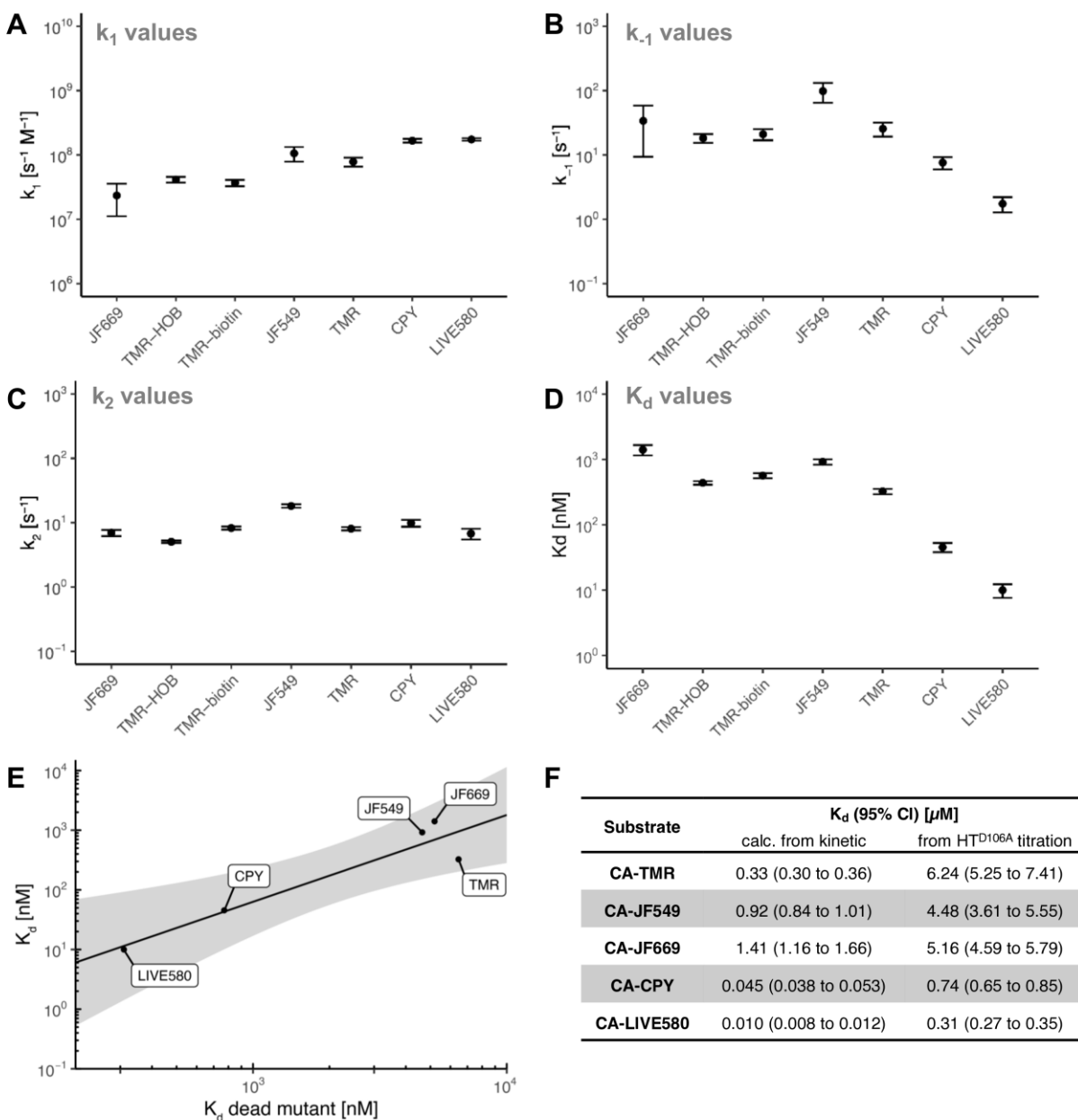
1  
2 **Figure S4:** Modeling of HT7 labeling kinetics using measured parameters to compare the kinetic models 1 and 2.  
3 **A.** Modeling of the fluorescence anisotropy response at different reactant concentrations using model 1 and 2 with parameters  
4 determined for HT7 labeling with CA-TMR. At concentrations below  $K_d$  (327 nM for CA-TMR) both models yield a rather similar  
5 response. At concentrations higher than  $K_d$  (1000 nM) the response for model 2 shows a strong biphasic character as observed in the  
6 measured data, which is not matching the monoexponential behavior of model 1. At very high concentrations (10000 nM) the response  
7 for model 2 is again close to a monoexponential curve but the kinetic is much faster than the model 1 curve. This happens since the  
8 rise in fluorescence anisotropy for model 2 in the first milliseconds is not due to covalent reaction but mostly binding ( $k_1$ ). The binding  
9 rate constant  $k_1$  is faster than  $k_{app}$  if  $k_{-1}$  is not zero ( $k_{app} = k_1 * k_2 / (k_2 + k_{-1})$ ). Hence directly estimating  $k_{app}$  from fluorescence anisotropy  
10 traces by fitting model 1 to the data is only valid for concentrations below  $K_d$  or if  $k_{-1} \ll k_2$ . **B.** Modeling the formation of covalently  
11 labeled product at different reactant concentrations using model 1 and 2 with parameters determined for HT7 labeling with CA-CPY.  
12 At concentrations below  $K_d$  (46 nM for CA-CPY) both models yield a rather similar behavior. At higher concentrations model 1 predicts  
13 a much faster product formation than model 2 since it does not account for enzyme saturation. **C.** Plot of the apparent first order  
14 reaction rate constant for product formation against substrate concentration for model 1 and 2 with parameters for CA-CPY. In contrast  
15 to model 1, model 2 accounts for enzyme saturation leading to a maximum reaction rate of  $k_{max} = k_2 = 9.9$   $s^{-1}$ . The models start to  
16 diverge significantly once the substrate concentration exceeds  $K_d$  (46 nM). As a consequence, model 2 should be used for predicting  
17 formation of labeled HT7 if labeling is performed at high concentrations.



1

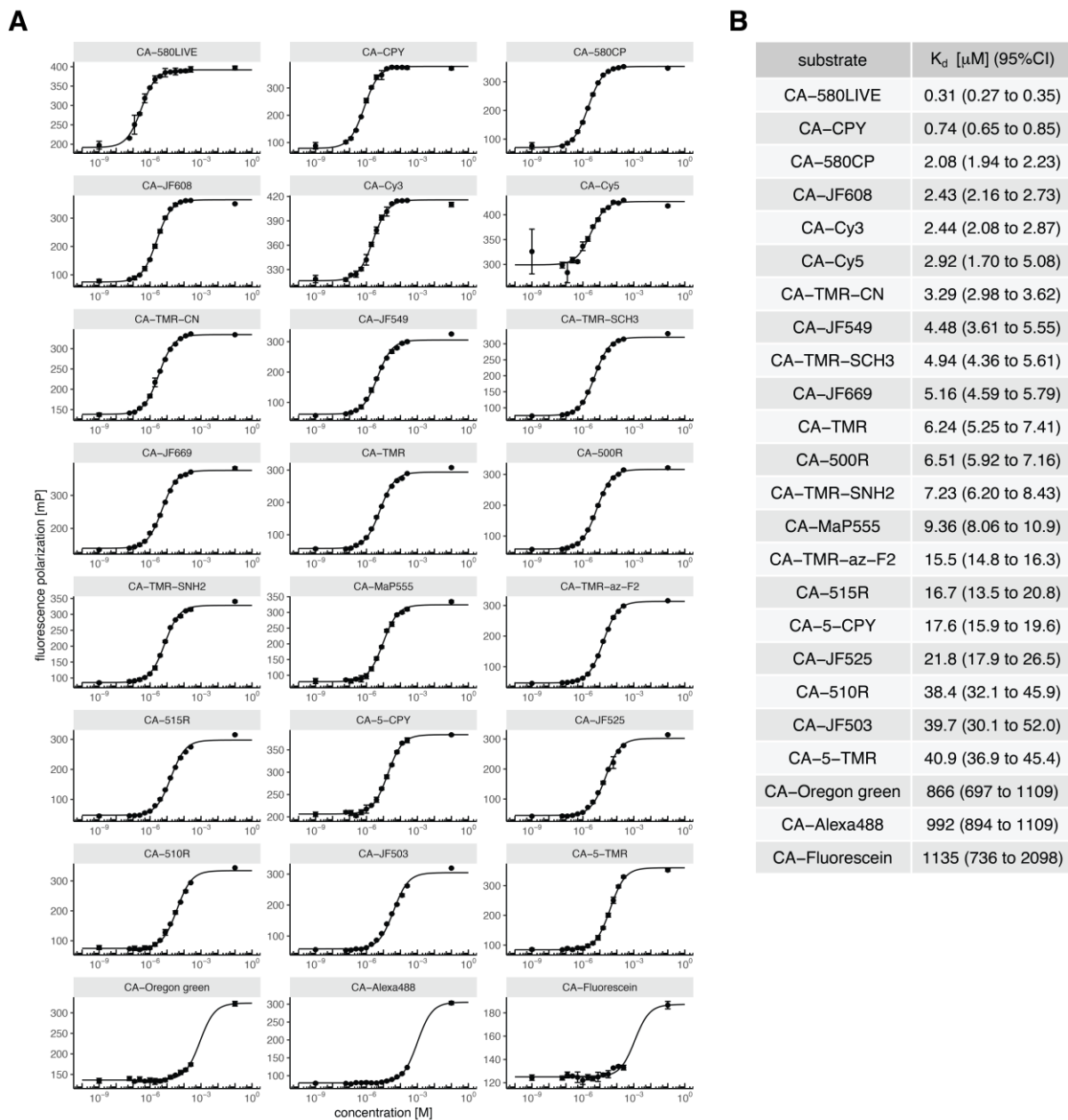
2 **Figure S5:** Labeling kinetics of HT7 and HOB with CA-TMR (A) and CA-Alexa488 (B).

3 **A:** Labeling kinetics of HT7 and HOB with CA-TMR. Full anisotropy traces (points) and predications of fits based on model 2 (lines)  
4 along with zoom on the initial part are represented on the top panels. Residuals from the fits are depicted in the bottom panels. Kinetics  
5 were recorded by following fluorescence anisotropy changes over time using a stopped flow device. All conditions are 1:1 mixtures of  
6 protein and substrate at the given concentrations (conc.). **B:** Labeling kinetics of HT7 and HOB with CA-Alexa488. Full fluorescence  
7 polarization traces (points) and predications of fits based on model 1 (lines) along with zoom on the initial part are represented on the  
8 top panels. Residuals from the fits are depicted in the bottom panels. Kinetics were recorded by following fluorescence polarization  
9 changes over time using a plate reader. All experiments were performed at a fixed substrate concentration of 50 nM with varying  
10 protein concentrations. For structures of CA substrates see **Fig. S1**.

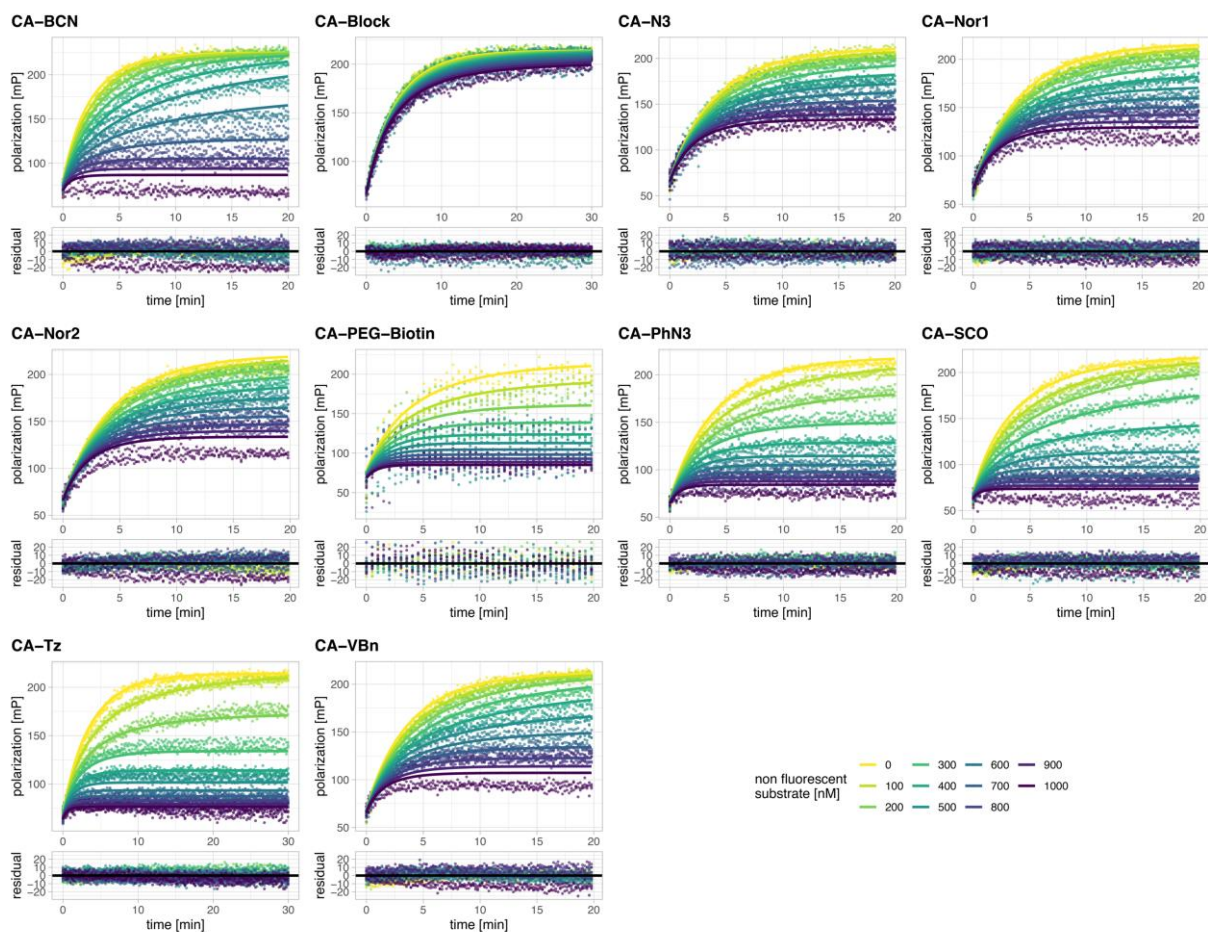


1  
2 **Figure S6:** Rate and equilibrium constants of HT7 labeling with various fluorescent CA substrates.

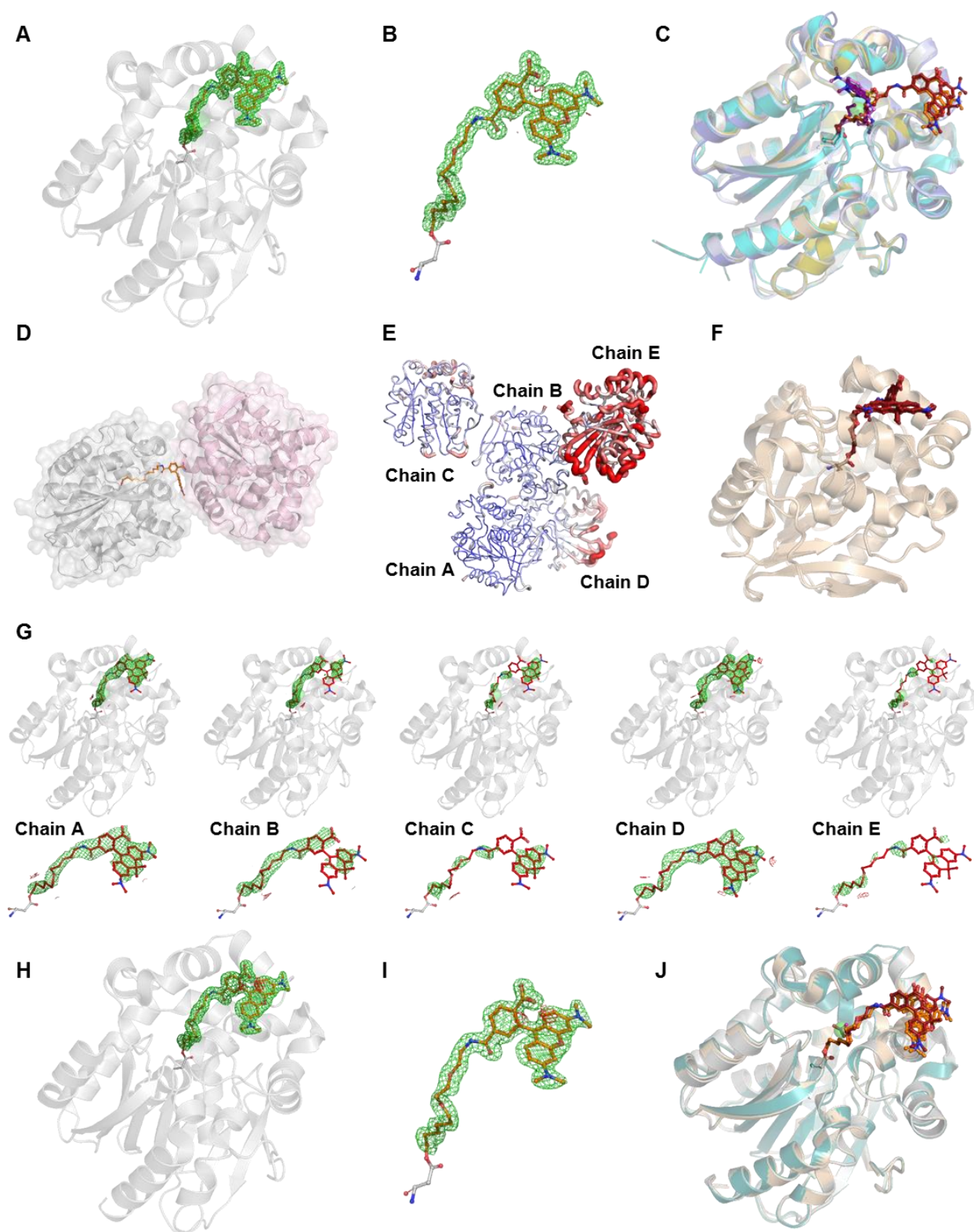
3 Rate constants  $k_1$  (**A**),  $k_{-1}$  (**B**),  $k_2$  (**C**) and the calculated dissociation constants ( $K_d = k_{-1}/k_1$ , **D**.) obtained from fitting model 2 to stopped  
4 flow labeling experiments of HT7 and HOB. The catalytic rate constant ( $k_2$ ) is rather constant among these substrates, while there are  
5 significant differences in the dissociation constant ( $K_d$ ). The  $K_d$  variations are due to large differences in  $k_{-1}$  and minor differences in  $k_1$ .  
6 As a result, differences in  $K_{app}$  can be mostly explained by affinity differences of HT7 towards its substrates. **E**. Correlation between the  
7 calculated  $K_d$  from the stopped flow kinetic experiments and the  $K_d$  obtained from titration experiments performed with the dead mutant  
8 HT7<sup>D106A</sup>. Log transformed values were fitted to a linear model ( $\log(y) = 1.455 * \log(x) - 2.567$ ; black line, 95% confidence bands  
9 in grey, depicting the area in which the true regression line lies with 95% confidence). The linear correlation in logarithmic space suggests  
10 that the  $K_d$  of CA rhodamine substrates with HT7<sup>D106A</sup> could represent a valid proxy to estimate their  $K_d$  with the native HT7. **F**  $K_d$  values  
11 of the tested substrates calculated from the kinetics ( $k_1/k_{-1}$ ) and measured by fluorescence polarization titration against the dead mutant  
12 HT<sup>D106A</sup>.



1  
 2 **Figure S7:** Affinity of the dead mutant HT7<sup>D106A</sup> to fluorescent CA substrates.  
 3 **A.** Titration curves of fluorescent CA substrates against HT7<sup>D106A</sup> measured via fluorescence polarization. The FP value of each dye  
 4 fully bound to native HT7 was added at  $c = 0.1$  M to improve fitting of the upper plateau. (See corresponding methods section for more  
 5 details). **B.** Table summarizing fitted  $K_d$  values with 95% confidence intervals. For structures of CA substrates see **Fig. S1**.



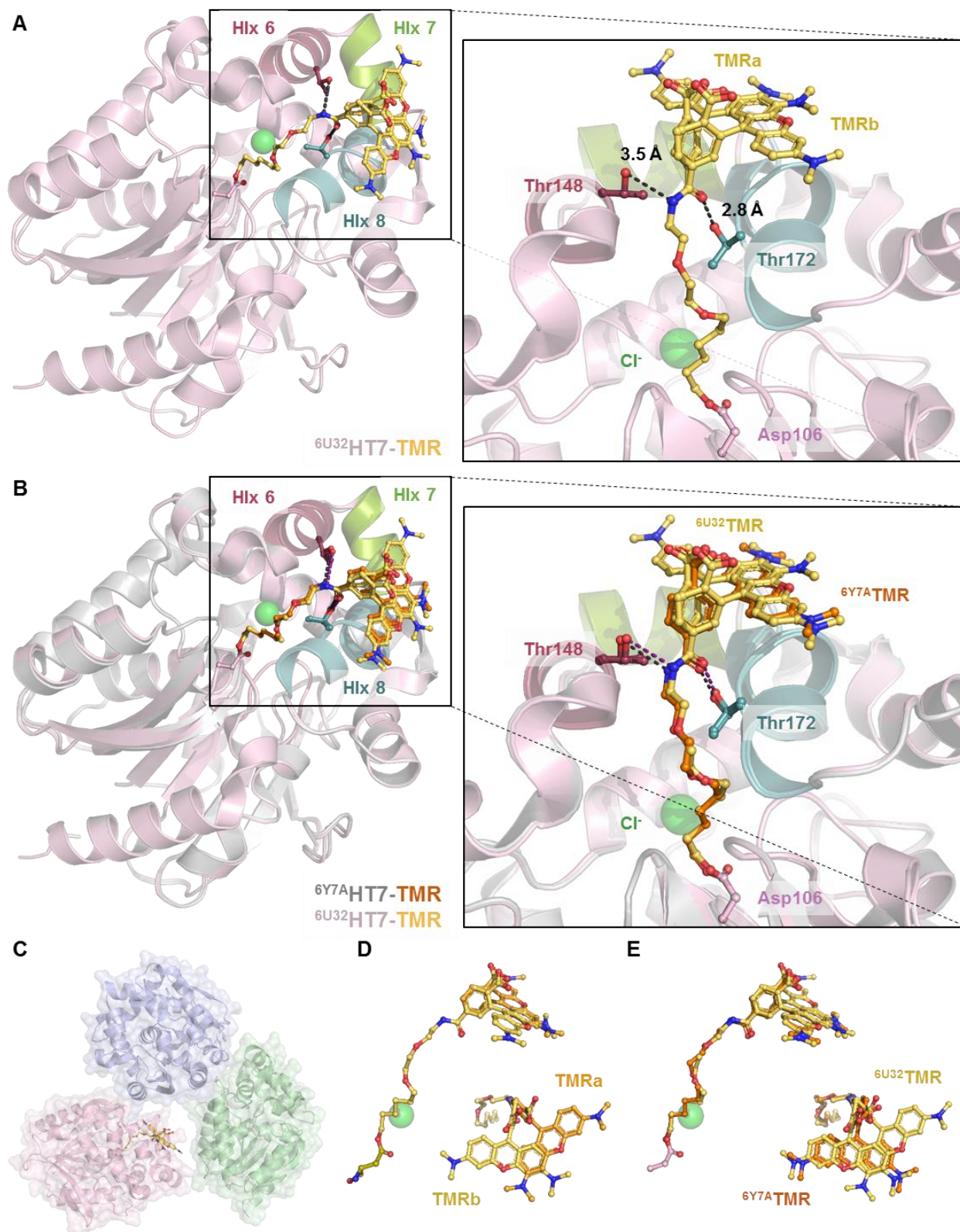
1  
2 **Figure S8:** Labeling kinetics of HT7 with non-fluorescent CA substrates.  
3 Fluorescence polarization traces (points) of kinetic competition assays and predications of fits (lines) based on a simple competitive  
4 model (see methods section for details) of HT7 labeling with CA-Alexa488 in the presence of different concentrations of non-fluorescent  
5 CA substrates are represented on the top panels. Residuals from the fits are depicted in the bottom panels. Kinetics were recorded by  
6 following fluorescence polarization changes over time using a plate reader. For structures of CA substrates see Fig. S1.



1  
2 **Figure S9:** Validation of HT7-TMR and HT7-CPY X-ray structures.  
3 **A.** Omit-map of the TMR ligand of the HT7-TMR X-ray structure. The protein is represented as grey cartoon with the catalytic aspartate  
4 (grey) and the TMR ligand (orange) represented as sticks. **B.** Zoom on the isolated labeled catalytic aspartate of HT7-TMR. The omit  
5 map of the alkane-TMR is contoured at 3  $\sigma$  and represented as green and red mesh for missing and extra density, respectively. **C.**

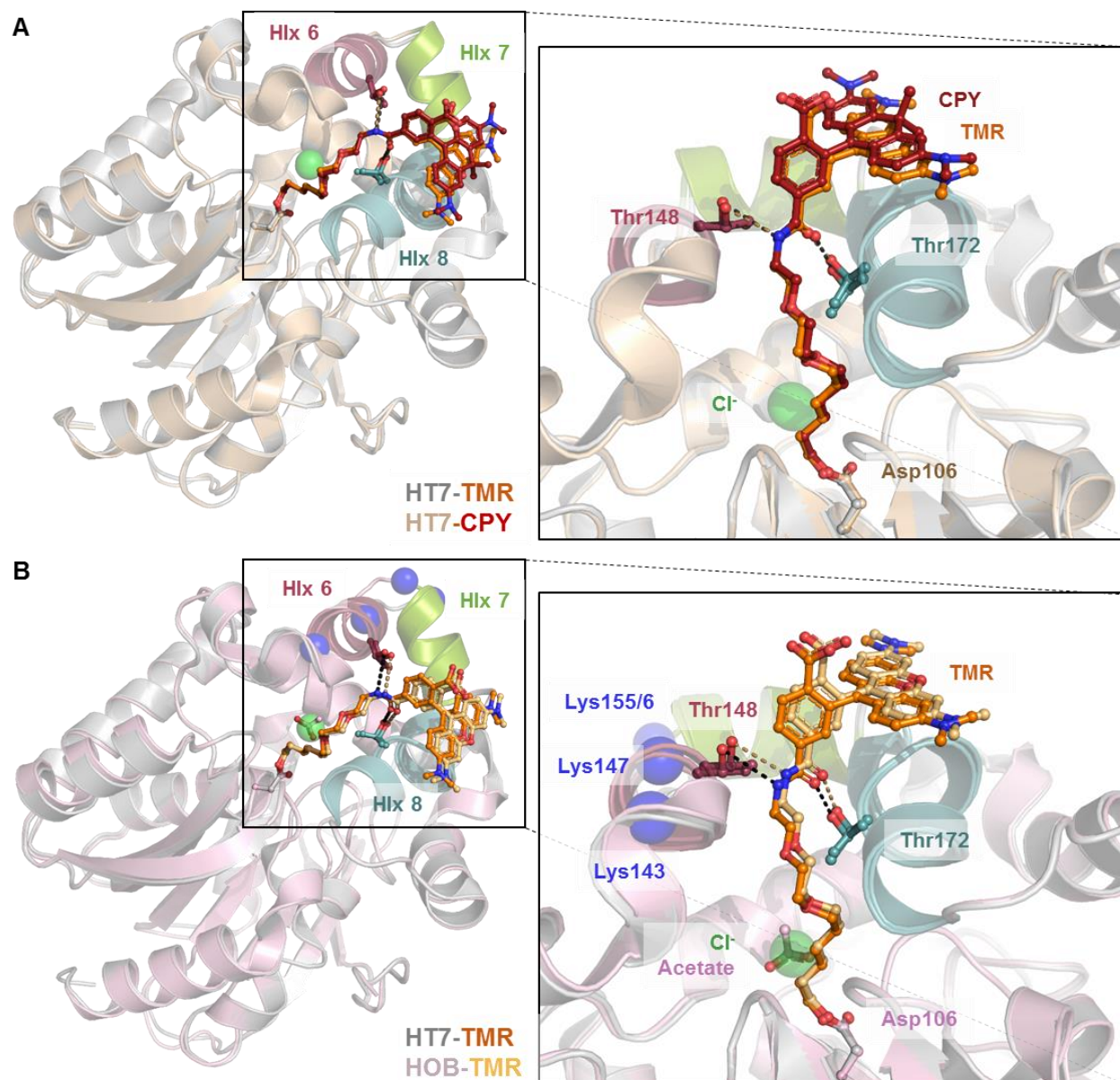


1 Structure alignment of HT7-TMR and HT7-CPY (chain A) with different X-ray structures of HaloTag. All structures are represented as  
2 cartoons with their respective catalytic aspartate and ligands represented as sticks. When present the chloride is represented as green  
3 sphere. **D.** Alkane-TMR constraints by the crystal packing. Two monomers of HT7-TMR are represented as grey and light-pink cartoons  
4 and surfaces. The conformation of alkane-TMR (orange sticks) of the grey monomer is constrained by the light-pink monomer that was  
5 generated as symmetry mate. **E.** B-factor putty representation of the different chains of the asymmetric unit of the HT7-CPY crystal  
6 structure. Blue = 15; Red = 120. Chain E and to a lesser extent Chain D present an overall higher B-factor compared the other  
7 monomers. **F.** Structure alignment of the different monomers in the asymmetric unit of the HT7-CPY structure. The monomers are  
8 represented as wheat cartoon with the catalytic aspartate and alkane-CPY represented as sticks; all featuring similar conformations.  
9 **G.** Omit-maps of the alkane-CPY ligands of the different monomers in the HT7-CPY asymmetric unit. Proteins are represented as grey  
10 cartoons with the catalytic aspartates (grey) and alkane-CPYs (firebrick) represented as sticks. **H.** Omit-map of the TMR ligand of the  
11 HOB-TMR X-ray structure. The protein is represented as grey cartoon with the catalytic aspartate (grey) and the TMR ligand (orange)  
12 represented as sticks. **I.** Zoom on the isolated labeled catalytic aspartate of HOB-TMR. The omit map of the alkane-TMR is contoured  
13 at  $3\sigma$  and represented as green and red mesh for missing and extra density, respectively. **J.** Structure alignment of HT7-TMR, HT7-  
14 CPY (chain A) and HOB-TMR. Proteins are represented as grey, wheat and dark-green cartoons, respectively. The alkane-TMR and  
15 -CPY ligands are represented as orange and firebrick sticks, respectively. The catalytic aspartate is represented as sticks of the same  
16 color as the cartoons.

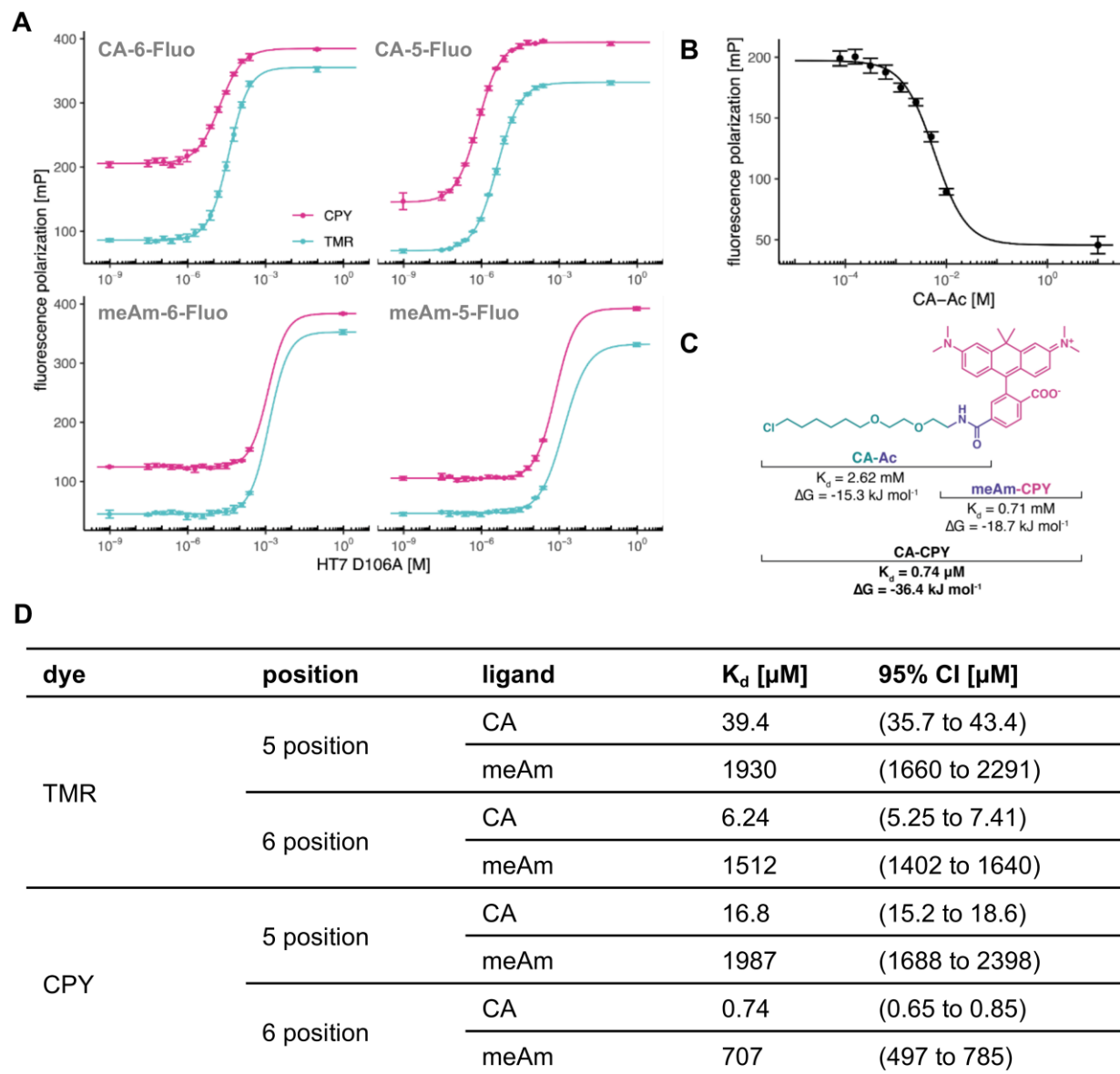


1  
2 **Figure S10:** Structural comparison between HT7-TMR structures from PDB IDs 6U32 and 6Y7A.  
3 **A.** Structure of HT7-TMR (PDB ID 6U32, previously published (16)) featuring two conformations of the alkane-TMR ligand **B.** Structural  
4 comparison between <sup>6U32</sup>HT7-TMR and <sup>6Y7A</sup>HT7-TMR (PDB ID 6Y7A, this study). Hydrogen bonds between <sup>6Y7A</sup>HT7-TMR and <sup>6U32</sup>HT7-

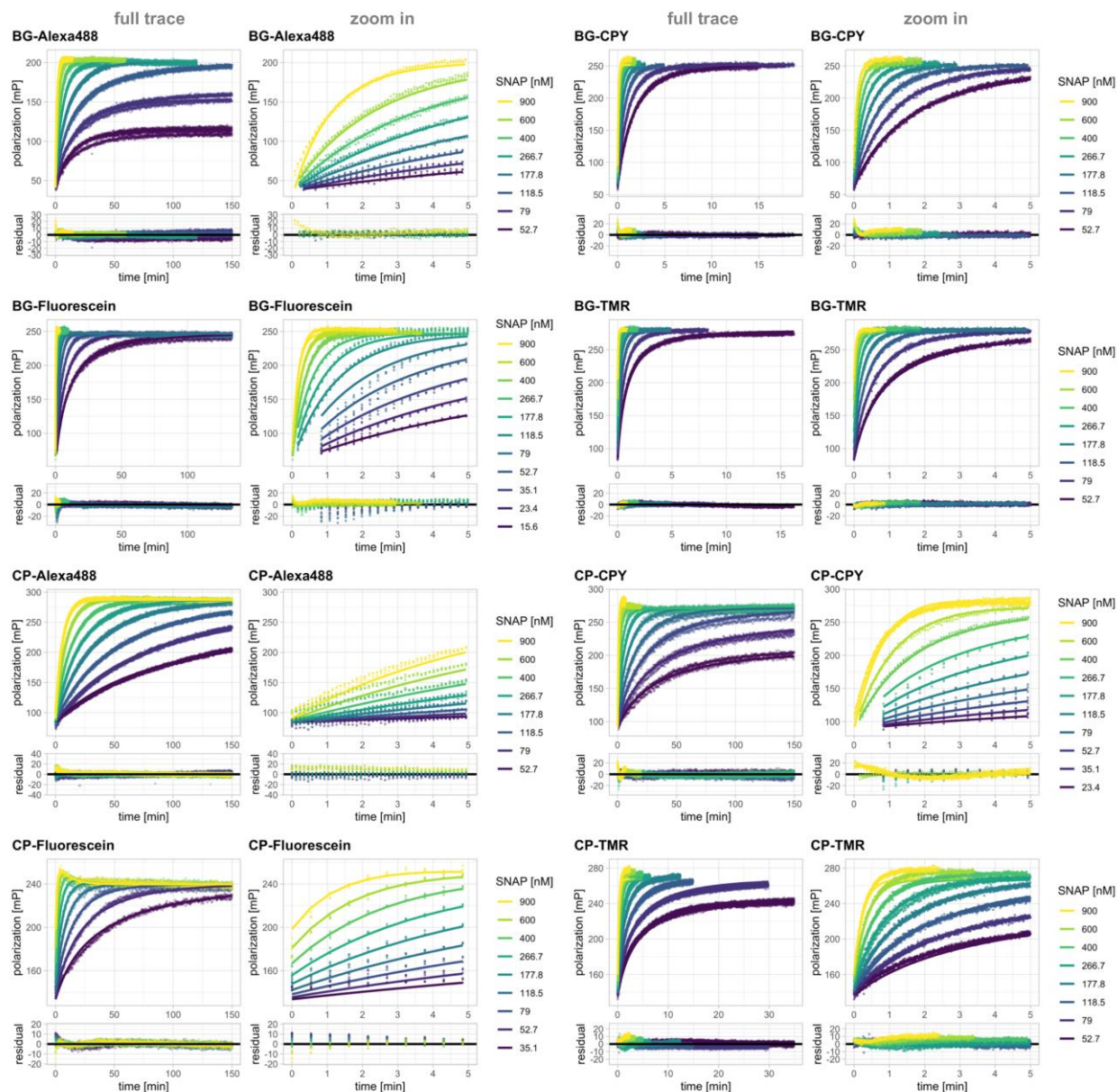
1 TMR and their respective reacted substrates are represented as black and dark-purple lines, respectively. **C.** <sup>6U32</sup>HT7-TMR crystal  
2 packing. Three monomers of HT7-TMR are represented as blue, green and pink cartoons. The conformation of the alkane-TMR  
3 (yellow/orange sticks) of the pink monomer is not constrained by the other symmetry mates. **D.** Zoom on the catalytic aspartate and  
4 alkane-TMR substrate highlighting the alternative conformations observed in the <sup>6U32</sup>HT7-TMR crystal structure. The two alternative  
5 TMR conformations (a and b) are represented as different tone of yellow/orange sticks. **E.** Structural comparison of the substrate  
6 positioning between <sup>6U32</sup>HT7-TMR and <sup>6Y7A</sup>HT7-TMR. Alkane-<sup>6U32</sup>TMR and alkane-<sup>6Y7A</sup>TMR are represented as yellow and orange  
7 sticks, respectively. The <sup>6Y7A</sup>TMR present a very similar conformation than one of the <sup>6U32</sup>TMR conformation which can't be observed  
8 due to the crystal packing in the <sup>6Y7A</sup>HT7-TMR crystal structure.



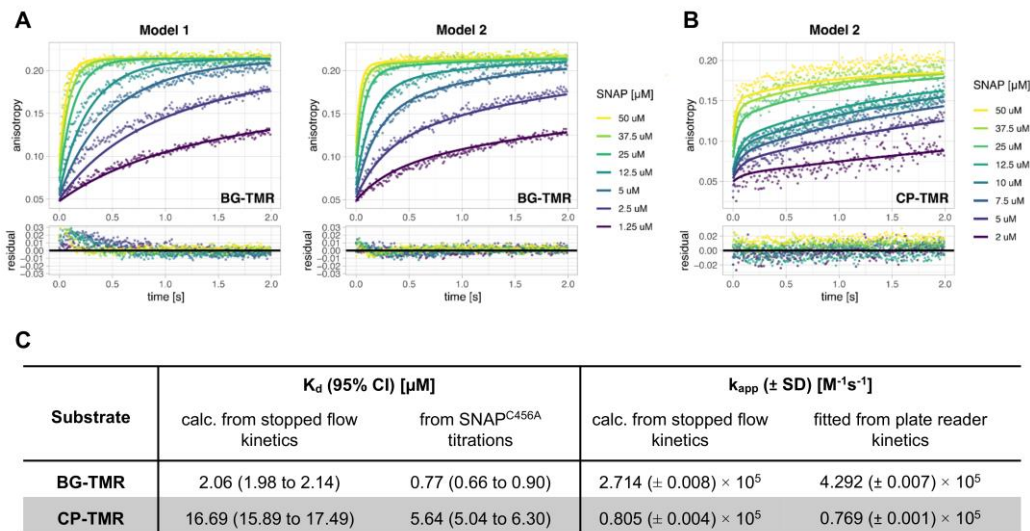
1  
2 **Figure S11:** Structural comparison between HT7-TMR, HT7-CPY (A) and HOB-TMR (B).  
3 **A.** Structural comparison between HT7-TMR and HT7-CPY. Hydrogen bonds between HT7-TMR and HT7-CPY and their respective  
4 reacted substrates are represented as black and sand dashed lines, respectively. **B.** Structural comparison between HT7-TMR and  
5 HOB-TMR. Hydrogen bonds between HT7 and HOB and their respective reacted substrates are represented as black and sand dashed  
6 lines, respectively.



1  
2 **Figure S12:** Biochemical study of the interaction of HT7 with CA-fluorophores.  
3 **A.** Affinity of the dead mutant HT7<sup>D106A</sup> towards different fluorophore derivatives measured via fluorescence polarization assay. The  
4 FP value of each dye as CA substrate fully bound to native HT7 was added at  $c = 0.1$  M or  $c = 1$  M in order to improve fitting of the  
5 upper plateau. **B.** Affinity of HT7<sup>D106A</sup> to CA-Ac measured via fluorescence polarization competition assay against CA-TMR. **C.**  
6 Summary of dissociation constants ( $K_d$ ) and calculated free binding energies ( $\Delta G$ ) of HT7<sup>D106A</sup> with CA-Ac, mAm-5-CPY and CA-5-  
7 CPY. The representation highlights the additive nature of the binding energies from the chloroalkane and the CPY moieties for the  
8 binding energy of the full substrate. **D.** Table summarizing values and confidence intervals (95%) of the fits.



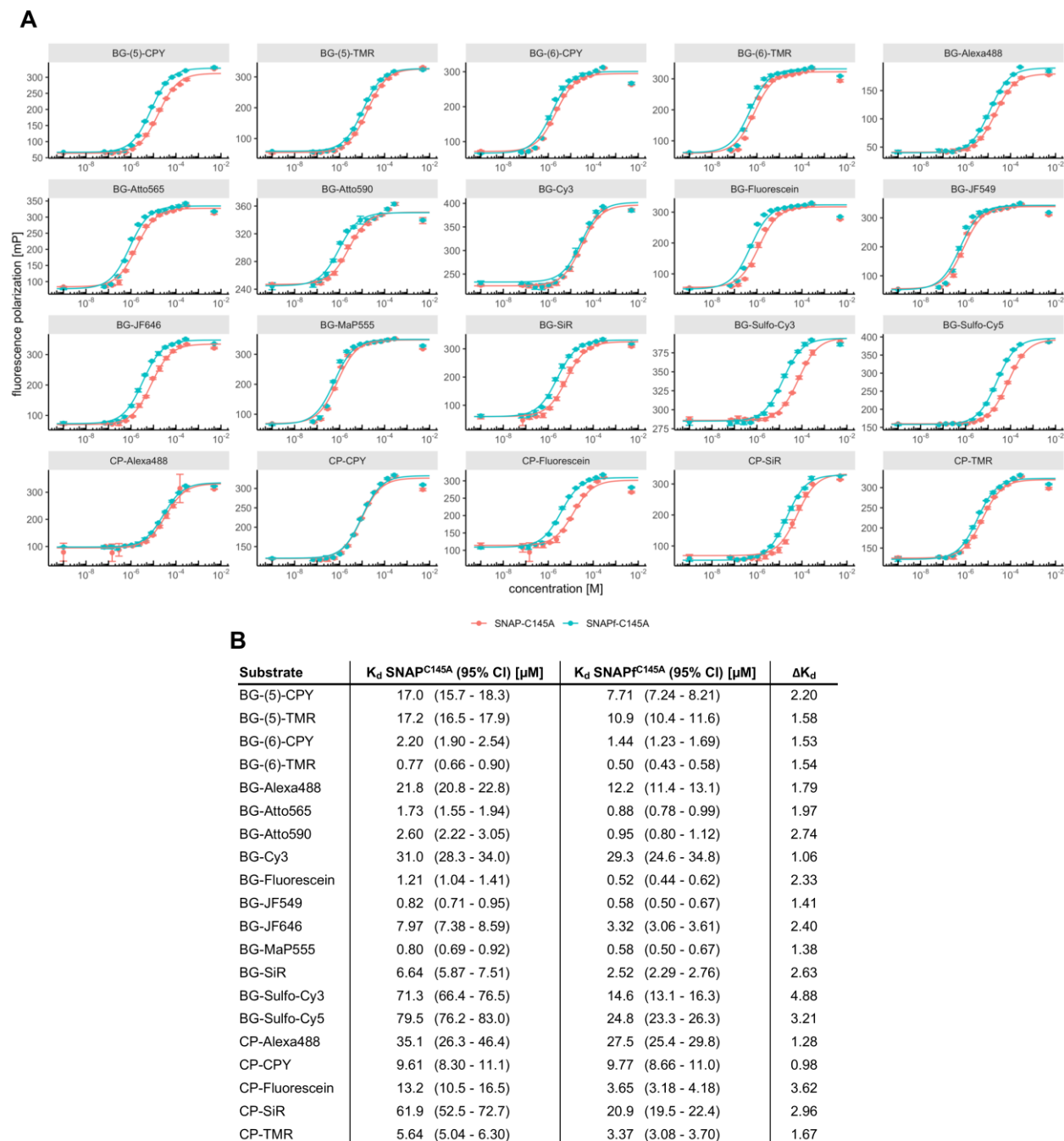
1  
2 **Figure S13:** Labeling kinetics of SNAP with fluorescent BG and CP substrates.  
3 Full fluorescence polarization traces (points) and predications of fits based on model 1 or 1.2 (lines) along with zoom on the initial 5  
4 minutes are represented on the top panels. Most substrates were fitted to model 1 except CP-Fluorescein and CP-CPY, which showed  
5 an additional phase (model 1.2). Residuals from the fits are depicted in the bottom panels. Kinetics were recorded by following  
6 fluorescence polarization changes over time using a plate reader. Labeling was performed at different concentrations of SNAP protein.  
7 Substrate concentrations were aimed at 20 nM based on the dyes extinction coefficient but fitted in the model since significant  
8 deviations from the expected stoichiometry were observed. For structures of BG and CP substrates see **Fig. S1**.



1

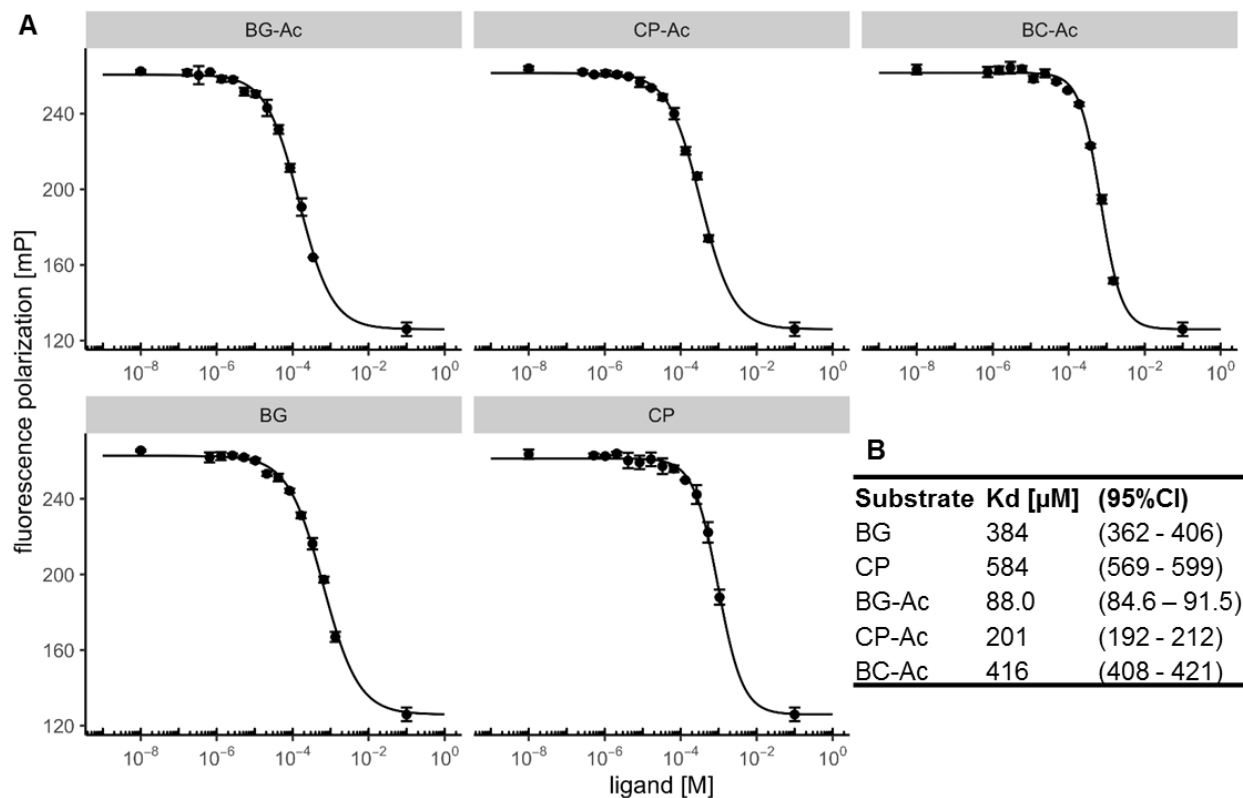
2 **Figure S14:** Labeling kinetics of SNAP measured by stopped flow fluorescence anisotropy.

3 **A.** Comparative data analysis of SNAP labeling kinetics with BG-TMR. Anisotropy traces (points) and predications of fits based on  
 4 either model 1 or model 2 (lines) of the labeling reaction between SNAP and BG-TMR are represented in the top panels. Residuals  
 5 from the fits are depicted in the bottom panels. Labeling was performed at different concentrations of SNAP protein and a constant  
 6 substrate concentration of 1  $\mu\text{M}$ . Model 2 describes the data better than the simplified model 1. (for model description see **Fig. 1**). **B.**  
 7 Kinetic traces of SNAP labeling with CP-TMR represented as previously explained and fit with model 2. For structures of BG and CP  
 8 substrates see **Fig. S1**. **C.**  $K_d$  and  $k_{app}$  values calculated from parameters obtained by fitting model 2 to stopped flow anisotropy data  
 9 ( $K_d = k_{-1}/k_1$ ,  $k_{app} = k_1 \cdot k_2 / (k_{-1} + k_2)$ ) compared to values directly fitted to fluorescence polarization assay with SNAP<sup>C145A</sup> ( $K_d$ ) and plate  
 10 reader kinetics at lower SNAP concentrations fitted with model 1 ( $k_{app}$ ).

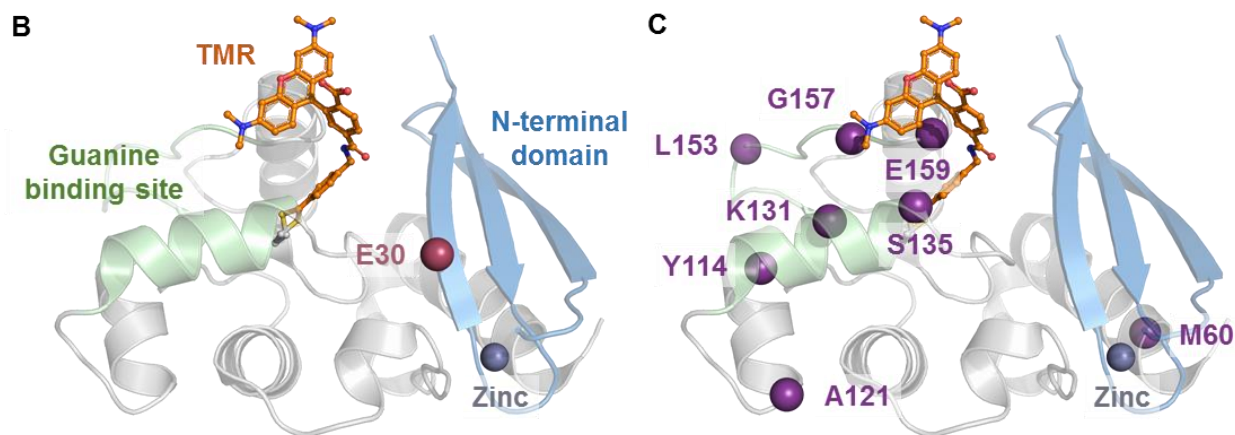
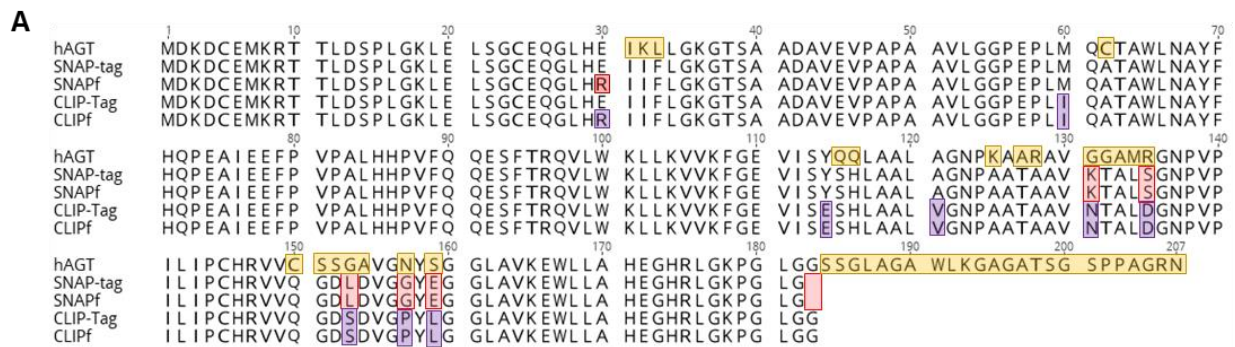


1  
2 **Figure S15:** Comparison of fluorophore substrate affinities between the dead mutants SNAP<sup>C145A</sup> and SNAP<sup>fC145A</sup>.  
3 **A.** Titration curves obtained for the dead mutants SNAP<sup>C145A</sup> and SNAP<sup>fC145A</sup> measured via fluorescence polarization. The FP value of  
4 each dye fully bound to native SNAP/SNAPf was added at  $c = 0.005$  M to improve fitting of the upper plateau. (See corresponding  
5 methods section for more details). **B.** Table summarizing fitted  $K_d$  values with 95% confidence intervals. For structures of BG and CP  
6 substrates see **Fig. S1**.

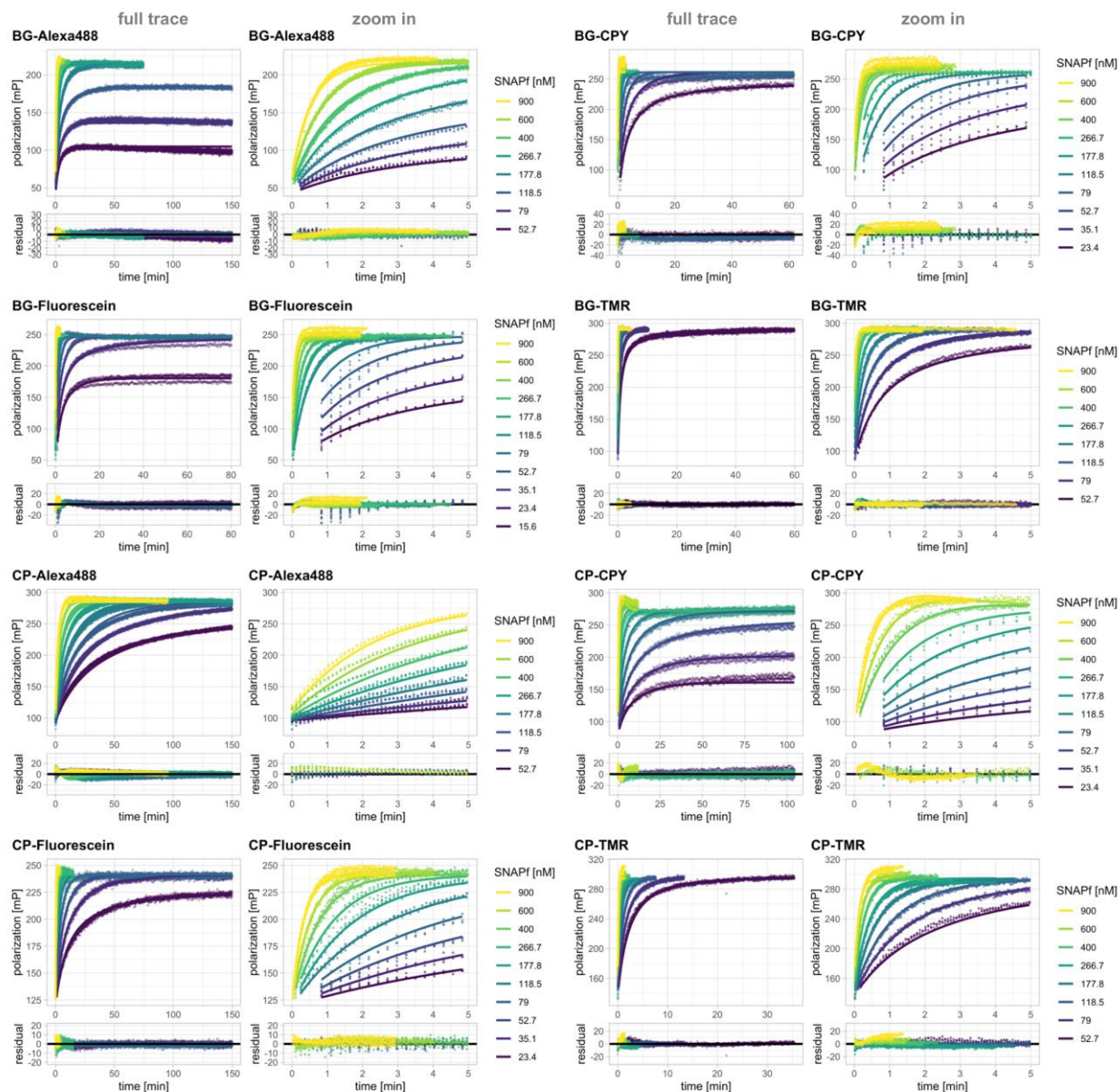




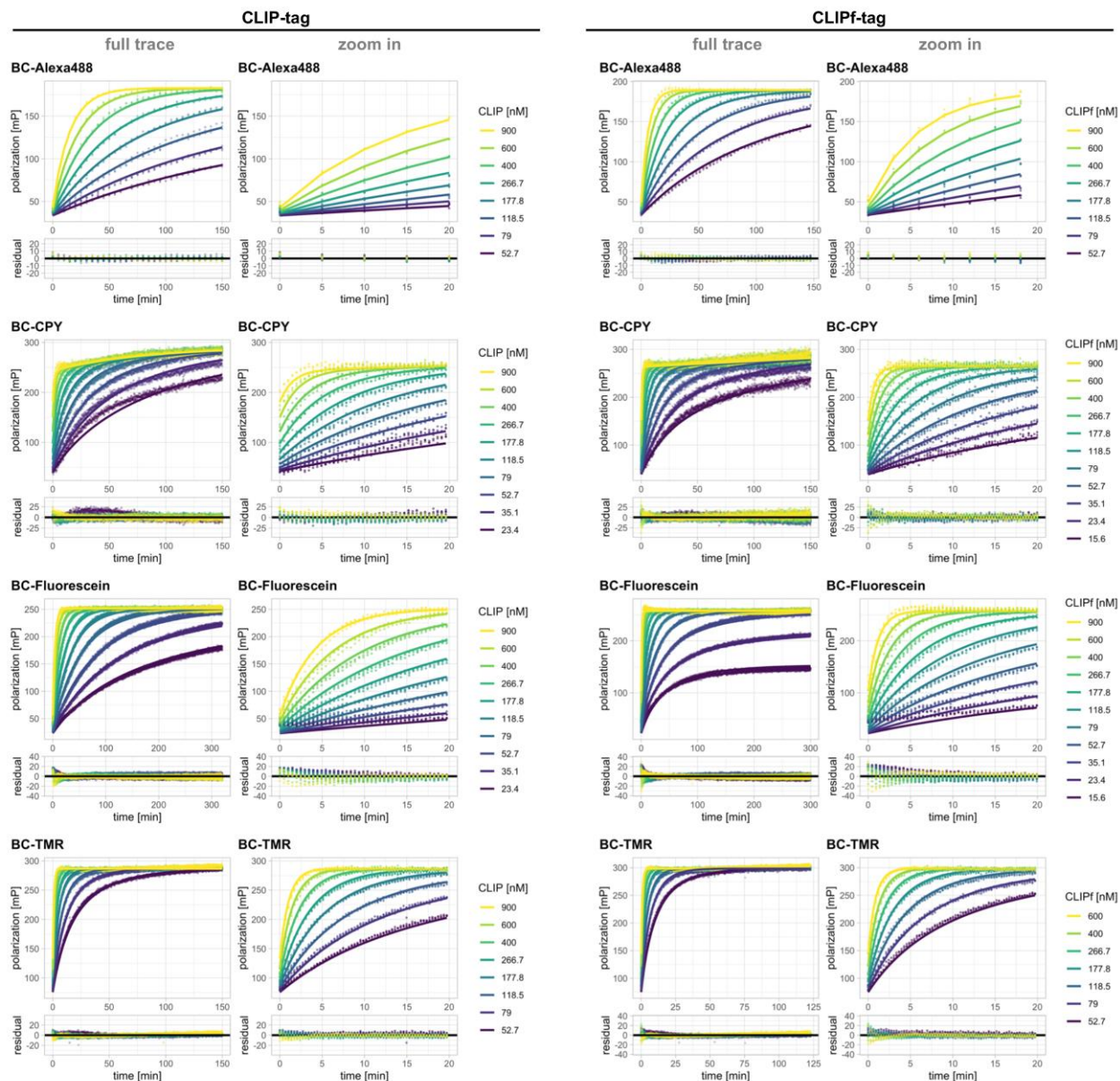
1  
2 **Figure S16:** Comparison of non-derivatized core substrate affinities with the dead mutant SNAP<sup>C145</sup>.  
3 **A.** Titration curves obtained for the dead mutant SNAP<sup>C145A</sup> measured via competitive fluorescence polarization. The FP value of free  
4 dye was added at  $c = 0.1$  M to improve fitting of the lower plateau. (See corresponding methods section for more details) **B.** Table  
5 summarizing fitted  $K_d$  values with 95% confidence intervals. For structures of substrates see **Fig. S1**.



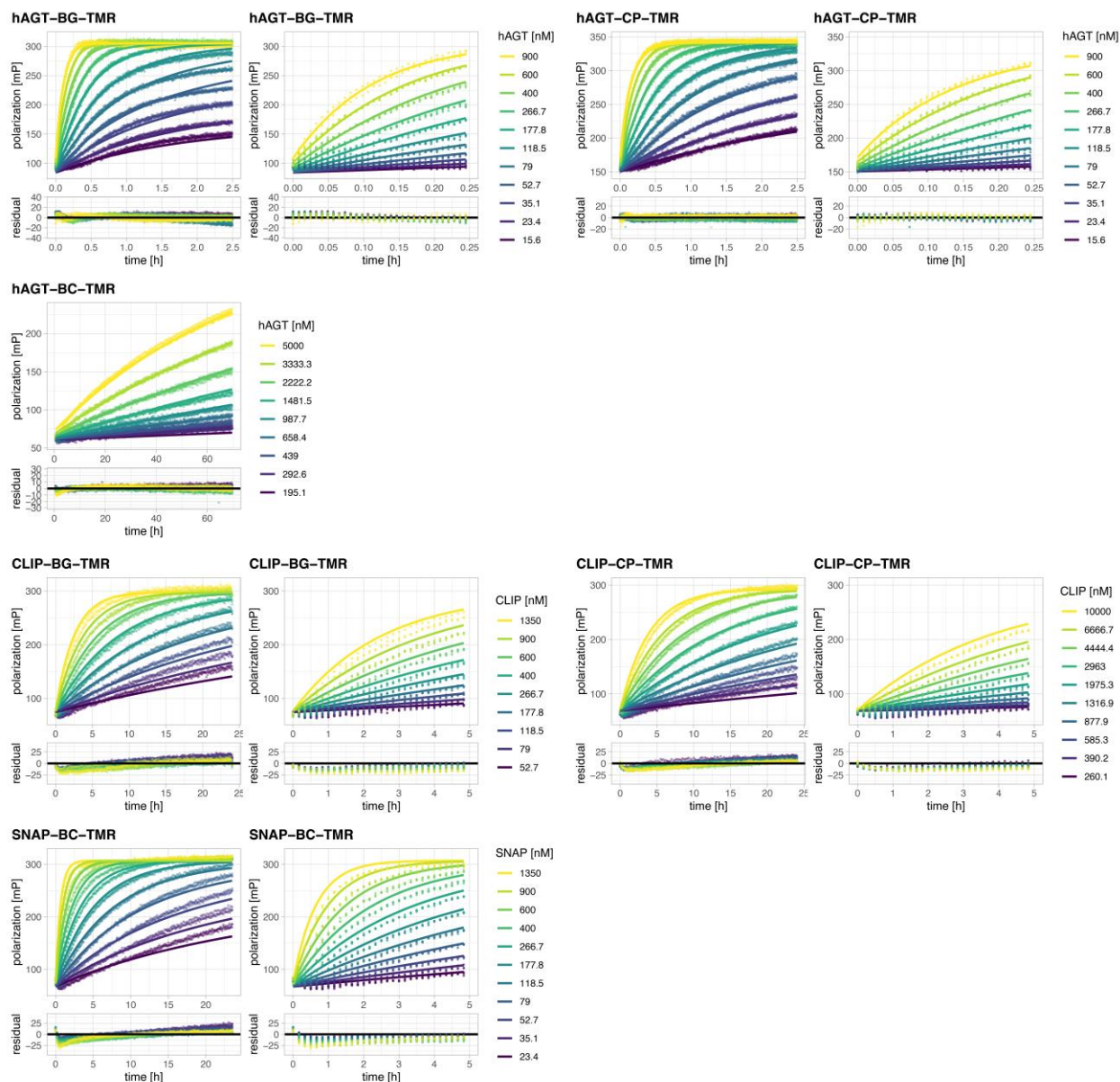
1  
2 **Figure S17:** Sequence alignment and structural comparison between SNAP and CLIP variants.  
3 **A.** Sequence alignment of hAGT, SNAP, SNAPf, CLIP and CLIPf. Differences are highlighted in yellow, red and violet in the hAGT,  
4 SNAP(f) and CLIP(f) sequences, respectively. **B.** Crystal structure of SNAP labeled with TMR. SNAP is represented as grey cartoon  
5 despite for the BG binding site and the N-terminal domain that are represented in green and blue, respectively. The catalytic cysteine  
6 is represented as grey sticks and the benzyl-TMR as orange sticks. The residue E30 which is mutated to an arginine (R) in SNAPf is  
7 highlighted as a red sphere. **C.** Crystal structure of SNAP labeled with TMR with  $\alpha$ -carbons of the residues that differ between SNAP  
8 and CLIP represented as purple spheres.



1  
2 **Figure S18:** Labeling kinetics of SNAPf with fluorescent BG and CP substrates.  
3 Full fluorescence polarization traces (points) and predictions of fits based on model 1 or 1.2 (lines) along with zoom on the initial 5  
4 minutes are represented on the top panels. All substrates were fitted to model 1 except CP-CPY, which showed an additional phase  
5 (model 1.2). Residuals from the fits are depicted in the bottom panels. Kinetics were recorded by following fluorescence polarization  
6 changes over time using a plate reader. Labeling was performed at different concentrations of SNAPf protein. Substrate concentrations  
7 were aimed at 20 nM based on the dyes extinction coefficient but fitted in the model since significant deviations from the expected  
8 stoichiometry were observed. For structures of BG and CP substrates see **Fig. S1**.

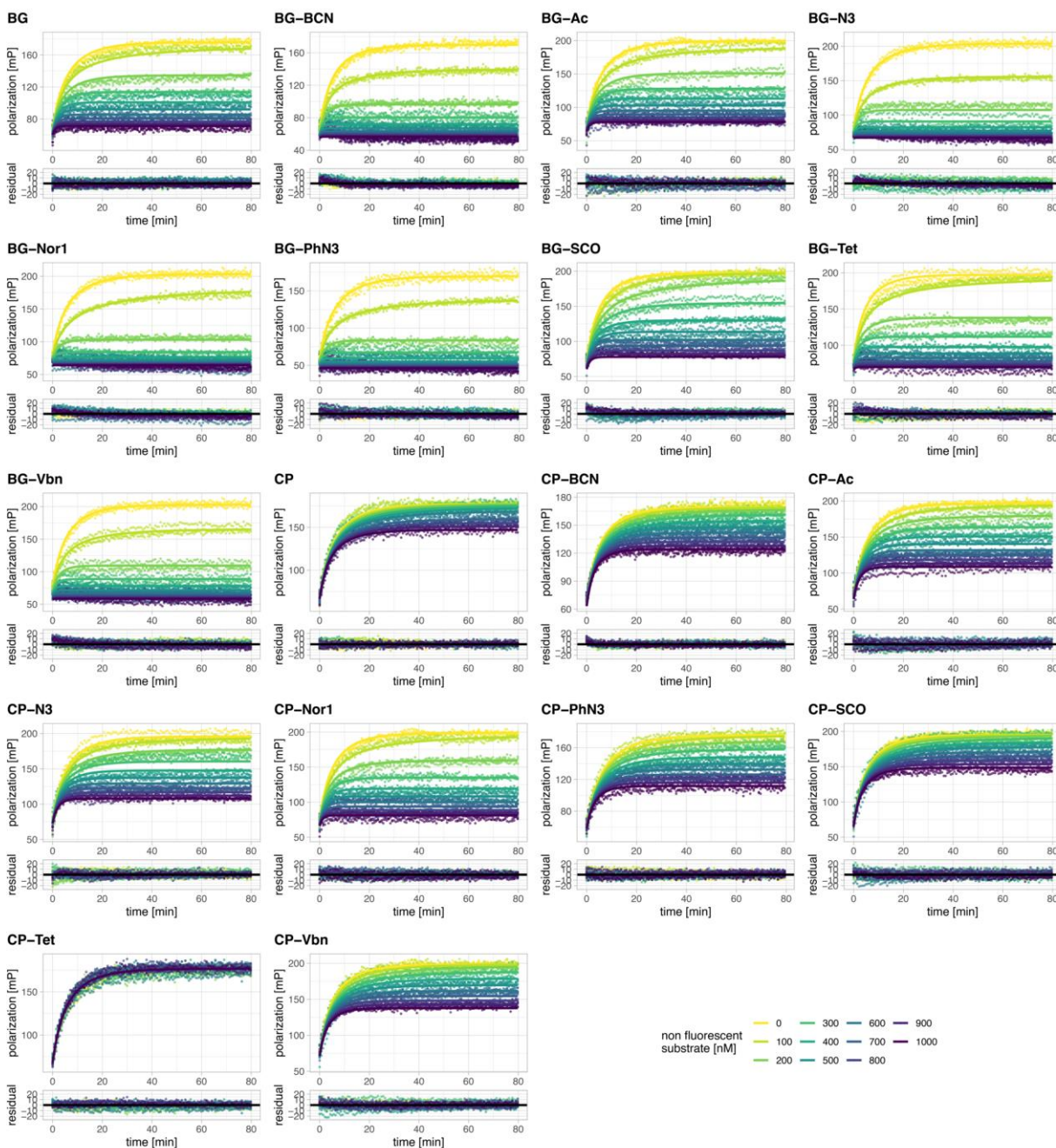


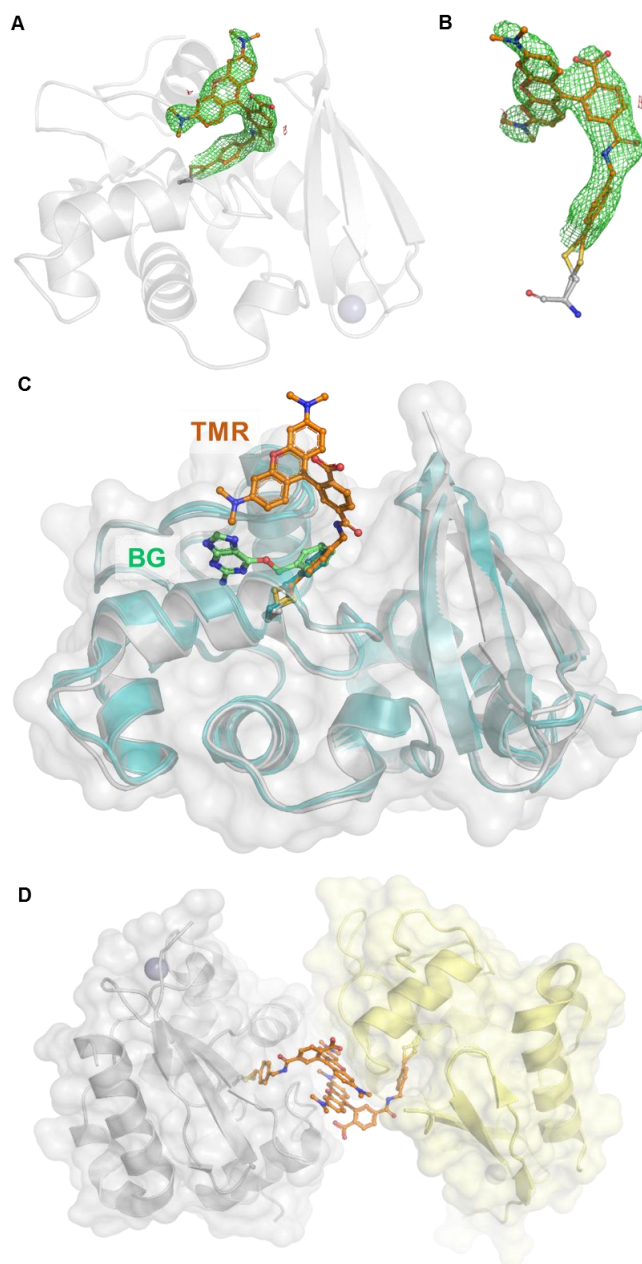
1  
2 **Figure S19:** Labeling kinetics of CLIP and CLIPf with fluorescent BC substrates.  
3 Full fluorescence polarization traces (points) and predications of fits based on model 1 or 1.2 (lines) along with zoom on the initial 20  
4 minutes are represented on the top panels. All substrates were fitted to model 1 except BC-CPY, which showed an additional phase  
5 (model 1.2). Residuals from the fits are depicted in the bottom panels. Kinetics were recorded by following fluorescence polarization  
6 changes over time using a plate reader. Labeling was performed at different concentrations of CLIP and CLIPf protein. Substrate  
7 concentrations were aimed at 20 nM based on the dyes extinction coefficient but fitted in the model since significant deviations from  
8 the expected stoichiometry were observed. For structures of BC substrates see **Fig. S1**.



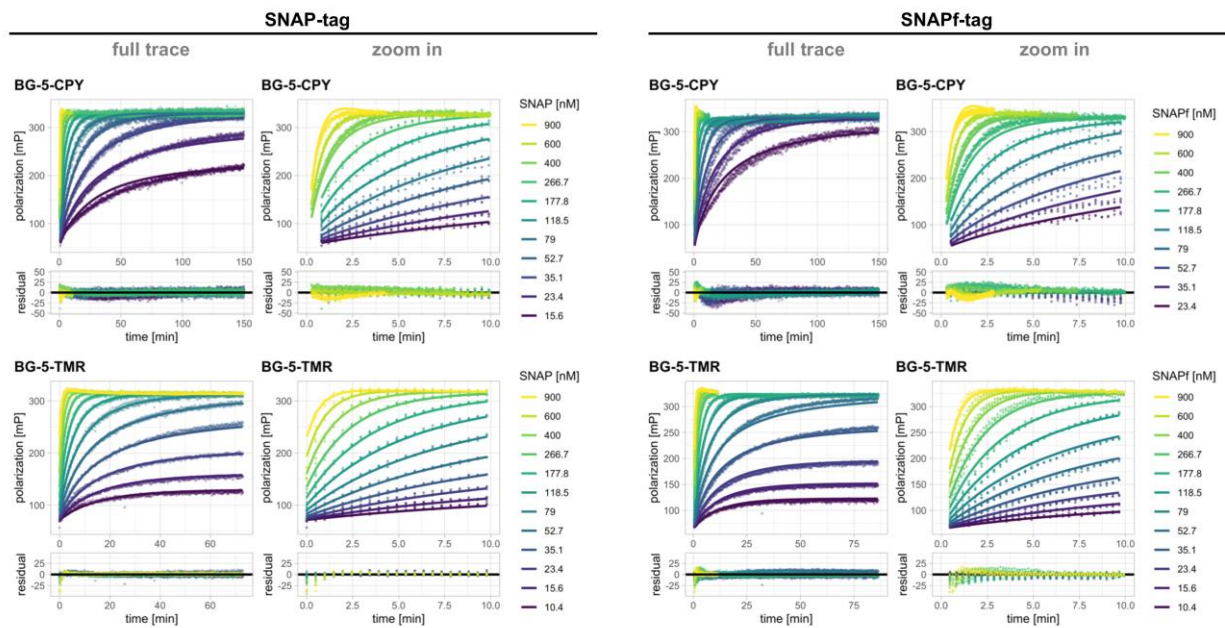
1  
 2 **Figure S20:** Labeling kinetics of hAGT, SNAP and CLIP with the non-respective BG-, CP- and BC-TMR substrates.  
 3 Full fluorescence polarization traces (points) and predications of fits based on model 1 along with zoom on the initial part (except for  
 4 BC-TMR and hAGT) are represented on the top panels. Residuals from the fits are depicted in the bottom panels. Kinetics were  
 5 recorded by following fluorescence polarization changes over time using a plate reader. Labeling was performed at different  
 6 concentrations of hAGT, SNAP and CLIP proteins. Substrate concentrations were aimed at 20 nM based on the dyes extinction  
 7 coefficient but fitted in the model since significant deviations from the expected stoichiometry were observed. For structures of BG, CP  
 8 and BC substrates see **Fig. S1**.

1



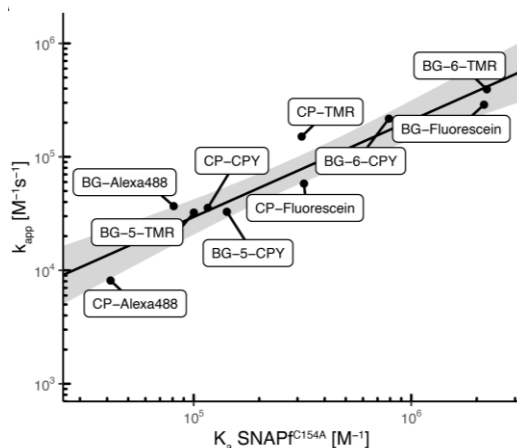


1  
2 **Figure S22:** Validation and analysis of the SNAP-TMR X-ray structure.  
3 **A.** Omit-map of the TMR ligand of the SNAP-TMR structure. The protein is represented as grey cartoon, TMR fluorophore-substrate  
4 as orange sticks and the catalytic cysteine as grey sticks. **B.** Zoom on the isolated labeled catalytic cysteine of SNAP-TMR. Omit-map  
5 contoured at  $3\sigma$ , represented as green and red mesh for missing and extra density, respectively. **C.** Comparison of the SNAP structure  
6 with available SNAP structures. SNAP-TMR is represented as previously explained. Apo SNAP (PDB ID 3KZY), benzylated SNAP  
7 PDB ID 3L00) and the BG bound dead mutant SNAP<sup>C145A</sup> (PDB ID 3KZZ) are represented as cartoon with different shades of blue-  
8 green. No major structural differences are observed with SNAP-TMR. **D.** Benzyl-TMR constraints by the crystal packing. Two  
9 monomers of SNAP-TMR are represented as grey and yellow cartoons. The conformation of the benzyl-TMR (orange sticks) of both  
10 monomers is constrained by the other monomer. Symmetry mates were generated within 4 Å radius and selected to highlight the  
11 packing constraints.



1  
2 **Figure S23:** Labeling kinetics of SNAP and SNAPf with BG-5-TMR and BG-5-CPY.  
3 Full fluorescence polarization traces (points) and predictions of fits based on model 1.2 (lines) along with zoom on the initial 10  
4 minutes are represented on the top panels. Residuals from the fits are depicted in the bottom panels. Kinetics were recorded by  
5 following fluorescence polarization changes over time using a plate reader. Labeling was performed at different concentrations of  
6 SNAP and SNAPf protein. Substrate concentrations were aimed at 20 nM based on the dyes extinction coefficient but fitted in the  
7 model since significant deviations from the expected stoichiometry were observed. For structures of BG substrates see **Fig. S1**.

8

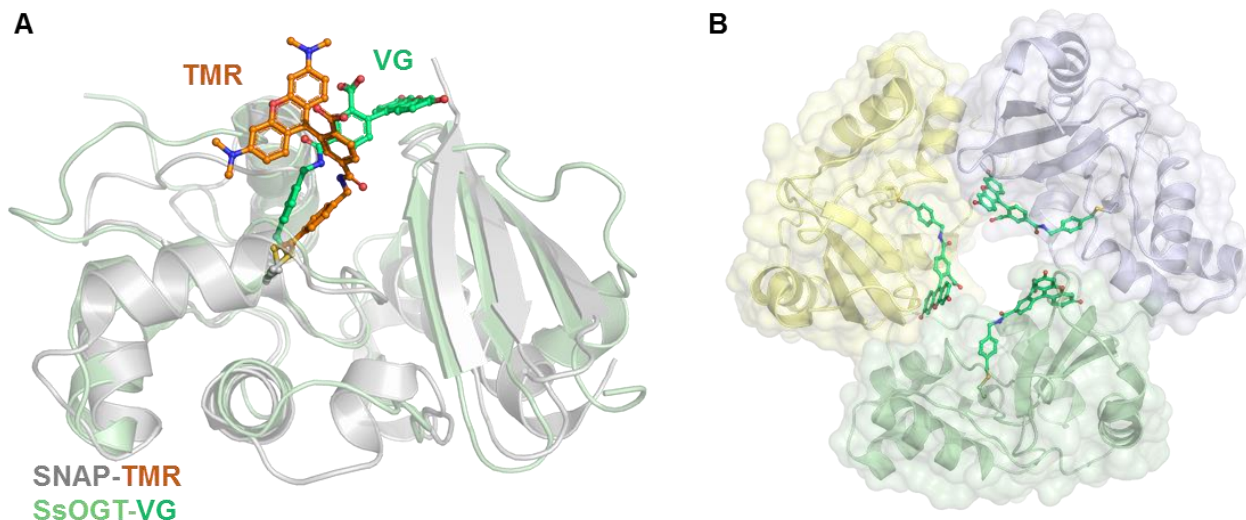


9

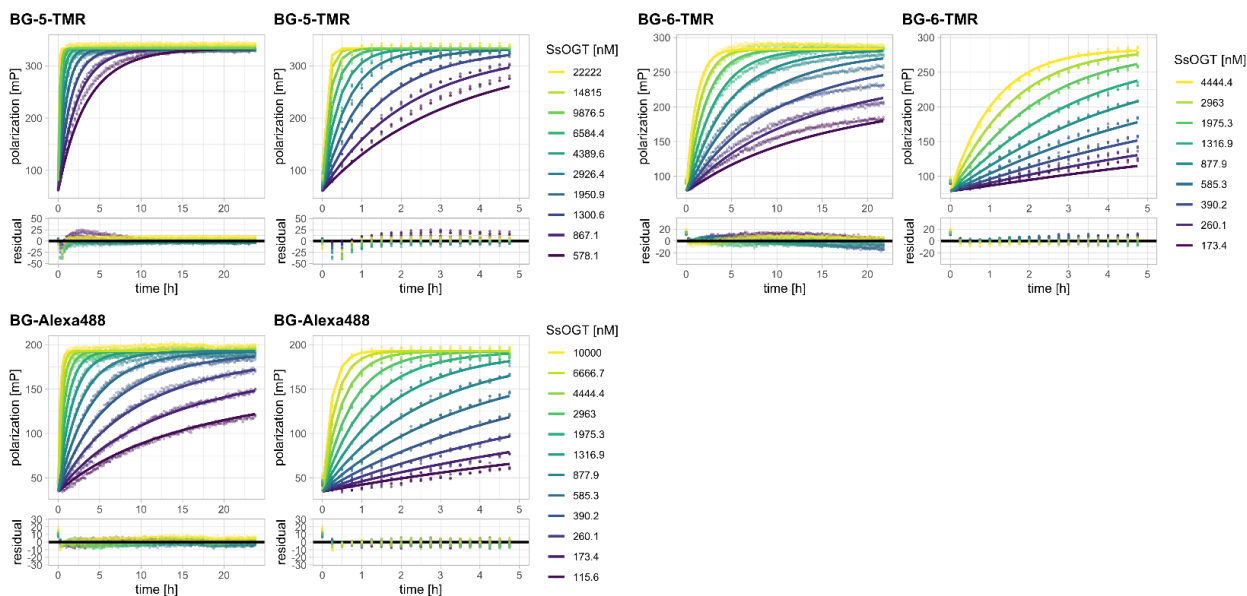
10 **Figure S24:** SNAPf kinetic and affinity correlations.

11 Correlation between SNAPf labeling kinetics ( $k_{app}$ ) and affinity ( $K_a = 1/K_d$ ) for different fluorophore substrates. Affinities were obtained  
12 with the catalytically dead mutant SNAPf<sup>C145A</sup>. Log transformed values were fitted to a linear model ( $\log(k_{app}) = 0.2568 +$   
13  $\log(K_a) * 1.0697$ , 95% confidence bands in grey, depicting the area in which the true regression line lies with 95% confidence). The  
14 linear correlation in logarithmic space suggests that the  $K_d$  of fluorescent SNAP substrates towards SNAPf<sup>C145A</sup> could represent a valid  
15 proxy to estimate their  $K_{app}$  towards native SNAPf.





1  
2 **Figure S25:** SsOGT-H<sup>5</sup>-VistaGreen alternative fluorophore conformation.  
3 **A.** Structural alignment of SNAP-TMR with SsOGT-H<sup>5</sup>-VG structure (PDB ID 6GA0) (17). **B.** Benzyl-VG constraints by the crystal  
4 packing. Three monomers of SsOGT-H<sup>5</sup>-VG are represented as blue, green and yellow cartoons. The conformation of the benzyl-VG  
5 (green sticks) of all monomers is constrained by the neighboring monomer. Symmetry mates were generated within 4 Å radius and  
6 selected to highlight the packing constraints.



8  
9 **Figure S26:** Labeling kinetics of SsOGT-H<sup>5</sup> with BG-Alexa488 and BG-TMR.

10 Full fluorescence polarization traces (points) and predications of fits based on model 1 (lines) along with zoom on the initial 5 hours  
11 are represented on the top panels. Residuals from the fits are depicted in the bottom panels. Kinetics were recorded by following  
12 fluorescence polarization changes over time using a plate reader. Labeling was performed at different concentrations of SsOGT-H<sup>5</sup>  
13 protein. Substrate concentrations were aimed at 20 nM based on the dyes extinction coefficient but fitted in the model since significant  
14 deviations from the expected stoichiometry were observed. For structures of BG substrates see **Fig. S1**.

1 **Table S1:** Kinetic parameters of HT7 labeling with fluorescent CA substrates.

Substrate	$k_1 (\pm \text{S.D.}) [\text{M}^{-1} \text{s}^{-1}]$	$k_{-1} (\pm \text{S.D.}) [\text{s}^{-1}]$	$k_2 (\pm \text{S.D.}) [\text{s}^{-1}]$	$k_{\text{app}} (\pm \text{S.D.}) [\text{M}^{-1} \text{s}^{-1}]$
CA-TMR	$7.84 (\pm 0.76) \times 10^7$	$2.56 (\pm 0.38) \times 10^1$	$8.06 (\pm 0.29)$	$1.88 (\pm 0.01) \times 10^7$
CA-JF549	$1.60 (\pm 0.16) \times 10^8$	$9.83 (\pm 2.04) \times 10^1$	$1.82 (\pm 0.07) \times 10^1$	$1.66 (\pm 0.01) \times 10^7$
CA-JF669	$2.35 (\pm 0.75) \times 10^7$	$3.39 (\pm 1.49) \times 10^1$	$6.94 (\pm 0.47)$	$4.03 (\pm 0.02) \times 10^6$
CA-CPY	$1.6.7 (\pm 0.067) \times 10^8$	$7.60 (\pm 0.98)$	$9.86 (\pm 0.73)$	$9.44 (\pm 0.18) \times 10^7$
CA-LIVE580	$1.74 (\pm 0.05) \times 10^8$	$1.75 (\pm 0.28)$	$6.77 (\pm 0.77)$	$1.39 (\pm 0.03) \times 10^8$
CA-TMR-biotin	$3.69 (\pm 0.25) \times 10^7$	$2.10 (\pm 0.25) \times 10^1$	$8.24 (\pm 0.28)$	$1.04 (\pm 0.01) \times 10^7$

2 Data analyzed using model 2.

3  
4 **Table S2:** Comparison  $k_{\text{app}}$  of HT7 labeling kinetics analyzed using models 1 and 2.

Substrate	$k_{\text{app}} (\pm \text{S.D.}) [\text{M}^{-1} \text{s}^{-1}]$	
	Model 1	Model 2
CA-TMR	$1.79 (\pm 0.01) \times 10^7$	$1.88 (\pm 0.01) \times 10^7$
CA-JF549	$1.46 (\pm 0.01) \times 10^7$	$1.66 (\pm 0.01) \times 10^7$
CA-JF669	$3.95 (\pm 0.02) \times 10^6$	$4.03 (\pm 0.02) \times 10^6$
CA-CPY	$1.10 (\pm 0.02) \times 10^8$	$9.44 (\pm 0.18) \times 10^7$
CA-LIVE580	$1.58 (\pm 0.02) \times 10^8$	$1.39 (\pm 0.03) \times 10^8$
CA-TMR-biotin	$9.00 (\pm 0.04) \times 10^6$	$1.04 (\pm 0.01) \times 10^7$

5  
6 **Table S3:** Comparison of HT7 and HOB labeling kinetics with fluorescent CA substrates.

Protein	Substrate	$k_1 (\pm \text{S.D.}) [\text{M}^{-1} \text{s}^{-1}]$	$k_{-1} (\pm \text{S.D.}) [\text{s}^{-1}]$	$k_2 (\pm \text{S.D.}) [\text{s}^{-1}]$	$k_{\text{app}} (\pm \text{S.D.}) [\text{M}^{-1} \text{s}^{-1}]$
HT7	CA-TMR	$7.84 (\pm 0.76) \times 10^7$	$2.56 (\pm 0.38) \times 10^1$	$8.06 (\pm 0.29)$	$1.88 (\pm 0.01) \times 10^7$
	CA-Alexa488	-	-	-	$2.57 (\pm 0.01) \times 10^4$
HOB	CA-TMR	$4.15 (\pm 0.26) \times 10^7$	$1.83 (\pm 0.17) \times 10^1$	$5.05 (\pm 0.13)$	$8.99 (\pm 0.04) \times 10^6$
	CA-Alexa488	-	-	-	$8.04 (\pm 0.02) \times 10^7$

7  
8

1 **Table S4:** Data collection and refinement statistics the X-ray crystal structures.

Data collections	SNAP-TMR	HT7-TMR	HT7-CPY	HOB-TMR
<b>PDB ID</b>	6Y8P	6Y7A	6Y7B	6ZCC
<b>Beamline</b>	ESRF ID29	PXII-X10SA, SLS	PXII-X10SA, SLS	PXII-X10SA, SLS
<b>Wavelength (Å°)</b>	0.976	1.00001	1.00006	0.99984
<b>Resolution (Å°)</b> <b>(last bin)</b>	36.88 - 2.3 (2.382 - 2.3)	50-1.40 (1.50-1.40)	50-3.10 (3.20-3.10)	50-1.50 (1.60-1.50)
<b>Space group</b>	<i>P</i> 3 <sub>2</sub> 21	<i>P</i> 12 <sub>1</sub>	<i>P</i> 321	<i>P</i> 2 <sub>1</sub> 2 <sub>1</sub> 2 <sub>1</sub>
<b>Unit cell dimensions</b>				
<b>a (Å°)</b>	65.5148	44.00	161.27	52.21
<b>b (Å°)</b>	65.5148	78.14	161.27	64.77
<b>c (Å°)</b>	97.067	45.24	124.66	78.85
<b>No. observed reflections</b>	119190 (12210)	160637 (29978)	231609 (21528)	228695 (8515)
<b>No. unique reflections</b>	11152 (1087)	50448 (9451)	34294 (3081)	38699 (3579)
<b>Completeness (%)</b>	99.94 (100.00)	96.5 (97.1)	99.8 (99.9)	88.9 (47.5)
<b>Rmerge</b>	0.1015 (0.8636)	0.063 (0.410)	0.196 (0.596)	0.042 (0.241)
<b>I/σ(I)</b>	13.48 (2.82)	9.59 (2.83)	8.53 (3.10)	18.87 (2.39)
<b>CC ½ (%)</b>	99.9 (19.3)	99.7 (86.4)	98.8 (85.7)	99.9 (93.4)
<b>Redundancy</b>	10.7 (11.2)	3.18 (3.17)	6.75 (6.99)	5.91 (2.38)
<b>Wilson B</b>	47.75	21.39	37.99	32.28
<b>Refinement statistics</b>				
<b>Resolution range (Å)</b>	36.88-2.3	39.19-1.40	49.32-3.10	43.53-1.52
<b>No. Reflections</b>	8878	50435	34290	38697
<b>Rwork (%)</b>	0.2385	0.1558	0.2074	0.1887
<b>Rfree (%)</b>	0.2694	0.1868	0.2594	0.2238
<b>No. protein atoms</b>	1231	2397	11750	2348
<b>No. water atoms</b>	50	348	0	312
<b>No. ligand atoms</b>	45	51	235	52
<b>Average B factor (Å<sup>2</sup>)</b>	73.06	18.93	51.23	31.74
<b>RMSD from ideal</b>				
<b>Bond lengths (Å°)</b>	0.007	0.013	0.004	0.009
<b>Bond angles (°)</b>	1.24	1.247	0.788	1.014

2

1 **Table S5:** Kinetic parameters of SNAP and CLIP labeling with fluorescent substrates analyzed using model 1.2.

Substrate	$k_{app} (\pm \text{S.D.}) [\text{s}^{-1}\text{M}^{-1}]$	$k_3 (\pm \text{S.D.}) [\text{s}^{-1}]$	$k_{app} (\pm \text{S.D.}) [\text{s}^{-1}\text{M}^{-1}]$	$k_3 (\pm \text{S.D.}) [\text{s}^{-1}]$
SNAP CP-Fluorescein	$1.42 (\pm 0.01) \times 10^4$	$1.61 (\pm 0.04) \times 10^{-3}$	-	-
SNAP CP-CPY	$1.59 (\pm 0.01) \times 10^4$	$1.26 (\pm 0.01) \times 10^{-2}$	$3.55 (\pm 0.02) \times 10^4$	$6.22 (\pm 0.13) \times 10^{-3}$
CLIP BC-CPY	$1.26 (\pm 0.01) \times 10^4$	$2.16 (\pm 0.09) \times 10^{-4}$	$2.65 (\pm 0.01) \times 10^4$	$9.02 (\pm 0.48) \times 10^{-7}$

2

3 **Table S6:** Kinetic parameters of SNAP labeling with TMR substrates measured via stopped flow.

Substrate	$k_1 (\pm \text{S.D.}) [\text{M}^{-1}\text{s}^{-1}]$	$k_{-1} (\pm \text{S.D.}) [\text{s}^{-1}]$	$k_2 (\pm \text{S.D.}) [\text{s}^{-1}]$	$k_{app} (\pm \text{S.D.}) [\text{M}^{-1}\text{s}^{-1}]$
BG-TMR	$4.93 (\pm 0.04) \times 10^5$	$1.02 (\pm 0.03)$	$1.24 (\pm 0.02)$	$2.71 (\pm 0.01) \times 10^5$
CP-TMR	$5.36 (\pm 0.30) \times 10^5$	$8.96 (\pm 0.71)$	$1.58 (\pm 0.04)$	$0.81 (\pm 0.01) \times 10^5$

Data analyzed using model 2

4

5

6 **Table S7:** Comparison of SNAP/CLIP with SNAPf/CLIPf labeling kinetics with fluorescent substrates.

Substrate		$k_{app} (\pm \text{S.D.}) [\text{s}^{-1}\text{M}^{-1}]$	
		Original	Fast variant
SNAP BG substrates	BG-Alexa488	$1.22 (\pm 0.01) \times 10^4$	$3.68 (\pm 0.64) \times 10^4$
	BG-Fluorescein	$1.17 (\pm 0.01) \times 10^5$	$2.88 (\pm 0.01) \times 10^5$
	BG-CPY	$2.17 (\pm 0.01) \times 10^5$	$2.17 (\pm 0.02) \times 10^5$
	BG-TMR	$4.29 (\pm 0.01) \times 10^5$	$3.94 (\pm 0.01) \times 10^5$
SNAP CP substrates	CP-Alexa488	$3.12 (\pm 0.003) \times 10^3$	$8.13 (\pm 0.01) \times 10^3$
	CP-Fluorescein	$1.42 (\pm 0.01) \times 10^4 (*)$	$5.81 (\pm 0.01) \times 10^4$
	CP-CPY*	$1.59 (\pm 0.01) \times 10^4 (*)$	$3.55 (\pm 0.02) \times 10^4 (*)$
	CP-TMR	$7.69 (\pm 0.01) \times 10^4$	$1.51 (\pm 0.01) \times 10^5$
CLIP BC substrates	BC-Alexa488	$1.26 (\pm 0.01) \times 10^3$	$3.10 (\pm 0.02) \times 10^3$
	BC-Fluorescein	$4.36 (\pm 0.01) \times 10^3$	$1.62 (\pm 0.01) \times 10^4$
	BC-TMR	$1.85 (\pm 0.01) \times 10^4$	$3.37 (\pm 0.01) \times 10^4$
	BC-CPY*	$1.26 (\pm 0.01) \times 10^4 (*)$	$2.65 (\pm 0.01) \times 10^4 (*)$

Data analyzed using model 1 or 1.2 (\*) which included an additional phase (see Table S5).

7

8

9 **Table S8:** Comparison of SNAP labeling kinetics with 5- and 6-fluorophores.

Substrate	SNAP		SNAPf	
	$k_{app} (\pm \text{S.D.}) [\text{s}^{-1}\text{M}^{-1}]$	$k_3 (\pm \text{S.D.}) [\text{s}^{-1}]$	$k_{app} (\pm \text{S.D.}) [\text{s}^{-1}\text{M}^{-1}]$	$k_3 (\pm \text{S.D.}) [\text{s}^{-1}]$
BG-6-TMR	$4.29 (\pm 0.01) \times 10^5$	-	$3.94 (\pm 0.01) \times 10^5$	-
BG-5-TMR (*)	$2.67 (\pm 0.01) \times 10^4$	$1.53 (\pm 0.12) \times 10^{-3}$	$3.23 (\pm 0.01) \times 10^4$	$2.18 (\pm 0.18) \times 10^{-3}$
BG-6-CPY	$2.17 (\pm 0.01) \times 10^5$	-	$2.17 (\pm 0.02) \times 10^5$	-
BG-5-CPY (*)	$2.51 (\pm 0.01) \times 10^4$	$2.11 (\pm 0.04) \times 10^{-2}$	$3.28 (\pm 0.01) \times 10^4$	$1.42 (\pm 0.03) \times 10^{-2}$

Data analyzed using model 1 or 1.2 (\*) which included an additional phase.

10

11

12 **Table S9:** Kinetic parameters of SsOGT-H<sup>5</sup> labeling.

Substrate	$k_{app} (\pm \text{S.D.}) [\text{s}^{-1}\text{M}^{-1}]$
BG-6-TMR	$6.78 (\pm 0.67) \times 10^1$
BG-5-TMR	$1.45 (\pm 0.92) \times 10^2$
BG-6-Alexa488	$1.24 (\pm 0.01) \times 10^2$

Data analyzed using model 1.

13

1 **Protein sequences:**

2 General color code: Hisx10-tag – TEV cleavage site – Protein sequence – Fast mutation – Catalytic residue

3  
4 >HT7  
5 MHHHHHHHHHHENLYFQJGIGTGFPDPHYVEVLGERMHYVDVGPRDGTPLFLHGNPTSSYVWRNIIPHVAPTHRCIAPDLIGMGKS  
6 DKPDLGYFFDDHVRFMDFIEALGLEEVVLVIH DWGSALGFHWAKRNPERVKGIAFMEFIRPIPTWDEWPEFARETFQAFRTTVDVGRK  
7 LIIDQNVFIEGTLPMGVVRPLTEVEMDHYREPFLNPVDREPLWRFPNELPIAGEPANIVALVEEYMDWLHQSPVKLLFWGTPGVLIPP  
8 AEAARLAKSLPNCKAVDIGPGLNLLQEDNPDIGSEIARWLSTLEI

9  
10 >HOB  
11 MHHHHHHHHHHENLYFQJGIGTGFPDPHYVEVLGERMHYVDVGPRDGTPLFLHGNPTSSYVWRNIIPHVAPTHRCIAPDLIGMGKS  
12 DKPDLGYFFDDHVRFMDFIEALGLEEVVLVIH DWGSALGFHWAKRNPERVKGIAFMEFIRPIPTWDEWP KFARKTFQAFRT KKVGR  
13 KLIIDQNVFIEGTLPMGVVRPLTEVEMDHYREPFLNPVDREPLWRFPNELPIAGEPANIVALVEEYMDWLHQSPVKLLFWGTPGVLIP  
14 PAEAARLAKSLPNCKAVDIGPGLNLLQEDNPDIGSEIARWLSTLEISG

15 Color code: mutations as compared to HT7  
16  
17 >SNAP  
18 MHHHHHHHHHHENLYFQJGMDKDCEMKRTTLDSPGKLELSGCEQGLHEIIFLGKGTSAADAVEVPAPAAVLGGPEPLMQATAWLNA  
19 YFHQPEAIEEFPVPALHHPVFQQESFTRQVLWKLKVVKFGVEVISYSHLAALAGNPAATAAVKTALSGNPVPIPIP CHRVVQGDLDVGG  
20 YEGGLAVKEWLLAHEGHRLGKPLG

21  
22 >SNAPf  
23 MHHHHHHHHHHENLYFQJGMDKDCEMKRTTLDSPGKLELSGCEQGLH RIIFLGKGTSAADAVEVPAPAAVLGGPEPLMQATAWLNA  
24 YFHQPEAIEEFPVPALHHPVFQQESFTRQVLWKLKVVKFGVEVISYSHLAALAGNPAATAAVKTALSGNPVPIPIP CHRVVQGDLDVGG  
25 YEGGLAVKEWLLAHEGHRLGKPLG

26  
27 >SNAP<sup>α</sup>  
28 MHHHHHHHHHHENLYFQJGDCEMKRTTLDSPGKLELSGCEQGLHEIIFLGKGTSAADAVEVPAPAAVLGGPEPLMQATAWLNAYFH  
29 QPEAIEEFPVPALHHPVFQQESFTRQVLWKLKVVKFGVEVISYSHLAALAGNPAATAAVKTALSGNPVPIPIP CHRVVQGDLDVGGYEG  
30 GLAVKEWLLAHEGHRLGKR

31  
32 >CLIP  
33 MHHHHHHHHHHENLYFQJGMDKDCEMKRTTLDSPGKLELSGCEQGLHEIIFLGKGTSAADAVEVPAPAAVLGGPEPLIQATAWLNAY  
34 FHQPEAIEEFPVPALHHPVFQQESFTRQVLWKLKVVKFGVEISESHLAALVGNPAATAAVNTALDGNPVPILIP CHRVVQGDSDVGPY  
35 LGGLAVKEWLLAHEGHRLGKPLGG

36  
37 >CLIPf  
38 MHHHHHHHHHHENLYFQJGMDKDCEMKRTTLDSPGKLELSGCEQGLH RIIFLGKGTSAADAVEVPAPAAVLGGPEPLIQATAWLNA  
39 YFHQPEAIEEFPVPALHHPVFQQESFTRQVLWKLKVVKFGVEISESHLAALVGNPAATAAVNTALDGNPVPILIP CHRVVQGDSDVGP  
40 YLGGLAVKEWLLAHEGHRLGKPLGG

41  
42 >hAGT  
43 *MAS*WSPQFEK *GADDDDK* *VPH*MDKDCEMKRTTLDSPGKLELSGCEQGLHEIKLLGKGTSAADAVEVPAPAAVLGGPEPLMQCTA  
44 WLNAYFHQPEAIEEFPVPALHHPVFQQESFTRQVLWKLKVVKFGVEISYQQLAALAGNPKAARAVGGAMRGNPVPILIPCHRVVCCSS  
45 GAVGNYSGLAVKEWLLAHEGHRLGKPLGGSSGLAGAWLKAGATSGSPAGRN *APGFSSISA*HHHHHHHHHH

46 Color code: Strep-Tag II, Enterokinase cleavage site, linkers

47

1 >SsOGT-H<sup>5</sup>  
2 MASWSHPQFEK GADDDDK VPHMLVYGLYKSPLGYITVAKDDKGFIMLDFCDCVEGNSRDDSSFTEFFHKLDLYFEGKPINLREPINK  
3 TYPFRLSVFKEVMKIPWGKVMYKQIADSLGTAPAAVKTALSENPELLIIPCHRVAENGIGGYERGVKLKRALLELEGVKIPELAPGFSSI  
4 SAHHHHHHHHHHH  
5 Color code: **Strep-Tag II**, **Enterokinase cleavage site**, *linkers*

## 1 Example DynaFit scripts:

2

## 3 HT7 stopped flow labeling kinetics model 2

```
[task]
  data = progress
  task = fit
  confidence = monte-carlo

[mechanism]
  P + S <==> P.S      :   k1   k-1
  P.S ----> Z         :   k2

[constants] ; units: uM, sec
  k1 = 10 ?
  k-1 = 10 ?
  k2 = 10 ?

[parameters]
  R = 0.2 ?

[data]
  Delay      0.022
  offset     0.0262
  directory  path/to/data
  sheet      data.csv
  column 6 | conc P = 1      | conc S = 1      | response Z = 1      * R |
response P.S = 1      * R | label c=1
  column 5 | conc P = 0.75 | conc S = 0.75 | response Z = 1.333 * R |
response P.S = 1.333 * R | label c=0.75
  column 4 | conc P = 0.5  | conc S = 0.5  | response Z = 2      * R |
response P.S = 2      * R | label c=0.5
  column 3 | conc P = 0.25 | conc S = 0.25 | response Z = 4      * R |
response P.S = 4      * R | label c=0.25
  column 2 | conc P = 0.1  | conc S = 0.1  | response Z = 10     * R |
response P.S = 10     * R | label c=0.1

[output]
  directory path/to/output/folder

[settings]
  {ConfidenceIntervals}
  LevelPercent = 95
  {Output}
  XAxisLabel = time [s]
  YAxisLabel = anisotropy
```

4 [end]

5

## 1 SNAP stopped flow labeling kinetics model 2

```
[task]
  data = progress
  task = fit
  confidence = monte-carlo

[mechanism]
  P + S <===> P.S      :   k1   k-1
  P.S ----> Z          :   k2

[constants] ; units: uM, sec
  k1 = 1 ?
  k-1 = 1 ?
  k2 = 1 ?

[concentrations] ; units: uM
  S = 2 ?

[responses]
  Z = 0.07 ?
  P.S = 1 * Z

[data]
  delay      0.022
  offset     0
  directory  path/to/data
  sheet      data.csv
  column 2 | conc P = 50 | label c=50
  column 3 | conc P = 37.5 | label c=37.5
  column 4 | conc P = 25 | label c=25
  column 5 | conc P = 12.5 | label c=12.5
  column 6 | conc P = 5 | label c=5
  column 7 | conc P = 2.5 | label c=2.5
  column 8 | conc P = 1.25 | label c=1.25

[output]
  directory path/to/output/folder

[settings]
  {ConfidenceIntervals}
    LevelPercent = 95
  {Output}
    XAxisLabel = time [s]
    YAxisLabel = anisotropy
```

2 [end]

3



## 1 HT7 microplate reader labeling kinetics model 1

2 (Time series of each condition were not averaged before DynaFit analysis since the TECAN plate reader has small inconsistencies  
3 in measurement intervals)

```
[task]
  data = progress
  task = fit
  confidence = monte-carlo

[mechanism]
  P + S ----> Z      :   k_app

[constants] ; units: uM, sec
  k_app = 1 ?

[concentrations] ; units: uM
  S = 0.05

[responses]
  Z = 4000 ?

[data]
  delay      1
  offset     87.118
  directory  path/to/data
  sheet      data.csv

  column 2 | conc P = 0      | label 0
  column 3 | conc P = 0      | label 0
  column 4 | conc P = 0      | label 0

  column 5 | conc P = 0.4    | label 400
  column 6 | conc P = 0.4    | label 400
  column 7 | conc P = 0.4    | label 400

  column 8 | conc P = 0.8    | label 800
  column 9 | conc P = 0.8    | label 800
  column 10 | conc P = 0.8   | label 800

  column 11 | conc P = 1.6   | label 1600
  column 12 | conc P = 1.6   | label 1600
  column 13 | conc P = 1.6   | label 1600

  column 14 | conc P = 3.2   | label 3200
  column 15 | conc P = 3.2   | label 3200
  column 16 | conc P = 3.2   | label 3200

  column 17 | conc P = 6.4   | label 6400
  column 18 | conc P = 6.4   | label 6400
  column 19 | conc P = 6.4   | label 6400

  column 20 | conc P = 12.8  | label 12800
  column 21 | conc P = 12.8  | label 12800
  column 22 | conc P = 12.8  | label 12800

  column 23 | conc P = 25.6  | label 25600
  column 24 | conc P = 25.6  | label 25600
  column 25 | conc P = 25.6  | label 25600

  column 26 | conc P = 51.2  | label 51200
  column 27 | conc P = 51.2  | label 51200
  column 28 | conc P = 51.2  | label 51200

[output]
  directory path/to/output/folder

[settings]
  {ConfidenceIntervals}
  LevelPercent = 95
  {Output}
  XAxisLabel = time [s]
  YAxisLabel = anisotropy
```

4 [end]

5

## 1 SNAP-/CLIP microplate reader labeling kinetics model 1

2 (Time series of each condition were not averaged before DynaFit analysis since the TECAN plate reader has small inconsistencies  
3 in measurement intervals)

```
[task]
  data = progress
  task = fit
  confidence = monte-carlo

[mechanism]
  P + S ----> Z          : k_app

[constants] ; units: nM, sec
  k_app = 0.0001 ?

[concentrations] ; units: nM
  S = 50 ?

[responses]
  Z = 2 ?

[data]
  delay      2.7
  offset     73.46
  directory  path/to/data
  sheet      data.csv

  column 2 | conc P = 52      | label 52
  column 3 | conc P = 52      | label 52
  column 4 | conc P = 52      | label 52

  column 5 | conc P = 79      | label 79
  column 6 | conc P = 79      | label 79
  column 7 | conc P = 79      | label 79

  column 8 | conc P = 118.5   | label 118.5
  column 9 | conc P = 118.5   | label 118.5
  column 10 | conc P = 118.5  | label 118.5

  column 11 | conc P = 177.7  | label 177.7
  column 12 | conc P = 177.7  | label 177.7
  column 13 | conc P = 177.7  | label 177.7

  column 14 | conc P = 266.6   | label 266.6
  column 15 | conc P = 266.6   | label 266.6
  column 16 | conc P = 266.6   | label 266.6

  column 17 | conc P = 400     | label 400
  column 18 | conc P = 400     | label 400
  column 19 | conc P = 400     | label 400

  column 20 | conc P = 600     | label 600
  column 21 | conc P = 600     | label 600
  column 22 | conc P = 600     | label 600

  column 23 | conc P = 900     | label 900
  column 24 | conc P = 900     | label 900
  column 25 | conc P = 900     | label 900

[output]
  directory path/to/output/folder

[settings]
  {ConfidenceIntervals}
    LevelPercent = 95
  {Output}
    XAxisLabel = time [s]
    YAxisLabel = anisotropy
```

4 [end]

5

## 1 SNAP-/CLIP microplate reader labeling kinetics model 1.2

2 (Time series of each condition were not averaged before DynaFit analysis since the TECAN plate reader has small inconsistencies  
3 in measurement intervals)

```
[task]
  data = progress
  task = fit
  confidence = monte-carlo

[mechanism]
P + S ----> Z      : k_app
Z      ----> Z2     : k_app_2

[constants] ; units: nM, sec
  k_app = 0.0001 ?
  k_app_2 = 0.0001 ?

[concentrations] ; units: nM
  S = 50 ?

[responses]
  Z = 2 ?
  Z2 = 2 ?

[data]
  delay      2.7
  offset     73.46
  directory  path/to/data
  sheet      data.csv

  column 2 | conc P = 52      | label 52
  column 3 | conc P = 52      | label 52
  column 4 | conc P = 52      | label 52

  column 5 | conc P = 79      | label 79
  column 6 | conc P = 79      | label 79
  column 7 | conc P = 79      | label 79

  column 8 | conc P = 118.5   | label 118.5
  column 9 | conc P = 118.5   | label 118.5
  column 10 | conc P = 118.5  | label 118.5

  column 11 | conc P = 177.7  | label 177.7
  column 12 | conc P = 177.7  | label 177.7
  column 13 | conc P = 177.7  | label 177.7

  column 14 | conc P = 266.6   | label 266.6
  column 15 | conc P = 266.6   | label 266.6
  column 16 | conc P = 266.6   | label 266.6

  column 17 | conc P = 400     | label 400
  column 18 | conc P = 400     | label 400
  column 19 | conc P = 400     | label 400

  column 20 | conc P = 600     | label 600
  column 21 | conc P = 600     | label 600
  column 22 | conc P = 600     | label 600

  column 23 | conc P = 900     | label 900
  column 24 | conc P = 900     | label 900
  column 25 | conc P = 900     | label 900

[output]
  directory path/to/output/folder

[settings]
  {ConfidenceIntervals}
  LevelPercent = 95
  {Output}
  XAxisLabel = time [s]
  YAxisLabel = anisotropy

4 [end]
5
```

1 **References:**

- 2 1. Butkevich AN, Mitronova GY, Sidenstein SC, Klocke JL, Kamin D, Meineke DN, et al. Fluorescent  
3 Rhodamines and Fluorogenic Carbopyronines for Super-Resolution STED Microscopy in Living Cells. *Angew*  
4 *Chem Int Ed Engl*. 2016;55(10):3290-4.
- 5 2. Mudd G, Pi IP, Fethers N, Dodd PG, Barbeau OR, Auer M. A general synthetic route to isomerically  
6 pure functionalized rhodamine dyes. *Methods and Applications in Fluorescence*. 2015;3(4).
- 7 3. Ueno Y, Jose J, Loudet A, Pérez-Bolívar Cs, Anzenbacher P, Burgess K. Encapsulated Energy-  
8 Transfer Cassettes with Extremely Well Resolved Fluorescent Outputs. *Journal of the American Chemical*  
9 *Society*. 2011;133(1):51-5.
- 10 4. Lukinavicius G, Umezawa K, Olivier N, Honigmann A, Yang G, Plass T, et al. A near-infrared  
11 fluorophore for live-cell super-resolution microscopy of cellular proteins. *Nat Chem*. 2013;5(2):132-9.
- 12 5. Wang L, Tran M, D'Este E, Roberti J, Koch B, Xue L, et al. A general strategy to develop cell  
13 permeable and fluorogenic probes for multicolour nanoscopy. *Nat Chem*. 2020;12(2):165-72.
- 14 6. Keppler A, Gendrezig S, Gronemeyer T, Pick H, Vogel H, Johnsson K. A general method for the  
15 covalent labeling of fusion proteins with small molecules in vivo. *Nature biotechnology*. 2003;21(1):86-9.
- 16 7. Srikun D, Albers AE, Nam CI, Iavarone AT, Chang CJ. Organelle-Targetable Fluorescent Probes for  
17 Imaging Hydrogen Peroxide in Living Cells via SNAP-Tag Protein Labeling. *Journal of the American Chemical*  
18 *Society*. 2010;132(12):4455-65.
- 19 8. Keppler A, Pick H, Arrivoli C, Vogel H, Johnsson K. Labeling of fusion proteins with synthetic  
20 fluorophores in live cells. *Proceedings of the National Academy of Sciences*. 2004;101(27):9955-9.
- 21 9. Correa I, Baker B, Zhang A, Sun L, Provost C, Lukinavicius Gz, et al. Substrates for Improved Live-  
22 Cell Fluorescence Labeling of SNAP-tag. *Current Pharmaceutical Design*. 2013;19(30):5414-20.
- 23 10. Hiblot J, Yu Q, Sabbadini MDB, Reymond L, Xue L, Schena A, et al. Luciferases with Tunable  
24 Emission Wavelengths. *Angew Chem Int Ed Engl*. 2017;56(46):14556-60.
- 25 11. Grimm JB, English BP, Chen J, Slaughter JP, Zhang Z, Revyakin A, et al. A general method to improve  
26 fluorophores for live-cell and single-molecule microscopy. *Nat Methods*. 2015;12(3):244-50, 3 p following  
27 50.
- 28 12. Gautier A, Juillerat A, Heinis C, Correa IR, Jr., Kindermann M, Beaufils F, et al. An engineered  
29 protein tag for multiprotein labeling in living cells. *Chem Biol*. 2008;15(2):128-36.
- 30 13. Bottanelli F, Kromann EB, Allgeyer ES, Erdmann RS, Wood Baguley S, Sirinakis G, et al. Two-colour  
31 live-cell nanoscale imaging of intracellular targets. *Nature communications*. 2016;7(1).
- 32 14. Zhang Y, So M-k, Loening AM, Yao H, Gambhir SS, Rao J. HaloTag Protein-Mediated Site-Specific  
33 Conjugation of Bioluminescent Proteins to Quantum Dots. *Angewandte Chemie International Edition*.  
34 2006;45(30):4936-40.
- 35 15. Masharina A, Reymond L, Maurel D, Umezawa K, Johnsson K. A fluorescent sensor for GABA and  
36 synthetic GABA(B) receptor ligands. *Journal of the American Chemical Society*. 2012;134(46):19026-34.
- 37 16. Deo C, Abdelfattah AS, Bhargava HK, Berro AJ, Falco N, Farrants H, et al. The HaloTag as a general  
38 scaffold for far-red tunable chemigenetic indicators. *Nature chemical biology*. 2021.
- 39 17. Rossi F, Morrone C, Massarotti A, Ferraris DM, Valenti A, Perugino G, et al. Crystal structure of a  
40 thermophilic O6-alkylguanine-DNA alkyltransferase-derived self-labeling protein-tag in covalent complex  
41 with a fluorescent probe. *Biochemical and Biophysical Research Communications*. 2018;500(3):698-703.

42